UNIVERSITY OF THESSALY

SCHOOL OF ENGINEERING

DEPARTMENT OF MECHANICAL ENGINEER

Diploma thesis

GENERATION OF ELECTRICITY IN FUEL CELLS WITH BIOETHANOL SUPPLY

by

PATSIAS ATHANASIOS

Supervisor:

Prof. Tsiakaras Panagiotis

Submitted in partial fulfillment of the requirements for the degree of Diploma in Mechanical Engineering at the University of Thessaly

Volos, 2024

ΠΑΝΕΠΙΣΤΗΜΙΟ ΘΕΣΣΑΛΙΑΣ
ΠΟΛΥΤΕΧΝΙΚΗ ΣΧΟΛΗ
ΤΜΗΜΑ ΜΗΧΑΝΟΛΟΓΩΝ ΜΗΧΑΝΙΚΩΝ

ΔΙΠΛΩΜΑΤΙΚΗ ΕΡΓΑΣΙΑ

ΠΑΡΑΓΩΓΗ ΗΛΕΚΤΡΙΣΜΟΥ ΣΕ ΚΥΨΕΛΕΣ ΚΑΥΣΙΜΟΥ ΜΕ ΤΡΟΦΟΔΟΣΙΑ ΒΙΟΑΙΘΑΝΟΛΗΣ

υπό

ΠΑΤΣΙΑΣ ΑΘΑΝΑΣΙΟΣ

Επιβλέπων:

Καθηγητής Τσιακάρας Παναγιώτης

Υπεβλήθη για την εκπλήρωση μέρους των απαιτήσεων για την απόκτηση του
Διπλώματος Μηχανολόγου Μηχανικού

Βόλος, 2024

Ο υπογράφων ΠΑΤΣΙΑΣ ΑΘΑΝΑΣΙΟΣ, γνωρίζοντας τις συνέπειες της λογοκλοπής, δηλώνω υπεύθυνα ότι η παρούσα εργασία με τίτλο «ΠΑΡΑΓΩΓΗ ΗΛΕΚΤΡΙΣΜΟΥ ΣΕ ΚΥΨΕΛΕΣ ΚΑΥΣΙΜΟΥ ΜΕ ΤΡΟΦΟΔΟΣΙΑ ΒΙΟΑΙΘΑΝΟΛΗΣ» αποτελεί προϊόν αυστηρά προσωπικής εργασίας και όλες οι πηγές που έχω χρησιμοποιήσει έχουν δηλωθεί κατάλληλα στις βιβλιογραφικές αναφορές. Τα σημεία όπου έχω χρησιμοποιήσει ιδέες, κείμενο ή και πηγές άλλων συγγραφέων, αναφέρονται ευδιάκριτα στο κείμενο με την κατάλληλη παραπομπή και η σχετική αναφορά περιλαμβάνεται στο τμήμα των βιβλιογραφικών αναφορών με πλήρη περιγραφή.
Ο ΔΗΛΩΝ

ΠΑΤΣΙΑΣ ΑΘΑΝΑΣΙΟΣ

I, PATSIAS ATHANASIOS, knowing the consequences of plagiarism, I declare hereby responsibly that the present paper entitled "GENERATION OF ELECTRICITY IN FUEL CELLS WITH BIOETHANOL SUPPLY" is a product of strictly personal work and all the sources I have used have been properly declared in the bibliographic references. Where I have used ideas, text and/or sources from other authors, they are clearly indicated in the text with appropriate citation and the relevant reference is included in the bibliography section with a full description.
THE DECLARANT

PATSIAS ATHANASIOS

Approved by the Committee on Final Examination:

Advisor	Dr. Tsiakaras Panagiotis (Supervisor) Professor of Department of Mechanical Engineering School of Engineering University of Thessaly
Member	Dr. Charalampous Georgios Assistant professor of Department of Mechanical Engineering School of Engineering University of Thessaly
Member	Dr. Brouzgou Angeliki Assistant Professor of Department of Energy Systems School of Technology Sciences University of Thessaly

Acknowledgements

I would like to express my sincere thanks to my thesis supervisor, Professor Tsiakaras Panagiotis, for his valuable help and guidance during the implementation of my thesis.

I am also grateful to the other members of the examination committee of my thesis, Associate Professors, Charalampous Georgios and Brouzgou Angeliki for the careful reading of my thesis and for their valuable suggestions.

I also thank my colleagues Molochas Kostas and Balkourani Georgia and Ms. Sotiria Kontou for their support and guidance.

Finally, I am grateful to my parents, Patsias Antonios and Giantsidou Maria, for their wholehearted love and support throughout the years.

Dedicated to my parents.

Ευχαριστίες

Θα ήθελα να εκφράσω τις ειλικρινείς μου ευχαριστίες στον επιβλέποντα καθηγητή της διατριβής μου, καθηγητή Τσιακάρα Παναγιώτη, για την πολύτιμη βοήθεια και καθοδήγησή του κατά τη διάρκεια της εκπόνησης της διατριβής μου.

Ευχαριστώ επίσης τα άλλα μέλη της εξεταστικής επιτροπής της διατριβής μου, τους Αναπληρωτές Καθηγητές, Χαραλάμπους Γεώργιο και Μπρούζγου Αγγελική για την προσεκτική ανάγνωση της διατριβής μου και για τις πολύτιμες υποδείξεις τους.

Ευχαριστώ τους συναδέλφους μου Μολόχα Κώστα και Μπαλκουράνη Γεωργία και την κα Σωτηρία Κόντου για την συμπαράσταση και την καθοδήγησή τους.

Τέλος, είμαι ευγνώμων στους γονείς μου, Πατσιάς Αντώνιος και Γιαντσίδου Μαρία, για την ολόψυχη αγάπη και υποστήριξή τους όλα αυτά τα χρόνια.

Αφιερωμένο στους γονείς μου.

Abstract

The impact on the human body from the exhaust fumes of conventional engines and the continuous increase of the greenhouse effect has led the scientific community to study and develop new environmentally friendly energy conversion methods. Fuel cells are devices of high interest as they directly convert the chemical energy of the fuel into electricity. They have many advantages for commercial use as they have no moving parts, provide higher yields in contrast to conventional machines, quiet in use and the fuel feedstock does not have to be from fossil fuels. When the fuel feedstock, like ethanol, comes from biomass, the carbon dioxide produced is equal to the amount of carbon dioxide that the biomass feedstock consumes to grow. In this way, there is no increase in the amount of carbon dioxide produced, which makes fuel cells ideal for commercial use.

Ethanol can be produced both from oil and biomass. When it comes from biomass it is called bioethanol. Bioethanol is a renewable energy source and the hydrogen it contains is called green while the hydrogen that comes from oil is called grey. Hydrogen transportation and storage can be challenging, thus ethanol, as a hydrogen-containing fuel, can be an easy fuel supply solution for fuel cells. In order to extract ethanol, biomass goes through a simple process where it includes pretreatment, hydrolysis, fermentation and finally distillation where pure ethanol is obtained. This process is called biochemical conversion. Another process that is not usually used is the thermochemical conversion.

In this study some of the main direct ethanol fuel cells are first analysed. Some of the most basic principles of electrochemistry are described and some examples such as batteries and capacitors are presented. Also, some of the techniques for producing hydrogen for use in fuel cells are described. In the following, PEMFCs and AEMFCs using bioethanol are analysed to a greater extent and at the same time, the case of NISSAN, which uses SOFCs with a reformer in its vehicles, is described.

Finally, a report is made on the main catalyst materials studied to date, analyzing their main characteristics. First, the two basic palladium and platinum monometallic catalysts are compared. Then, some of the most important and widely studied palladium-based bimetallic and trimetallic catalysts are discussed. Finally, the catalysts PdSn-SnO_2/C and Pd/$Ni(OH)_2$ are analysed in terms of their main characteristics.

Περίληψη

Οι επιπτώσεις στον ανθρώπινο οργανισμό από τα καυσαέρια των συμβατικών κινητήρων και η συνεχής αύξηση του φαινομένου του θερμοκηπίου έχουν οδηγήσει την επιστημονική κοινότητα στη μελέτη και την ανάπτυξη νέων μεθόδων μετατροπής ενέργειας φιλικών προς το περιβάλλον. Οι κυψέλες καυσίμου είναι συσκευές υψηλού ενδιαφέροντος, καθώς μετατρέπουν άμεσα τη χημική ενέργεια του καυσίμου σε ηλεκτρική ενέργεια. Έχουν πολλά πλεονεκτήματα για εμπορική χρήση, καθώς δεν έχουν κινούμενα μέρη, παρέχουν υψηλότερες αποδόσεις σε αντίθεση με τις συμβατικές μηχανές, είναι αθόρυβες στη χρήση και η πρώτη ύλη του καυσίμου δεν χρειάζεται να προέρχεται από ορυκτά καύσιμα. Όταν η πρώτη ύλη καυσίμου, όπως η αιθανόλη, προέρχεται από βιομάζα, το παραγόμενο διοξείδιο του άνθρακα είναι ίσο με την ποσότητα διοξειδίου του άνθρακα που καταναλώνει η πρώτη ύλη βιομάζας για να αναπτυχθεί. Με αυτόν τον τρόπο, δεν αυξάνεται η ποσότητα του παραγόμενου διοξειδίου του άνθρακα, γεγονός που καθιστά τις κυψέλες καυσίμου ιδανικές για εμπορική χρήση.

Η αιθανόλη μπορεί να παραχθεί τόσο από πετρέλαιο όσο και από βιομάζα. Όταν προέρχεται από βιομάζα ονομάζεται βιοαιθανόλη. Η βιοαιθανόλη είναι μια ανανεώσιμη πηγή ενέργειας και το υδρογόνο που περιέχει ονομάζεται πράσινο, ενώ το υδρογόνο που προέρχεται από το πετρέλαιο ονομάζεται γκρι. Η μεταφορά και η αποθήκευση υδρογόνου μπορεί να είναι δύσκολη, επομένως η αιθανόλη, ως καύσιμο που περιέχει υδρογόνο, μπορεί να αποτελέσει μια εύκολη λύση παροχής καυσίμου για τις κυψέλες καυσίμου. Για την εξαγωγή αιθανόλης, η βιομάζα περνάει από μια απλή διαδικασία που περιλαμβάνει προεπεξεργασία, υδρόλυση, ζύμωση και τέλος απόσταξη όπου λαμβάνεται καθαρή αιθανόλη. Η διαδικασία αυτή ονομάζεται βιοχημική μετατροπή. Μια άλλη διαδικασία που συνήθως δεν χρησιμοποιείται είναι η θερμοχημική μετατροπή.

Στην παρούσα μελέτη αναλύονται αρχικά ορισμένες από τις κυριότερες κυψέλες καυσίμου απευθείας αιθανόλης. Περιγράφονται ορισμένες από τις βασικότερες αρχές της ηλεκτροχημείας και παρουσιάζονται ορισμένα παραδείγματα, όπως οι μπαταρίες και οι πυκνωτές. Επίσης, περιγράφονται ορισμένες από τις τεχνικές παραγωγής υδρογόνου για χρήση σε κυψέλες καυσίμου. Στη συνέχεια, αναλύονται σε μεγαλύτερο βαθμό οι PEMFC και AEMFC που χρησιμοποιούν βιοαιθανόλη και παράλληλα περιγράφεται η περίπτωση της NISSAN, η οποία χρησιμοποιεί SOFC με αναμορφωτή στα οχήματά της.

Τέλος, γίνεται αναφορά στα κυριότερα υλικά καταλυτών που έχουν μελετηθεί μέχρι σήμερα, αναλύοντας τα κύρια χαρακτηριστικά τους. Αρχικά, συγκρίνονται οι δύο βασικοί μονομεταλλικοί καταλύτες παλλαδίου και πλατίνας. Στην συνέχεια αναλύονται κάποιοι από τους σημαντικότερους και τους πιο διαδεδομένα μελετημένους διμεταλλικούς και τριμεταλλικούς καταλύτες με βάση το παλλάδιο. Τέλος αναλύονται οι καταλύτες $PdSn\text{-}SnO_2/C$ και $Pd/Ni(OH)_2$ ως προς τα κυριότερα χαρακτηριστικά τους.

Contents

LIST OF TABLES

LIST OF FIGURES

Chapter 1

INTRODUCTION

To date, most of the research that has been carried out involves fuel cells with proton exchange membranes (PEM-DEFCs) [1]. Due to their many disadvantages and in combination with their low efficiency [2], interest is now turning to fuel cells with anion exchange membranes in alkaline media (AEM-DEFCs) [3]. In the context of this thesis, the study of the fuel cell with an anion exchange membrane in an alkaline media with ethanol feed will be attempted, utilizing the knowledge and experience of previous research. Through a series of experiments that several scientists have carried out, valuable results will be obtained, which will help to better understand the principles of cell operation. After this process, the results will be analyzed and appropriate conclusions will be drawn for the AEM-DEFC.

In nature, most chemical reactions are very slow, and some compounds do not interact at all. Thus, in applications where high rates of chemical reactions are required, catalysts had to be developed that would allow the compounds to react in a reasonable amount of time. Today, in most if not all electrochemical devices, reactions have to occur rapidly in order to be efficient. For this reason, depending on the electrochemical device, appropriate catalysts are used to allow these high conversion rates [4, 5].

In Chapter 2, first, a brief description of the fundamentals of electrocatalysis will be given [5-13]. The aim is to understand the reasons for its development, the principles of its operation and its various possible applications in electrochemical devices. Next, electrochemical devices for energy conversion and storage will be developed. In particular, the most studied fuel cells will be analyzed in terms of their structure, listing the reactions that govern them, the improvements in their operation that they are amenable to and their challenges [14-21]. In the following, the theoretical principles of the electrolysis process for the production of hydrogen as a more environmentally friendly fuel will be developed, listing some of the most common materials used to carry out the reactions and the principle of operation [22]. Moving on to the same chapter, a brief analysis of hydrogen fuel will be given [23]. First, some of its main applications will be described, such as its use in railways, ships, heavy-duty on road vehicles and aviation. Then, the hydrogen economy in terms of energy transport will be discussed.

On the need to develop energy storage and supply technologies, scientists have studied devices such as batteries [24-27]. Batteries are an easy solution for applications of everyday life that require

autonomy in energy and its use at the discretion of the person who needs it at a time different from the moment it was stored. In this chapter, an analysis of the operation of a variety of batteries such as lithium-ion, lithium-air and Zn-air batteries will be presented. In particular, the basic principles of operation are discussed, some of the main materials in which they are made and the various applications they are used in are given [28]. In addition, as a continuation of batteries, capacitors are described based on the literature of recent years and their main characteristics are analysed [29]. Next, a report on electrochemical sensors will be given [30]. The main objective is to understand their operating principles and to describe different types of sensors in a variety of applications [31, 32].

In chapter 3, high and low temperature fuel cells will be analysed. In particular, PEM and AEM fuel cells using ethanol will be examined [33, 34], setting out the main principles of operation, giving the reactions and some of the basic materials used in them [35]. Then, there will be a detailed description of the ethanol extraction process from biomass [36-40]. First, biomass itself will be analyzed in terms of its definition, how it is produced, and the different types that exist [38]. Then, a detailed examination of all the steps followed in the industry to safely extract bioethanol will be carried out [37].

In chapter 4, a brief comparison of the two main monometallic catalysts will be made first. Then, through experiments carried out by the scientific community, all the results obtained will be discussed with a full description of the main factors such as performance and stability in terms of ethanol oxidation reaction.

Chapter 2

FUNDAMENTAL OF ELECTROCHEMICAL DEVICES

The field of science and engineering is often confronted with physical obstacles that either prevent or delay certain processes. A common phenomenon is that reactions in nature do not occur naturally but under violent conditions such as very high temperatures or very high pressures. Also, many substances will take many hundreds of years to react, while other substances do not interact at all. Thus, it was necessary to create a new technological field called electrocatalysis, which deals with finding techniques that enable, enhance and accelerate the reactions of various substances [7, 8]. With the passage of time and the need to find a way to accelerate reactions on an industrial level, the first catalysts were created [4, 41-46]. The term catalyst refers to the substance in the presence of which the acceleration of chemical reactions is achieved while leaving the mass and chemical composition of the reactants almost unchanged. Depending on the phase of the catalyst and the reactants being catalyzed, catalysis is divided into two categories called homogeneous and heterogeneous catalysis. In homogeneous catalysis, the catalyst and the reactants are in the same phase, while in heterogeneous catalysis the catalyst and the catalyzed system are in different phases. In the case of solid catalysts, the reactions take place on their surface, so it can be concluded that increasing the surface area will lead to a more efficient reaction at a higher rate.

For substances to react with each other, a minimum energy is required, described by the term activation energy, introduced by Swedish scientist Svante Arrhenius in 1889. The term activation energy corresponds to the minimum energy that the reacting molecules must possess, i.e. appropriate velocity and orientation, in order to produce products. The lower this energy is, the faster the reaction takes place as many more molecules can cross the energy barrier and produce products. The mechanism of catalysis offers a different way for molecules to react faster. In particular, instead of reacting with each other, the substances adhere to the catalyst by making an intermediate apparent reaction and then interact with each other leading to the regeneration of the catalyst according to the following reaction:

Requested reaction (slow):

$A + B \rightarrow AB$ Where A and B are the reactants

Reaction offered by the catalyst:

$A + K \rightarrow AK$ (fast reaction)

$AK + B \rightarrow AB + K$ (fast reaction)

A special class of catalysts is provided by nature itself and is enzymes or biocatalysts [47, 48]. These compounds are protein-based and are used both in living organisms and their metabolism and in animal

and plant waste through the decomposition mechanism. In the biomass industry, biocatalysts are used in an important process called fermentation, which leads to the formation of bioethanol to produce a more environmentally friendly fuel.

An extension of catalysis is electrocatalysis, on which many of the electrochemical devices discussed in the second part of this chapter are based [5, 49, 50]. In addition to its importance in the technological world, electrocatalysis is often found in nature through processes such as plant photosynthesis and the neurological system of the human body. It is therefore necessary to understand its function and its usefulness in various technological devices that make up our daily life. Electrocatalysis, unlike simple catalysis, does not involve the collision of molecules to form products but creates an electrical circuit that includes elements (electrodes) that can give and receive electrons. For example, in fuel cells, an oxidation reaction is achieved at one electrode through a catalyst whereby electrons are delivered. The electrons are directed through an external circuit that includes a charge, such as a rotor, and then go to the second electrode where the reduction reaction of another substance using these electrons takes place. These reactions are carried out via a catalyst and involve the yielding or receiving of electrons rather than the collision of the reactants as in simple catalysis. The second part of this chapter will provide a first analysis of how electrochemical devices involving electrocatalysis work and how they operate.

Electrocatalysis, as mentioned above, is carried out with the help of substances called electrocatalysts [50]. The aim of electrocatalysts is to improve the efficiency of the respective reactions by adding as many electrons as possible to the system. Thus, electrocatalysts must meet certain important specifications in order to be used on a large scale. First of all, they must be able to catalyze the reactions they are assigned to in a satisfactory time frame and with increased efficiency. Also, they must have good resistance since they will often be exposed to corrosive substances. At the same time, they must have good mechanical stability and be able to operate for a long time without reducing their performance. Last but not least, they need to have a low cost price in order to be widely used. Many catalysts consist not only of one element but of two and three elements. Thus, they should be able to meet the specifications in small quantities in order to minimize their cost.

Electrocatalysis is the main mode of mechanism of many electrochemical devices of daily use. Such devices are used in our daily life facilitating it in many areas and making it more pleasant. One such device is the battery of our mobile phone and the battery of our computer. These batteries are mostly lithium-ion batteries and are based on electrocatalysis technology. The electrochemical sensors used in our everyday life also work through the electrocatalysis method. Sensors to detect dopamine in the human body and other substances, lambda sensors in the automotive industry to detect the fuel air ratio are some of these devices [30]. Fuel cells have also attracted the interest of scientists in order to optimize their operation for widespread use and thus replace the hitherto widespread conventional internal

combustion engines and make the transition to more environmentally friendly energy-efficient devices [51]. Especially, when the fuel used in electrocatalysis comes from renewable energy sources then it makes them as devices of utmost importance.

In this context, some general characteristics of different types of fuel cells in acidic and alkaline environments are first presented [1, 19, 34]. The main reactions that take place are described and an initial reference is made to some of their sovereign operating principles. This is followed by a review of the water electrolysis process, citing recent studies that will help improve green hydrogen production techniques for a smooth transition from fossil fuels to more environmentally friendly energy sources [22]. This will lead to an initial attempt to describe hydrogen as a fuel in everyday applications and machines such as fuel cells and a review of how hydrogen is stored and the hydrogen economy. Then, some of the main electrochemical devices for storing and supplying electricity such as lithium-air, lithium-ion and Zn-air batteries are described [9, 10]. Electrochemical capacitors and pseudo capacitors are then referred to with a general description and some of their main applications are listed. Finally, a brief description of electrochemical sensors such as lambda sensors, the pH meter, and the three-electrode system for detecting substances such as dopamine is given.

2.1 FUEL CELLS

Fuel cells are devices of high interest as they directly convert the chemical energy of a fuel into electricity. As far as the anatomy of fuel cells is concerned, the following applies. They consist, firstly, of the anode electrode where the fuel oxidation reaction takes place. The resulting electrons go through an external circuit to the cathode electrode where the oxygen reduction reaction takes place. Between the anode and cathode electrodes is the electrolyte, which is a non-metallic electrical conductor in which the stack current is carried by the movement of the ions. Fuel cells are ideal for commercial use as evidenced by their various advantages. In particular, they have no moving parts, so there is no loss of efficiency due to mechanical friction and no risk of damage, unlike conventional internal combustion engines [52]. They are also independent of fossil fuels and can use fuels such as bioethanol and methanol [33, 52, 53]. In this case they help to reduce carbon dioxide as they do not produce additional exhaust gas. They are silent with high efficiency and high-power quality and are simple to manufacture.

Fuel cells are divided into two major categories depending on their operating temperature. First, some fuel cells operate at high temperatures and are called solid oxide fuel cells (SOFCs). Next, some operate at low temperatures and are divided into two subcategories depending on the type of membrane. Those in which a hydrogen proton is transferred in an acidic media are called proton exchange membrane fuel cells (PEM-FCs) and those in which a hydroxyl anion is transferred in an alkaline media are called anion exchange membrane fuel cells (AEM-FCs).

2.1.1 SOLID OXIDE FUEL CELLS (SOFCs)

A well-studied fuel cell is a solid oxide fuel cell that operates at high temperatures (typically 600-800 ^{o}C) [21, 54, 55], and due to those temperatures there is no need of precious metal electrocatalysts such as Pt, Pd and Ru [56, 57]. Solid electrolyte fuel cells consist of the anode electrode, the cathode electrode, and the electrolyte which is sandwiched between the two electrodes. SOFCs have the advantage that can be configured at will and can have a tubular shape [58]. In particular, solid oxide fuel cells can exist in either a planar or tubular shape. The first SOFC-type fuel cells used were planar-shaped, and so their manufacturing technology developed quite a bit, following a simpler assembly method that makes them more economical compared to tubular cells. Planar SOFCs also offer higher power density because the electrons follow a shorter path from the anode to the cathode. However, their main disadvantage is that they cannot maintain the same temperature constantly on their surface. This problem does not seem to exist in tubular SOFC cells. Although their construction represents a higher investment, tubular is better sealed and is a smart space-saving solution. However, they offer lower-density power because they have longer current paths.

SOFCs can be divided into two groups depending on the conducting ions. Solid electrolyte fuel cells that conduct protons are called H-SOFCs while those that have an electrolyte that conducts oxygen ions are called O-SOFCs as illustrated in **Figure 2.1** [59]. In O-SOFCs, oxygen is reducted at the cathode electrode to form O^{2-} ions, which in turn pass through the electrolyte to the anode. At the anode, the oxidation reaction takes place producing water and releasing electrons which go to the cathode via an external circuit. In H-SOFCs, hydrogen is oxidized to create H^{+} protons that pass through the electrolyte to the cathode. In the cathode, the oxygen reacts with the protons and the electrons to produce water with the electrons that produced at the anode of the cell go to the cathode via an external circuit.

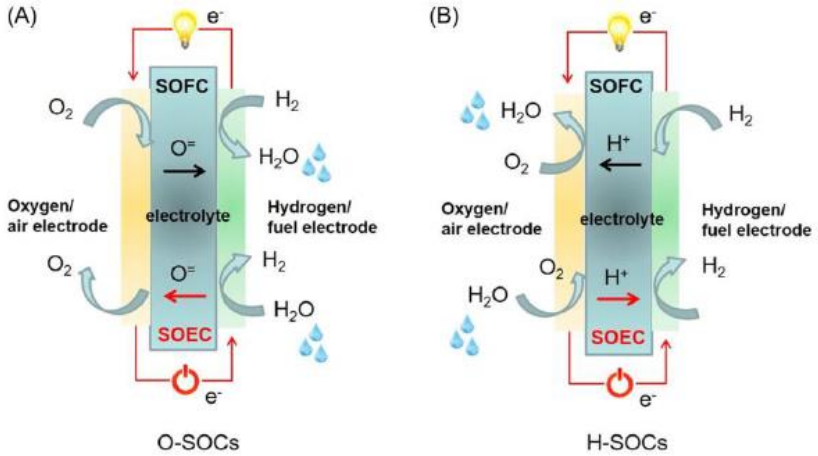

Figure 2.1. O-SOCs and H-SOCs types of solid oxide fuel cells [59].

Reactions that take place:

H-SOFCs:

ANODE: $H_2 \rightarrow 2H^+ + 2e^-$

CATHODE: $\frac{1}{2} O_2 + 2H^+ + 2e^- \rightarrow H_2O$

O-SOFCs:

ANODE: $H_2 + O^{2-} \rightarrow H_2O + 2e^-$

CATHODE: $\frac{1}{2} O_2 + 2e^- \rightarrow O^{2-}$

The picture also shows the solid oxide electrolysis cells with the corresponding reactions that take place depending on the electrolyte. These types of cells are mainly used to store renewable energy from solar panels and wind turbines in hydrogen fuel.

The choice of anode, electrolyte, and cathode materials must be made with great care as they need to meet certain specifications for the fuel cell to operate at maximum efficiency. The anode materials need to be such that they enhance the oxidation reaction but also facilitate the transfer of electrons to the cathode. Unlike the anode, the electrolyte materials must have very low electronic conductivity, but very fast ionic conductivity to enhance the efficiency of the cell and finally, high temperature resistant materials must be used in the cathode. Today the most common anode materials are of the perovskite-type due to their ionic and catalytic characteristics [60]. Perovskite is a crystalline material with an ABX_3 formula. Sites A and B are cations while X is an anion that bonds to both cations. Perovskite is a very convenient material as almost every metal on the periodic table can integrate on the A-site or B-site. Here are the elements that can occupy A-, B- and X-sites [61]:

A: Sr, Ba, Na, K, Rb, Cs, Y, Ag, Pb, Bi and some rare earth materials like Nd, La, Sm, Gd, Pr, Yb, and Ce

B: Mg, Cu, Ni, Fe, Co, Cr, V, W, Zn, Ga, Rh, Al, Si, Sc, Ti, Cr, Mn, Mo, Zr, Fe, Zr, Nb, Yb, Sn, Hf, Ta, and U

X: O, H, F, S, Cl, Se, and Br

Electrodes are divided into two categories, air and hydrogen or fuel electrodes. Air electrodes catalyze oxygen reduction reaction (ORR). The most used material for those electrodes is lanthanum strontium manganite (LSM) due to its catalytic activity. Lanthanum strontium manganite is often combined with yttrium stabilized zirconia (YZS) in order to increase its ion conductivity. On the other hand hydrogen or fuel electrodes catalyze the hydrogen oxidation reaction (HOR). The anode electrode is usually from Ni combined with Y_2O_3 stabilized ZrO_2. It has a porosity of 20 to

40% to enhance mass transport of the reactants and gas products. On the other hand, the cathode electrode is usually made out of lanthanum manganite, which is a p-type perovskite oxide, and is doped with a divalent ion such as calcium or strontium in order to enhance its electronic conductivity.

Electrolyte is the main part of a fuel cell. It needs to be from a material that has very low electronic conductivity but very good ion conductivity. Yttrium stabilized zirconia is the most used material for electrolytes that is usually doped with scandium stabilized zirconia (ScSZ) in order to increase its ion conductivity.

Fuel cells of this type are distinguished by their many advantages such as high efficiency, long-term stability, and fuel flexibility. However, due to the high operating temperature, they require longer start-up times and have mechanical and chemical compatibility issues.

As mentioned earlier, fuel cells of this type are distinguished by their flexibility in terms of the fuel they operate on. Ethanol is a very convenient fuel as it is an easy way to store and transport hydrogen. Based on current technology and the catalysts available, ethanol cannot be fully oxidized to carbon dioxide and water due to the strong C-C bond. Thus, feeding the fuel cell directly with ethanol is not appropriate since it does not deliver all the available electrons, resulting in low cell operating efficiency. This problem seems to have been solved by the NISSAN automotive industry using ethanol reformulation technology. This process involves an external reformer into which the ethanol is fed. The reforming process is then started, taking as product hydrogen together with other carbon compounds such as carbon monoxide. The presence of the monoxide prohibits the use of the final product of the reforming process for feeding into low-temperature fuel cells such as PEMs except in the presence of another reactor which would purify the solution from carbon monoxide which would increase the operating costs discretely.

2.1.2 PROTON EXCHANGE MEMBRANE FUEL CELLS (PEMFCs)

Fuel cells that use a proton-conducting membrane as the electrolyte are called proton exchange membrane fuel cells (PEM-FCs). PEM fuel cells consist of a proton exchange membrane sandwiched between the anode and cathode electrodes [1, 19, 21]. Between the membrane and the electrodes is an electrically conductive porous support layer, and the electrocatalyst is at the interface of the layer and the membrane. Finally, there are the flow channels from which the fuel and air are fed into the cell. The membrane needs to be constantly hydrated and not dried out in order for the cell to operate efficiently but in a quantity that does not cause flooding.

The operating temperature of fuel cells plays an important role in cell performance. PEMs are low temperature fuel cells; however a slight increase in temperature results in higher kinetics of the

reactions at the electrodes and also reduces the ohmic resistance of the electrolyte. Despite of that, the temperature increase cannot be unlimited as it will cause changes in the water pressure within the membrane causing dehydration and a decrease in ionic conductivity.

In PEM fuel cells the fuel is fed directly to the anode electrode where the oxidation takes place producing protons and electrons that transfer through an external circuit. In the cathode, the oxygen reacts with the protons and electrons to form water. Protons are transferred through the electrolyte from the anode to the cathode to complete the reduction of oxygen. When the fuel is hydrogen the reactions that occur are the followings:

ANODE: $H_2 \rightarrow 2H^+ + 2e^-$

CATHODE: $2H^+ + ½\ O_2 + 2e^- \rightarrow H_2O$

ION TRANSPORT IN ELECTROLYTE: H^+

In general, scientists over the years have studied proton exchange membrane fuel cells a lot because their optimization will greatly help in the development of technologies that will reduce the environmental footprint. During the research, they found many advantages of fuel cells to replace the conventional engines used so far, but also some disadvantages that make PEM-type fuel cells unusable on a large scale for the time being [62, 63]. Initially, the goal of creating fuel cells was to get rid of fossil fuels that destroy the environment and have a major impact on people's health, negatively affecting the respiratory system in the long term and causing cancer. Fuel cells have the potential to use more environmentally friendly fuels such as ethanol. In particular, when ethanol is obtained through extraction from biomass, it is considered a green fuel and enables fuel cells to operate with zero additional exhaust gases. They also have the ability to have short start up times making them quite easy to use since one does not have to wait in the car for hours until they finally start [64, 65]. Also, fuel cells in general have the potential to have a more stable structure without including moving parts like conventional engines. Thus, they can operate for longer periods of time without experiencing problems. At the same time, due to their compact structure, they reduce the operating noise considerably, thus contributing to the better well-being of people. Last but not least, a fuel cell has a much higher efficiency than conventional internal combustion engines since it has the ability to directly convert the chemical energy of the fuel into electricity. They often achieve efficiencies that are up to twice as high as those of currently available engines. Fuel cells are promising for the future and this is supported by their many advantages over conventional energy conversion engines. However, further optimization is necessary in order to overcome the problems that are an obstacle to their use on an industrial scale [2]. A major problem is the cost of catalysts. Catalysts such as platinum, although they have excellent performance in fuel cells, are often

characterized by high costs, making them not economically viable. Thus, it is necessary to further study new catalysts and their combination in order to keep fuel cells within cost limits. Another important problem is that in order to achieve good fuel cell performance, hydrogen must be available in sufficient quantities, and at relatively low cost. The electrolysis of water described below is very costly and is an unprofitable process. At the same time, hydrogen at ambient temperature is in gaseous form. Thus, in order to store and transport it safely, cryogenic methods are used which further increase the cost and risk. Another disadvantage especially when PEM fuel cells operate with direct ethanol injection is that a parasitic or leakage current is created due to ethanol crossover. This results in a negative effect and a significant reduction in the fuel cell open circuit voltage and a reduction in the discharge behavior of the fuel cell [2]. Finally, carbon monoxide has a negative effect on the overall performance of PEMs. In particular, CO competes with hydrogen in occupying the active sites and binding to platinum, thus reducing the reaction rate of HOR and thus reducing the efficiency. The presence of CO, even as a trace in the fuel, causes serious problems in the operation of PEMs and is perhaps one of the main drawbacks that delay their widespread use.

Proton exchange membrane fuel cells have been thoroughly investigated over the years by the scientific community leading to their evolution and the increasing possibility of their placement in some hybrid systems as combinatorial applications. Although a fairly significant optimization has been achieved, their widespread use is still not possible since there are factors such as cost and even distrust of investments that make technologies such as PEMs take a back seat. In the coming years, with environmental conditions and people's living conditions getting worse, it is expected that the green light will be given to use more environmentally friendly energy supply technologies such as PEMs.

2.1.3 ANION EXCHANGE MEMBRANE FUEL CELLS (AEMFCs)

Fuel cells that have an anion exchange membrane in alkaline media are called AEMFCs [18]. More and more scientists are turning their attention to anion exchange membrane fuel cells in the alkaline media due to their higher efficiency and higher kinetics of oxidation reactions compared to lower pH fuel cells. These types of fuel cells consist of two electrodes, which are called anode and cathode respectively, with an anion exchange membrane sandwiched between these two. At the cathode electrode, the oxygen reduction reaction takes place in which oxygen reacts with water and electrons to form hydroxyls. In contrast, the anode electrode is fed with hydrogen, which is oxidized in the presence of hydroxyls to form H_2O and produce electrons. Hydroxyl ions pass through the membrane from the cathode to the anode while the electrons follow the opposite direction moving in an external circuit. The typical AEM fuel cell when is fueled by hydrogen as described above is illustrated at **Figure 2.2**. In the third chapter a more in-depth analysis of how AEM fuel cells work

through the corresponding reactions will be carried out using ethanol as fuel. In this chapter a first description of the history of AEMs and their evolutionary path is given.

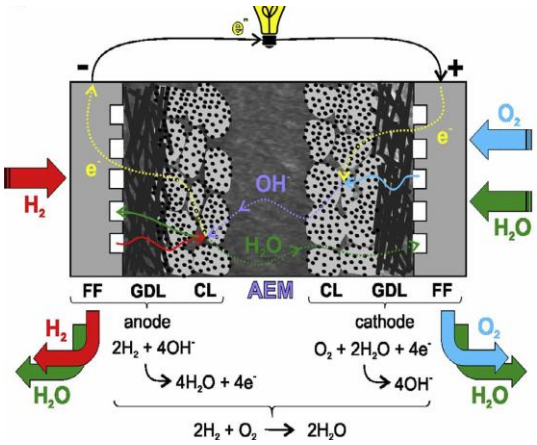

Figure 2.2. A typical H_2-AEMFC [66].

The first AEM-type fuel cells had already appeared in the 1960s and were applied to the Apollo space vehicle [67]. The vehicle's main source of electricity was a set of three fuel cells, each cell using hydrogen as fuel which was oxidized via hydroxyls and a catalyst to produce water and electrons. The water was not wasted but used for drinking by the astronaut crew. Each cell on the cathode side used oxygen and water causing the oxygen reduction in the presence of electrons. The above reactions are described below [68]:

Cathode oxygen reduction reaction: $O_2 + 2H_2O + 4e^- \rightarrow 4OH^-$

Anode hydrogen oxidation reaction: $2H_2 + 4OH^- \rightarrow 4H_2O + 4e^-$

Each fuel cell power plant is made up of 31 individual cells that are linked in series and in combination they produced between 27 and 31 volts. Every power plant has a maximum power output of 2300 watts and a typical power output of 563 to 1420 watts. The hydrogen electrode was made of nickel and the oxygen electrode of nickel and nickel oxide. The details of the electrodes, the way the cells are connected, and the power values were taken from the website of the National Air and Space Museum. AEM fuel cells have so far failed to be deployed on a large scale because their performance is reduced in the presence of CO_2. However, overall, it has been found that their performance is much better than PEMs in terms of electrochemical kinetics, weaker corrosion and the lower cost of the catalysts used, leading to the conclusion that AEMs can replace PEMs to a satisfactory extent under the right conditions. In comparison, the two types of fuel cells show similar behavior with the only difference being in the membrane where the PEMs use an acidic membrane while the AEMs use a solid anion exchange membrane. However, AEMs are amenable to the use of non-precious metal catalysts lowering the overall cost.

Despite the initial better performance of AEMs, in order to replace PEMs on an industrial scale they need to be obviously better and at a much lower cost in order to yield investment. Thus, some problems that are an obstacle to effective change and delay the development of AEMs need to be addressed. Initially, because the water is in liquid form at the cathode electrode where the oxygen reduction reaction takes place, it must be diffused and eventually removed from the cathode to prevent its accumulation [69]. Problems such as local flooding delay the reactions and the fast and efficient transport of hydroxyls [68]. It has also been shown that the presence of exhaust gases such as carbon dioxide negatively affects their performance by reducing the reaction kinetics and mass transfer effects since they are highly reactive with hydroxyls from ORR. Studies show that the overall voltage reduction is noteworthy and ranges from 100 to 400 mV [69-71]. Finally, to achieve the replacement of PEMFCs with AEMFCs it must be sufficiently cost-effective. Thus, it makes sense to get rid of the use of costly catalysts such as platinum metals and to use non noble ones. Using PGM-free (platinum-group metals) catalysts like Me-N-C (Me = Fe/Co/Cu/Ni), researchers have conducted experiments and reported their findings in several articles published in the literature [66, 72-75].

AEM fuel cells are supported by a wide range of advantages and when combined with economical, yet efficient catalysts can replace PEM in applications such as transport vehicles, passenger vehicles and municipal buses. A more detailed study is expected in the future for use both in initial stages in combination with internal combustion engines and in hybrid systems with batteries in electric vehicles.

2.2 ELECTROLYSIS

Electrolysis is a process in which applying an electric current causes the decomposition of the substances being studied. Concerning water electrolysis, by applying electricity, the positively charged hydrogen ions are transported to the cathode where the reduction reaction takes place through the capture of electrons to form hydrogen atoms [22, 76]. Due to the need to develop green hydrogen fuel formation technologies that will result in the reduction of fossil fuel use, water electrolysis is a good but so far costly solution [77-82]. Generally, hydrogen and oxygen are produced at the cathode and anode respectively, and in order to increase the rate of formation of these atoms, suitable catalysts are used to enhance the kinetics of the reactions on both electrodes. So far, the catalysts commonly used in the hydrogen evolution reaction (HER) are platinum, while for OER they are iridium or ruthenium oxides. In order to avoid using different catalysts each fulfilling only one reaction at the respective electrodes, it is legitimate to develop bifunctional catalysts that will be efficient in both reactions [83-86]. The choice of catalysts is very important since it must combine both low cost and enhanced reaction performance. In addition, the choice of electrodes must also be appropriate so that they are resistant to the solution environment to which they are exposed. Reviews have shown that metallic glass (MG) electrodes have

good resistance to both acidic and alkaline media. However, they lag behind in their overall performance setting the goal to significantly improve them through various strategies combining appropriate catalyst selection. There are two strategies for the improvement of MG electrodes. First, it is necessary to make the right composition of materials and then increase their surface area. In order to increase their surface area various techniques have been developed such as thermal plastic forming [87], templated electrodeposition [88], magnetron sputtering [89] and electrochemical modification. Several studies have shown that a very good method for surface area increase by creating porous nanostructured MGs is the de-alloying technology resulting in the creation of durable but also increased electrode yields [90-93]. Depending on the materials selected for use in the MGs, different characteristics are imparted according to the properties of the metals. Tantalum in particular has a high melting point of 3017 degrees Celsius making it more resistant to applications that are dangerous to overheating like electronic devices and furthermore, it can replace platinum in laboratory equipment since Pt has a high cost and simultaneously tantalum is combined with satisfactory properties. Ming-Xing Li et al. created Ir–Ni–Ta–(B) glasses which showed high resistance to high temperatures [94]. Later, Dongqing Liu et al. in their review proceeded to formulate the $Ir_{25}Ni_{33}Ta_{42}$ MG into ribbon applying the melt-spinning technique while for the formation of nano-porous structure; high-temperature chemical de-alloying was applied. The researchers, in their review, presented the results of their experiments and concluded that the mesoporous MG ribbon showed satisfactory electrocatalytic activity for both the hydrogen evolution reaction and the oxygen evolution reaction in an alkaline environment. Due to the high cost and the scarcity of catalysts based on Pt, Ru and Ir, the scientific community was led to the development of catalysts that would be able to replace the aforementioned catalysts without reducing the good properties they provide. During the last few years, transition metal catalysts such as phosphides, nitrides, carbides and oxides have been used experimentally showing satisfactory results in catalyzing reactions for the electrolysis of water to extract green hydrogen fuel. Of the aforementioned metals, phosphides (Fe_xP, Co_xP, Ni_xP), due to a variety of properties such as high stability, non-toxicity, fast charge transfer and electrical conductivity, are established as a very good alternative to catalysts composed of noble metals for hydrogen evolution reaction. Also, recent studies demonstrate that transition metal oxyhydroxides (MOOH, M = Fe, Co, Ni) perform well in terms of catalyzing the oxygen evolution reaction. As mentioned above, the development and the possibility of widespread use of catalysts that will efficiently catalyze both the cathode and anode reactions is one of the main concerns of scientists to achieve lower catalyst costs, higher stability and better performance.

Water electrolysis to obtain green hydrogen fuel is an easy method on which much research has been carried out in recent years. However, since the noble metal catalysts used so far are expensive and that the process of forming hydrogen atoms in large quantities is relatively slow are major

obstacles to the widespread use of this method. Over the years, studies have been carried out to develop better catalysts that will overcome these obstacles and make water electrolysis a practical solution for a smooth transition from fossil fuels to more environmentally friendly energy sources.

2.3 HYDROGEN

Hydrogen is the first element on the periodic table because it has an atomic number of one, implying that it has only one electron in its atom. Henry Cavendish was the first scientist to identify hydrogen as an element. It is the lightest element and, under standard temperature and pressure conditions, exists as a gas of diatomic molecules with the formula H_2. It is colorless, odorless, tasteless, non-toxic, and extremely flammable [95]. Hydrogen, because of its much lower density than air, is found in fairly small quantities in the free state, and is almost always found in various compounds with carbon and oxygen [95, 96]. At 101.283 kPa hydrogen has a boiling point at -253 ^{0}C and a melting point at -259 ^{0}C while density of the gas at boiling point and 1 atm is 1.331 kg/m^3.

Hydrogen can be used as a fuel in both passenger vehicles and public transport because of its many advantages. Initially, hydrogen has a higher heating value up to 141.8 MJ/kg at 298 K and a lower heating value up to 120 MJ/kg at 298 K. Comparatively, gasoline has 44 MJ/kg at 298 K, which means that hydrogen has a higher energy content [97-100]. Hydrogen is a very good alternative to fossil fuels since a) it does not produce CO, CO_2 and SO_2, b) more energy and c) only water is produced [101, 102]. In order to reduce the emissions of exhaust gases into the atmosphere, various devices such as fuel cells are being studied using hydrogen as a fuel. During its combustion reaction, hydrogen does not produce carbon dioxide or other exhaust emissions according to the following reaction:

$$2H_2\,(g) + O_2\,(g) \rightarrow 2H_2O\,(l)\ \Delta H^o = -242\ kJ\ (120kJ/g)$$

Since hydrogen exists in a minimal amount in the free state, techniques have been developed to produce it through other reactions involving compounds containing hydrogen [103]. Among these techniques are natural gas steam reforming, wind electrolysis and coal gasification [102, 104].

First, as is well known, the main component of natural gas is methane, but significant quantities of other compounds such as ethane, propane and butane, as well as carbon dioxide, nitrogen, hydrogen, helium and hydrogen sulphide are also present. Natural gas is collected and stored once it has been recovered from various sources and reserves. It is then chemically treated before being piped to fuel processing units that are located at the already existing gasoline refueling stations. There, through a combination of steam reforming and fuel oxidation, the desired hydrogen is produced [102, 105]. The processed hydrogen is then compressed and sent for use in vehicles that use hydrogen fuel. These types of systems have the advantage that they can use existing fueling stations. Depending on the gas connection and transport network and using the same pipelines, the natural gas is transported to the

refueling points where hydrogen and heat are produced. This method exploits the network without requiring changes to their materials and using the same supply points, keeping overall costs low and within reasonable limits. Otherwise, the hydrogen is produced at the fuel processing plants and from there it is transported through the same network again to the hydrogen demand centers. However, since with the second method hydrogen is circulating inside the pipelines, the existing network needs to be changed and replaced with reinforced steel materials, increasing the production costs much more. For a natural gas steam reforming plant for hydrogen production, the system described in **Figure 2.3** is used. Natural gas is first identified and then produced from the various deposits. It is then stored and chemically treated in fuel processing plants. In a decentralized system, it is transferred through a network of pipelines to fuel supply stations where the needed hydrogen is created. At the same time, it is cleansed on-site, stored, and eventually ready for use in vehicles.

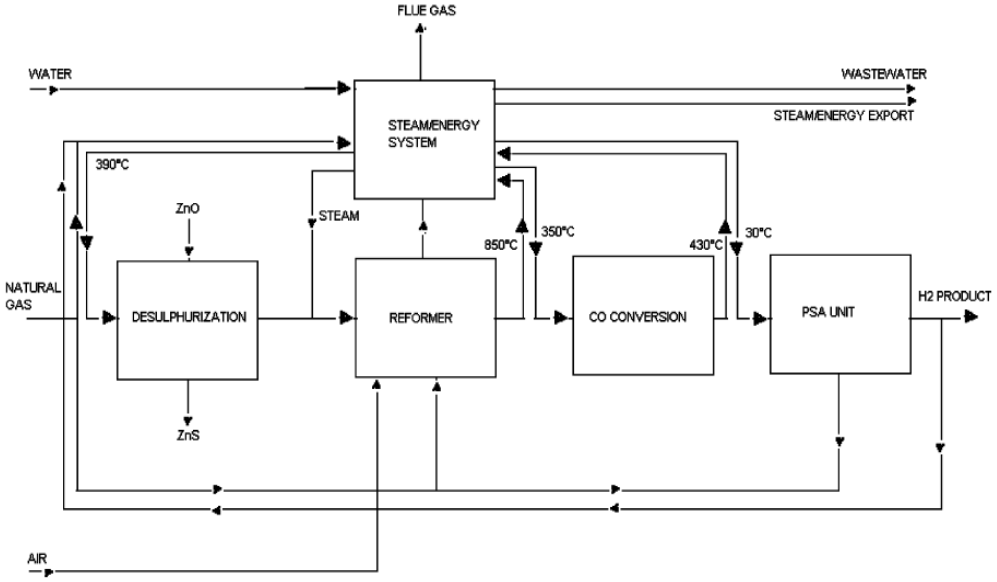

Figure 2.3. Hydrogen production from natural gas steam reforming [104].

Hydrogen is being studied in depth as a potential fuel with some cars already running exclusively on it such as the Toyota Mirai and Hyundai Nexo. The reason is because hydrogen is quite flammable without producing exhaust gases as mentioned above so it is environmentally friendly when burned. However, in the case of hydrogen created by natural gas steam reforming, it is required to quantify the total amount of exhaust gas produced by this procedure in order to conduct a full assessment of hydrogen production and consumption. Initially, United Technology Corporation's (UTC) PureCell commercial steam reformer was used as a reference system so that any new system being developed could be compared. As a result, emerging technologies that employ optimal methodologies and higher performance catalysts should exhibit much improved characteristics [102, 106, 107]. The emission factors for the steam reformer utilized in the 200kWe stationary hydrogen fuel cell system are presented

in the **Table 1** below [102], with the natural gas steam reforming process described by the following reactions:

Steam reforming reaction: $CH_4 + H_2O \rightarrow 3H_2 + CO$

Water gas shift reaction: $CO + H_2O \rightarrow H_2 + CO_2$

According to the foregoing reactions, the steam reforming reaction creates three moles of molecular hydrogen for every mole of methane reacted, whereas the water gas shift reaction produces one mole of hydrogen for every mole of carbon monoxide produced by the first reaction. The overall steam reforming reaction, resulting from the combination of the previous two is as follows:

$CH_4 + 2H_2O \rightarrow 4H_2 + CO_2$

Finally, and according to W.G. Colella et al., an emission factor for the fuel reformer of 2.65 kg CO_2 kg^{-1} of natural gas is obtained which is in agreement with the UTC's equivalent of 2.7kg CO_2 kg^{-1} of natural gas.

Table 1: Natural gas steam reformer [102].

Emissions	Emission factor (kg of pollutant kg^{-1} of natural gas fuel)
NO_x	0.0000459
CO	0.00000328
Nonmethane hydrocarbons (NMHC)	0.000000655
SO_x	Negligible
Particulates	Negligible
CH_4	0.0000475

Secondly, a widely known but not so economical method is that of electrolysis of water described earlier. The reaction is carried out endothermically and is described below:

$2H_2O\ (l) \rightarrow 2H_2\ (g) + O_2\ (g)\ \Delta H^{o} = +572kJ$

To be certified as environmentally friendly hydrogen utilized as a fuel must not only not emit exhaust gases during combustion, but also have emissions of chemicals such as CO_2 minimized or even eliminated during manufacture. Water electrolysis electricity is wisely supplied from renewable energy sources such as wind turbines. The generated electricity is then transported to electrolyzers at distributed hydrogen refueling stations, which are located in the same points as today's gasoline stations. The number of wind turbines required to generate adequate electricity to produce the specified quantity of hydrogen can then be estimated. Meaning the number of wind

turbines by n, the total mass of hydrogen consumed yearly by all vehicles by m_{H2C}, with H_h the higher heating value of hydrogen (140 MJ kg^{-1}), with E_T the yearly energy result of a turbine (kWh/year), η_{AC} the effectiveness of changing over the turbine's variable AC power to constant frequency AC (~97%), η_{LH} the efficiency of changing over the turbine's low voltage electricity up to high voltage electricity for conveying across significant distances (~95%), η_T the high voltage transmission grid efficiency that includes wire resistance (~97%), η_D the low voltage transmission grid efficiency including wire resistance (~93%) and η_E the electrolyzer effectiveness (~73%), the number of wind turbines can be estimated according to the following equation [102]:

$n = \frac{mH2C\ Hh}{ETnACnLHnTnDnE}$, while E_T is calculated through: $E_T = 8760Pr\ (0.087V - \frac{P}{D^2})$, 8760 is the hours in a year, Pr is the rated power of the turbine (kW), V the mean annual Rayleigh distributed wind speed (m s^{-1}) at turbine hub height, and D the diameter (m) of the turbine [108, 109].

The third hydrogen production process to be described is coal gasification. This process, as in natural gas steam reforming, follows a series of cascading steps. First, the coal is identified and then taken from the various mines. Subsequently, the coal is processed and transported to special coal gasification plants. These are the plants that are currently used as conventional coal combustion plants. It is therefore necessary to use the centralized system, where hydrogen-rich gas will be produced and then transported from there through a network of pipelines to the hydrogen refueling points.

The coal gasification process is not a simple process, but a complex one that combines both chemical and thermal conversion of the solid mineral into a gaseous mixture that includes significant amounts of hydrogen and other compounds such as carbon monoxide and hydrocarbons such as methane. In the first step, the coal is heated to a high temperature and pressure and then hydrogen and CO are produced in the presence of steam. Hydrogen and carbon monoxide are the result of incomplete fuel combustion where a small amount of oxygen is used to partially oxidize the fuel and are referred to as syngas. CO is then converted to carbon dioxide through the water gas shift reaction in the presence of steam and finally producing additional hydrogen. Coal itself contains much less hydrogen inside than other compounds such as hydrocarbons. Typically, the hydrogen to carbon ratio for coal is close to 0.8, while fuels such as natural gas have a ratio of close to 4, so the method used is to combine coal with other hydrogen-containing substances such as water. The consequence of this is that dangerous exhaust emissions such as CO_2 depend on the steam to carbon ratio used by each gasification plant. Some indicative values are shown in **Table 2** [102]:

Table 2: Coal gasification emissions [102].

Emissions	Emission factor (kg of pollutant kg^{-1} of dry coal fuel)
SOx as SO2	0.000762
NOx as NO2	0.000108
CO	0.00734
VOC	0
Particulates	0
CO2	2.37

At **Figure 2.4** is illustrated a schematic diagram of a typical Integrated Gasifier for Hydrogen Production plant. Initially, coal is added in combination with oxygen and steam to the gasifier and then the syngas is produced. In a second step, it is transferred through a network to heat exchangers and finally led to a water gas shift reactor. However, the mixture produced consists of carbon dioxide and hydrogen sulphide and thus has to be purified. After purification and CO_2 capture, pure hydrogen is obtained. Also, from hydrogen sulphide, sulphur can be recovered as a commercial product through the Claus process [110].

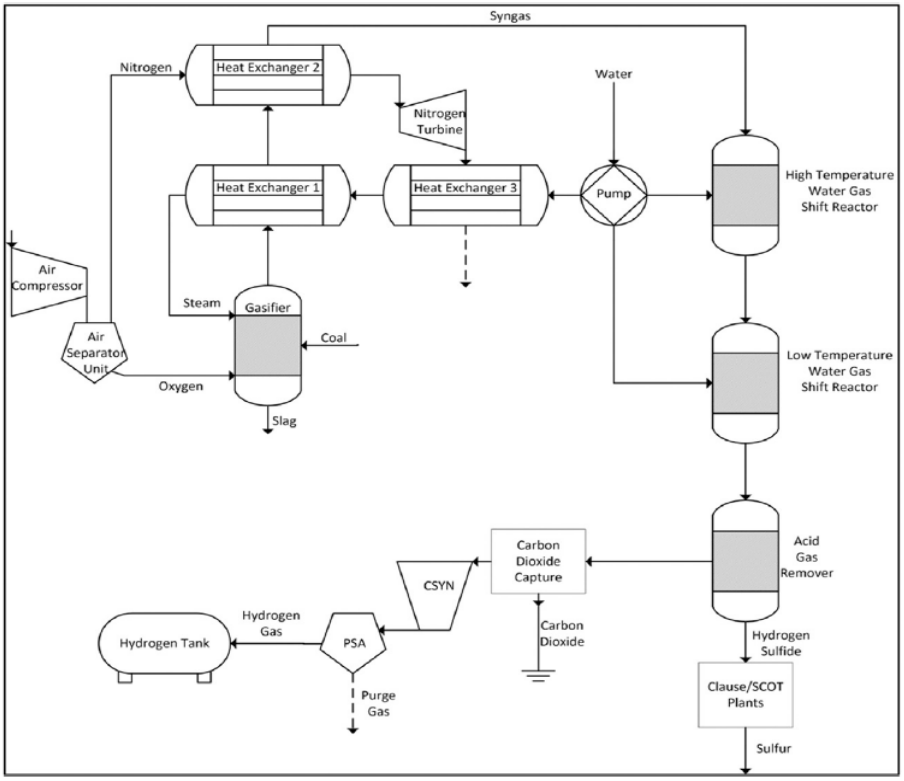

Figure 2.4. Schematic diagram of an Integrated Gasifier for Hydrogen Production plant [111].

With the continuous increase in fuel prices of conventional engines and the dangerous exhaust emissions that contribute to the deterioration of the environment, more and more companies have

turned to the study of hydrogen as a friendlier option and the creation of efficient technologies such as fuel cells. The transport sector is the largest sector of energy use with passenger vehicles and motorcycles taking the largest share as shown in **Figure 2.5**.

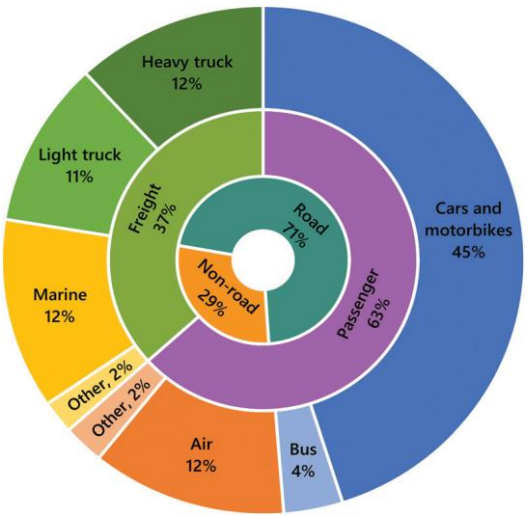

Figure 2.5. Breakdown of energy usage in the transport sector globally in 2015 [112].

At the same time as passenger cars are expected to grow from 1 to 2.5 billion globally by 2050, national emissions need to be reduced to a substantial level. Hydrogen as mentioned above is a promising option that can replace fossil fuels that come with harmful properties for humans. However, despite avoiding the time-consuming process of charging electric vehicles, they remain at a disadvantage due to the lower cost of EVs and the available infrastructure. In particular, electric vehicles powered by batteries require close to 45 minutes to fully recharging, while those powered by hydrogen can be refueled within 10 minutes. **Figure 2.6** shows a typical example of a vehicle using a fuel cell with a hydrogen tank. Electric fuel cell vehicles mainly use PEM fuel cells that offer high performance and cold start properties. For European cars, it is standard practice to use a 60 kW fuel cell.

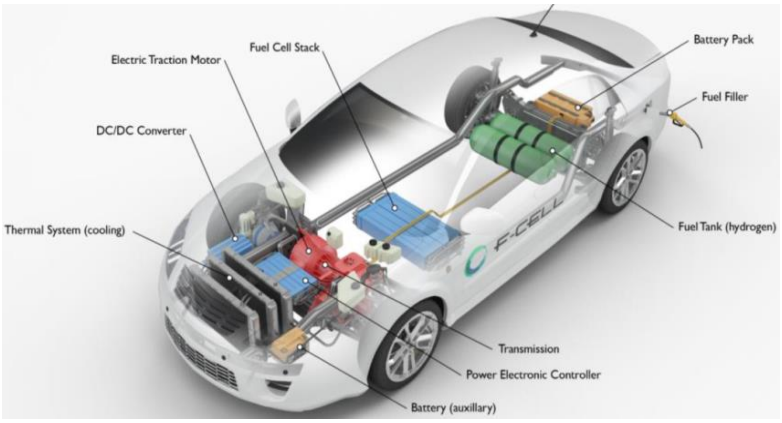

Figure 2.6. Block diagram of a hydrogen car [113].

One sector in which hydrogen fuel cells seem to be developing tremendous appeal is that of heavy vehicles such as trucks in the commercial sector and buses in the public transport sector. In

these vehicles, conventional engines take up a lot of space, greatly increasing the weight and size of the truck or bus, while at the same time increasing costs to levels beyond the customers' reach, often resulting in drivers not buying newer, low-emission vehicles and staying with the outdated ones. Thus, if hydrogen fuel cell vehicles gain the durability of the corresponding internal combustion engines and the cost of fuel cells, which is currently estimated to be up to 5 times higher than that of ICE, is reduced, then a smooth and promising transition to more environmentally friendly technologies will be possible.

An application of hydrogen fuel cells has begun to take its first steps in the rail sector. As of 2018, Alstom introduced the first passenger train using hydrogen fuel cells for a 100-kilometre journey in Germany. Since then, two Alstom trains in Germany have travelled over 180 thousand kilometers using exclusively fuel cells. Although the cost of manufacturing hydrogen trains is 1.5 times higher than that of their diesel counterparts, the overall long-term investment is more favourable due to lower fuel costs.

Finally, two other sectors in which hydrogen fuel cells are applied are those of navigation and aviation. In the former, an attempt has already been made to integrate fuel cells in various ferries, however due to the time and duration of various voyages; they result in the requirement of significant amounts of hydrogen and therefore the possibility of storing it by cryogenic methods. This increases both the cost and the risk of transport and storage. On the other hand, in aviation, it is less possible to replace current technologies and implement hydrogen fuel cells. Although they could be used to a large extent in commercial flights, their favourable contribution to the environment is questioned. As mentioned in a previous section, water is produced during the operation of PEM cells with hydrogen. The disadvantage, however, is that water vapor at high altitudes, although remaining for a short time causes radiation and therefore contributes to the net warming. But it seems to be gaining ground even in some early stages in Unmanned Aerial Vehicles [33]. This is because firstly they are less noisy, secondly they have fewer oscillations, thirdly they are lighter than others that use batteries and fourthly they are more efficient than fossil fuel UAVs.

The development of hydrogen-fuelled technologies and their use could replace fossil fuels and create a hydrogen-dependent society. John Bockris in a presentation at the General Motors Technical Center in 1970 first introduced the term "hydrogen economy", which refers to the replacement of fossil fuels in the industrial, transport and residential sectors [114]. The use of hydrogen as a fuel would have a positive impact on the environment and people's lives in the long term while mitigating the detrimental properties of fossil fuels. In particular, it would reduce the rate of depletion of natural resources and the rate of deposition of environmentally hazardous compounds such as carbon dioxide, which contributes to the increase in global average temperature. Moreover, if hydrogen replaces other

fuels such as coal and oil, phenomena such as photochemical smog, soot production and acid rain will be eliminated. An obstacle to the development of the widespread use of hydrogen is both the cost of its production and its low density, which makes storage techniques necessary and increases the risk [115-121]. However, more and more countries are taking the step forward and investing in hydrogen-fuelled energy systems. Hydrogen is currently a critical need for the EU in the work to accomplish the goals of the European Green Arrangement and "Europe's change to clean energy". The 2019 European agreement discussed the overarching goal of climate neutrality by 2050. At the same time, the European Union's objective by 2020 was to diminish air pollutant emissions as much as possible compared to 1990, which was accomplished three years earlier by 22% in 2017. In this setting, the European Union, a pioneer in climate emergency decision-making, chose to assist in decreasing emanations by up to 55% by 2030 compared to 1990 under the 2016 Paris Agreement. Hydrogen is therefore expected to contribute effectively and play an important role in achieving these agreements in energy exploitation applications. In fact, in November 2018, the European Commission announced to the European Parliament that the share of hydrogen in Europe's energy pie will increase from 2% to 13-14% by 2050.

However, as promising as the use of hydrogen to reduce greenhouse gas emissions is, nothing could be possible without harmonizing both the costs of investment and the revenues from these technologies. Thus, both the European Commission and, at the domestic level, the Ministry of Environment and Energy, have assessed both the potential investments and sales revenues for each year. It was therefore found that investments for 'green' hydrogen could amount to between EUR 180 and 470 billion by 2050, and for 'grey' hydrogen between EUR 3 and 18 billion. These investments are accompanied on the one hand by the employment of close to one million people by all means and on the other hand by sales of close to EUR 630 billion per year from purified hydrogen, covering 24% of international energy demand.

The hydrogen economy is based on two main systems already mentioned above. One is called a decentralized and the other a centralized system, and their definition depends on the location where the pure hydrogen is produced. For hydrogen production systems such as those of coal gasification they use a centralized production scenario. In particular, as mentioned in the previous paragraph, these systems involve some chain steps where first the coal is collected, stored and then transported to the coal gasification plants [102]. The total production of hydrogen is carried out on site, thus making the centralized coal gasification system. The hydrogen is then transported through a network of dedicated pipelines to the various hydrogen demand distribution points. This scenario implies high investment costs for hydrogen pipeline networks, which include thicker pipes made of durable steel, increasing the cost of construction and maintenance procedures, while at the same

time, transporting hydrogen from a residential location guarantees many risks. The tactical use of centralized scenarios does not seem to be the focus of research and investment since, in conjunction with international agreements to reduce harmful substances, decarbonize fuels and get rid of fuels such as coal; it seems to be losing ground. On the other hand, a more appropriate technique seems to be the use of the decentralized scenario. This method includes both hydrogen production through natural gas steam reforming and electrolysis through wind power. Concerning the first method, the natural gas is driven through the pipeline network from the plants where it has been purified to the existing hydrogen refueling sites. The advantage of the method is that hydrogen is produced on-site at the fuel demand points ready for use in cars at any time. At the same time, the method takes advantage of the existing well-designed and constructed natural gas distribution network, avoiding the cost of pipeline reinforcement. Thus, an amount of required investment is avoided altogether while at the same time, no newer safety rules are introduced. However, it is understandable that due to various informal market rules the fuel used individually by each refueling station will be significantly more than it would be in a factory plant. This will increase each customer's costs because of the need to push the natural gas to various remote points rather than to one location in total. However, depending on demand, transporting costs and taxation can be set fairly for the customer. Finally, the electrolysis method belongs to the same category where when the power is taken from wind farms, the current is fed through an existing grid to the supply stations where the electrolyzers are located and the process of electrolysis of water to produce hydrogen takes place. **Figure 2.7** shows a chart of the feedstock contribution to hydrogen production, as described above.

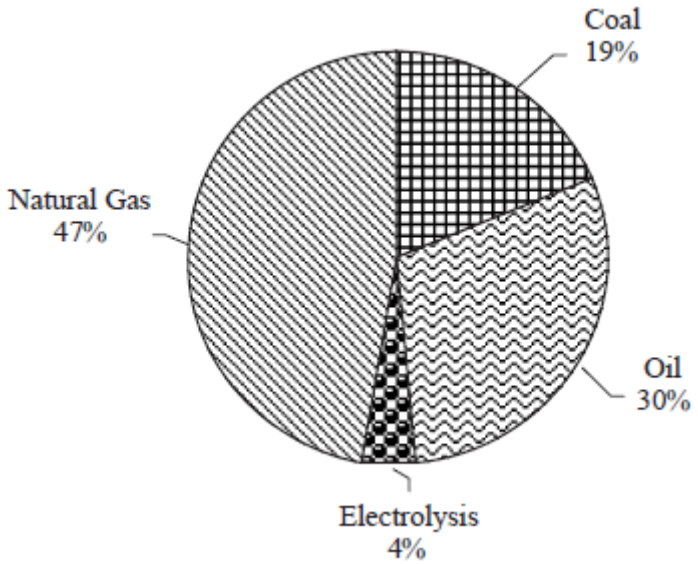

Figure 2.7. Feedstock contribution to hydrogen production [122].

2.4 LITHIUM-AIR BATTERIES

Lithium-air batteries are among the most popular rechargeable batteries in today's technology [27, 123-125]. This is because they offer high durability, long runtime, high performance and fast charging [126]. However, the main advantage compared to other batteries is that they have one of the highest energy densities. For instance, Li-O_2 batteries have a theoretically energy density of 11700 Wh kg^{-1} exceeding the energy density of other common batteries [127]. This is due to the fact that lithium has an energy density of 3860 mAh g^{-1} which is very high and at the same time oxygen is supplied by the air perpetually [128]. Having a great energy density also means that they can store a satisfactory quantity of energy in a small amount of weight reducing the space and the cost required. Along with the many advantages of this type of battery, there are also some disadvantages that, if solved, will greatly improve their performance. For example, the oxygen reduction reaction that occurs at the cathode electrode is significantly slow resulting in a reduced rate of Li-O_2 synthesis. Thus, it is important to develop cathode electrode catalysts that will enhance the reactions by eventually overcoming the barrier of reaction kinetics. Metals such as Pt and Ru have high costs making their widespread use difficult although they help to achieve higher yields in reactions. As a result, other materials, such as N-doped carbon with embedded cobalt, had to be developed [128]. Recent studies have shown that in order to increase the electrochemical activity of ORR, carbon materials derived from biomass are an economical, easy and smart solution for the improvement of Li-O_2 batteries [124]. Biomass has also the advantage of containing significant amounts of heteroatoms (atoms that are not carbon or hydrogen) such as N (nitrogen), S (sulfur) and P (phosphorus). Recent studies have found that carbon materials doped with heteroatoms derived from different biomass varieties offer higher capacity for applications such as lithium batteries [129]. For instance, Zeng et al. used biomass algae to fabricate catalysts in Li-O_2 batteries from N-doped carbon with a graphene-like nanosheet structure [124, 130]. S Jing et al. in their study list a variety of possible catalysts derived from different types of biomass such as wood and shrimp shells that show excellent performance on the reduction reaction in the cathode [124].

2.5 LITHIUM-ION BATTERIES

Today's most commercialized electrochemical storage devices for electronic systems are Lithium-ion batteries [10, 27, 28]. This is because lithium-ion batteries are non-toxic, provide very good cycle efficiency and have a high energy density [131]. Nevertheless, Li-ion batteries tend to overheat and at high voltages their capacitance tends to weaken [131, 132]. Also, the electrolyte at its core is flammable making it dangerous at high-temperature use [132]. The comparison of energy density and power density for different energy storage devices is illustrated at **Figure 2.8**.

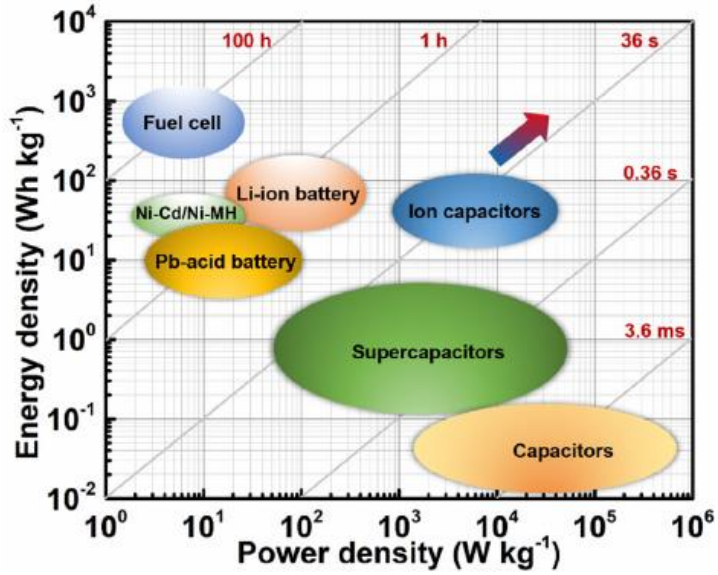

Figure 2.8. The comparison of energy density and power density for different energy storage devices [133].

Lithium-ion batteries have a wide variety of technological applications. Most of today's mobile phones, tablets, PCs, Bluetooth's and even small electrical toys use Li-ion batteries [132]. Their most important applications may be in electric cars, plug-in hybrid electric vehicles (PHEVs), photovoltaic systems and vehicles that combine fuel cells with lithium-ion batteries [134]. Because of the greenhouse effect and the effects of climate change in general, it was necessary for scientists to develop new energy storage and conversion technologies that are more environmentally friendly. Lithium-ion batteries are a smart solution with the advantages mentioned above but at the same time promise an even better performance with the ever-developing more efficient materials. Xiaopeng Chen et al. at their study compare lithium-ion batteries with lead-acid batteries, nickel-cadmium batteries (Ni-Cd) batteries and nickel-metal hydride (Ni-MH) batteries. In particular, the comparison is made with respect to various factors such as energy density, power density, nominal voltage, overload tolerance, self-discharge, reference temperature and life cycle [134]. According to them, lithium-ion batteries have an energy density ranging from 110W/Kg to 160 W/Kg with the second best being Ni-MH from 60 W/Kg to 120 W/Kg. In terms of power density, the ranking of the two batteries is the aforementioned with lithium-ion batteries having close to 1800W/Kg and Ni-MH batteries ranging from 250W/Kg to 1000 W/Kg. Lead-acid batteries come third with 180 W/Kg while Ni-Cd batteries are in last place with 150W/Kg. Also, lithium-ion batteries can operate for a range of temperatures including average ambient temperatures of one year and up to 60 degrees Celsius. But what makes them particularly special is their long cycle life with very little self-discharge. In particular, lithium-ion batteries have a cycle life that starts at 500 to 1000 cycles, while Ni-Cd batteries come second with a cycle life of 1500.

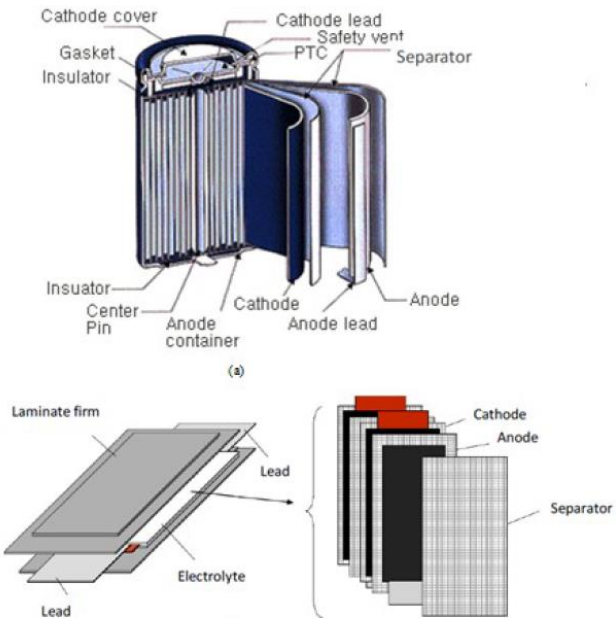

Figure 2.9. Structure of Li-ion batteries [134].

Li-ion battery in general consists of two electrodes that are called anode and cathode respectively [134, 135]. Anode is the negative electrode while cathode is the positive [136]. The electrolyte is sandwiched between the electrodes and it contains the separator as illustrated at **Figure 2.9** [134, 135]. At discharge, the operating principle of lithium-ion batteries is based on the oxidation of Li_xC at the anode producing lithium ions (Li^+) and electrons that move toward the cathode [137]. The electrons move through an external circuit. At the cathode, the reduction of lithium occurs resulting in the formation of $LiMO_2$. The reactions described are shown below [138]:

Discharge

Anode (Negative electrode): $Li_xC \rightarrow C + xLi^+ + e^-$

Cathode (positive electrode): $Li_{1-x}MO_2 + xLi^+ + xe^- \rightarrow LiMO_2$ Where M is a transition metal.

When we have the charging, oxidation take place at the cathode and reduction at the anode according to the follow reactions:

Charge

Anode (Negative electrode): $C + xLi^+ + xe^- \rightarrow Li_xC$

Cathode (Positive electrode): $LiMO_2 \rightarrow Li_{1-x}MO_2 + xLi^+ + xe^-$ Where M is a transition metal.

The process described above is illustrated by diagrams in **Figure 2.10 A)** and **Figure 2.10 B)**.

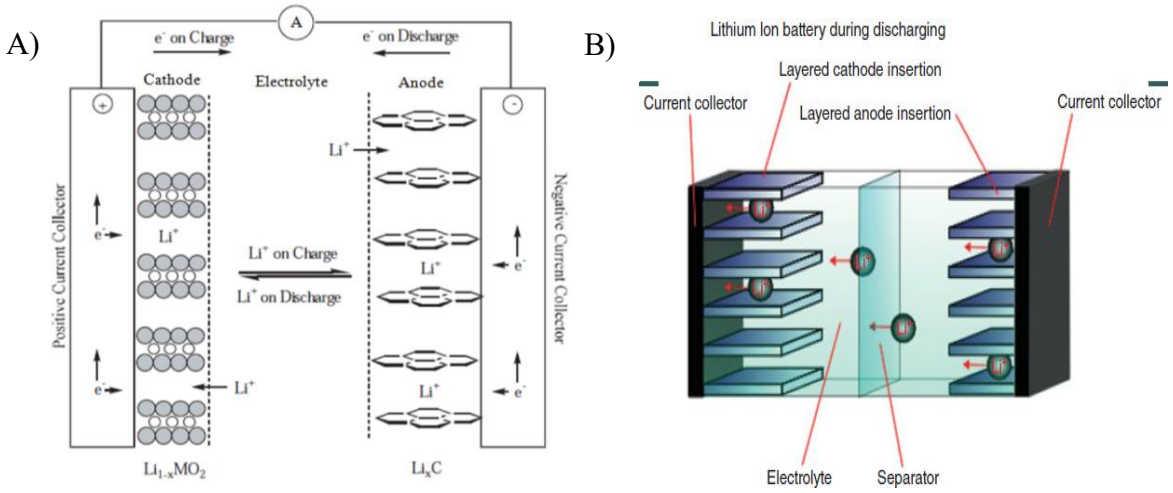

Figure 2.10. A) Lithium-ion cells and B) Lithium-ion battery during discharging [134, 139].

Overall, lithium-ion batteries consist of three individual cells divided into primary, secondary and tertiary. The two electrodes, the separator and the electrolyte mentioned above is located in the secondary cell and it is only in this cell that the charging and discharging to the cathode and anode electrodes take place through the previous reactions. A typical lithium-ion battery consists of several secondary cells next to each other connected electrically in order to boost either voltage or capacity.

A particular advantage of lithium-ion batteries is their flexibility in various shapes in order to facilitate their use in various applications that require limited space depending on the available budget and ease of construction. Currently, the two main categories are cylindrical and prismatic geometry. The prismatic geometry can be further divided into two more categories which are called prismatic hard-case cell and prismatic pouch cell. A typical picture of the shapes of lithium-ion batteries and the way the electrodes are formed in their structure is shown in **Figure 2.11**.

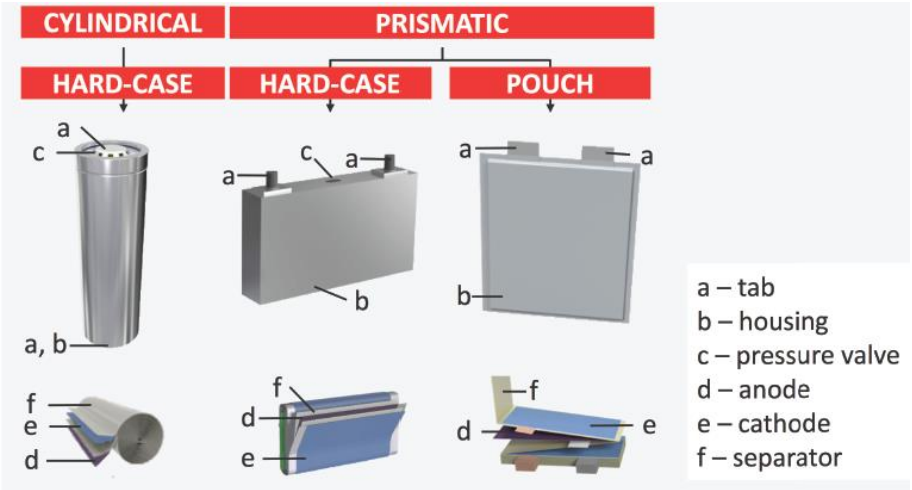

Figure 2.11. Different types of shapes of lithium-ion batteries [136].

2.6 METAL-AIR BATTERIES

With the passage of time and the ever-increasing pollution of the environment, it became necessary to develop new technologies for energy storage and supply. Zn-air batteries are a promising technology for the future for a variety of applications due to their high energy density of up to 1086Wh kg^{-1} [9, 27, 140]. However, there is a need to develop enhanced catalysts that will increase the efficiency and kinetics of the oxygen evolution and reduction reactions (OER and ORR) that occur during charging and discharging, respectively. Metals such as Pt and Ru have been studied in detail in the past as catalysts for such reactions and have been found to exhibit excellent performance by significantly enhancing the kinetics of the reactions. However, their scarcity and high cost make them difficult to use for such applications, leading the scientific community to research and select other materials. Dandan Lyu et al. in their review on Zn-air rechargeable batteries used catalysts for OER and ORR reactions composed of transition metal sulfides and graphitized carbon, doped with heterogeneous atoms materials [140]. In particular, the catalysts were prepared via Co_9S_8 encapsulation in N, S co-doped carbon matrix (Co_9S_8@N, S-C) [140]. In general, in order to avoid the use of noble metal catalysts, an effort has been made to develop alternative catalysts that will work efficiently for both oxygen reduction and evolution reactions (ORR and OER) and thus have a dual function. Bimetallic transition metal oxides like Fe, Co, Mn and Ni exhibit good stability, low cost and bifunctionality and can replace noble metal catalysts. However, with the existing technology compared to the noble metals they lag in the aforementioned parameters and need improvement for their development and efficient use in zinc-air batteries. What is common is the doping of metallic heteroatoms such as copper inside bimetallic oxide nanoparticles in order to enhance their overall performance. However, the doping mode significantly affects the catalysts and is the main study of researchers in order to achieve the best possible performance. One strategy for the incorporation of Cu heteroatoms into bimetallic oxides is to dope cobalt manganese oxides with metallic Cu to form $Cu_{0.1}Co_{0.3}Mn_{0.6}O_2$ nanosheets and then to go on to further incorporate N and P elements into the nanosheets. Through this process it is possible to increase the efficiency and performance of the oxygen reduction and evolution reactions.

Overall, due to the increasing pollution of the environment and the irrational use of fossil fuels, it is necessary to develop new methods of energy storage and supply. Batteries are a smart solution that over time are expected to improve in terms of cost, stability, robustness and performance so they can be used in a wider range of applications in everyday life.

2.7 ELECTROCHEMICAL CAPACITORS

Electrochemical capacitors or supercapacitors (ECs) are ideal devices for energy storage [29, 141-143]. Unlike batteries that store chemical energy, in supercapacitors, electricity is stored through two storage principles, static double-layer capacitance, and electrochemical pseudocapacitance; and the distribution of the two types of capacitance depends on the material and structure of the electrodes. The ability to store energy in the case of electrochemical double-layer super-capacitors is based on the surface reactions of electrode materials, without ion diffusion within the bulk of materials as in batteries, enables rapid delivery of the required energy and very fast charging, making them ideal for use in hybrid and electric vehicles (EVs). In **Figure 2.12** and **Figure 2.13 A)** is illustrated a typical electrochemical double layer supercapacitor and its combination with power generation systems like fuel cells. However electrochemical capacitors give lower energy density compared to batteries due to the rapid charging and discharging, but with the use of the latest technology of nanostructured lithium electrodes, the energy density of supercapacitors has significantly approached that of batteries at the cost of a lower cycle life and power [144]. Electrochemical capacitors also have the advantage of operating over a range that includes room temperatures and usually ranges from -20^0C to 55^0C. Furthermore, their capacitance ranges from 0.043 to 2700F and life cycles up to 100,000 charge-discharge cycles [144]. Unlike batteries, electrochemical double-layer supercapacitors are a promising technology for widespread use since the charging and discharging time is very short, ranging between 0.3 and 30 seconds. On the contrary, batteries have charging and discharging times of up to 5 and 3 hours respectively, which makes them very difficult to use for applications that require fast charge supply. Also, supercapacitors have a cycle efficiency of over 0.85 to 0.98.

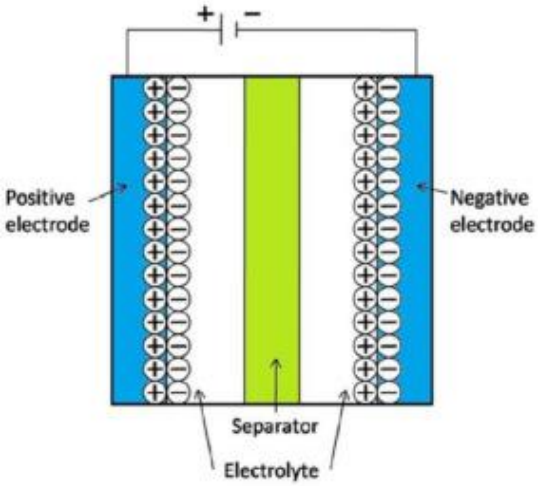

Figure 2.12. Electrochemical double layer supercapacitors [145].

Electrochemical capacitors are used in a wide range of electrical and mechanical devices. They are used in military applications in fire control systems and as backup power for electronics, power electronics, in hybrid cars, and adjustable speed drives (ASDs) [146, 147]. In particular, there is the

possibility of combining fuel cell technology with supercapacitors in a quite ambitious and efficient project for their application in cars, airplanes and public transport as shown at **Figure 2.13 B)**.

A) B)

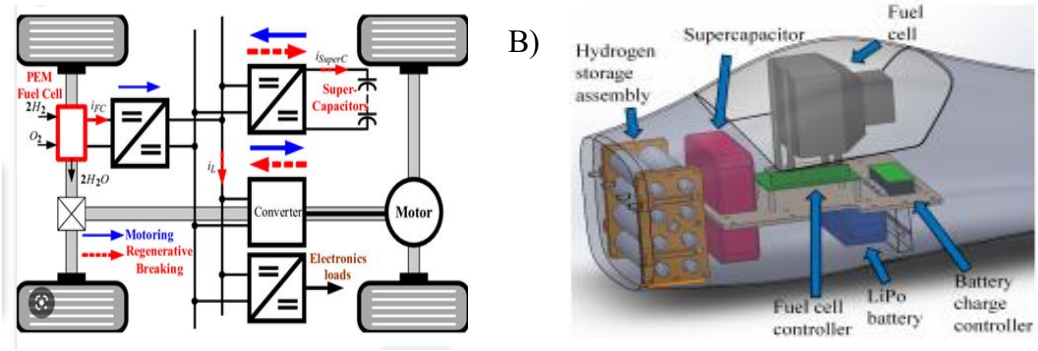

Figure 2.13. A) Fuel cell and supercapacitors hybrid system and B) Combined system of fuel cell with supercapacitor and battery in an airplane [148, 149].

2.7.1 ELECTROCHEMICAL DOUBLE-LAYER SUPERCAPACITORS

Electrochemical double-layer supercapacitors consist of two electrodes with an electrolyte sandwiched between them that can be either solid or liquid solution. They are based on electrostatic effects that occur between two carbon electrodes with high specific surface areas per volume [143]. When these capacitors occur with solid electrolyte, ions are conducted and the positive electrode is separated from the negative electrode. While a liquid electrolyte supercapacitor has an inert porous separator sheet that the ions pass through. Positive charges that are found at the positive electrode attract negative ones near the electrode from the electrolyte side creating the electric double-layer as shown at **Figure 2.12**.

2.7.2 ELECTROCHEMICAL PSEUDOCAPACITORS

Electrochemical pseudocapacitors use metal oxide or conductive polymer electrodes with a high amount of electrochemical pseudocapacitance. The amount of electric charge stored in a pseudocapacitance is linearly proportional to the applied voltage. Electrochemical pseudocapacitors (EPs) differ from electrochemical double-layer supercapacitors in the way they are charged. In particular, in EPs, the charge is transferred through a thermodynamically and kinematically favored reduction-oxidation reaction, adsorption or intercalation. The redox reactions of electroactive species occur through a faradaic process on the electrode and electrolyte surface [143]. The way in which charge is stored according to the literature is divided into three categories: a) underpotential deposition, b) redox pseudocapacitance, c) intercalation pseudocapacitance [147]. Underpotential deposition happens due to adsorption and reduction on the electrode surfaces. For instance, lead elements are deposited on a gold electrode because the Pb-Au compound is more favourable than Pb-Pb. Under redox pseudocapacitance there is a faradaic charge mechanism in which there is a charge transfer between the ions of the liquid electrolyte and those of solid electrode. A typical example of redox pseudocapacitance is shown at the **Figure 2.14 B)**. This type of

pseudocapacitance is also the most popular [150]. The third type of pseudocapacitance called intercalation pseudocapacitance consists of tunnels or layers of redox active materials that ions transfer through their bulk as shown at **Figure 2.14 A)**. This process is so fast that the whole operation reminds that of typical supercapacitors with the electrode reactions rather than that of batteries. Pseudocapacitor materials are metal oxides like RuO_2, NiO, MnO_2, Fe_3O_4, TiO_2 and conducting polymers like polyaniline and polypyrrole [144, 147, 150].

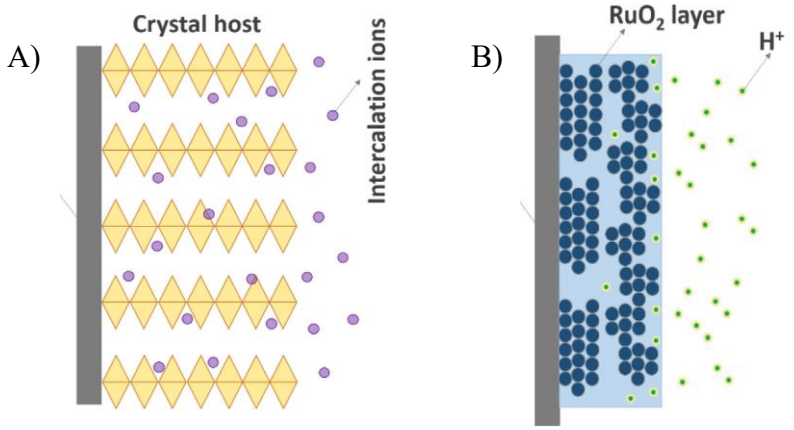

Figure 2.14. A) Intercalation pseudocapacitance and B) Redox pseudocapacitance [150].

2.8 ELECTROCHEMICAL SENSORS

Electrochemical sensors are devices that use a chemical reaction to measure the concentration of a target analyte and give information about the composition of a system in real time [30, 151-154]. They provide quantitative information about a particular chemical species of interest through oxidation and reduction reactions. They have a wide range of applications due to their ease of use. Electrochemical sensors can be used at environmental applications to measure gas pollutants, air quality and water quality. They are also used at industrial applications, for detection of exhaust and other industrial gases like CO and VOCs, and at automotive industry with lambda sensors and H_2-sensors. In addition, they find application at food industry and healthcare sector for microbial pathogens, toxins and viruses' detection, drugs detection, cancer biomarkers detection respectively. Electrochemical sensors can be constructed differently depending on the application, and therefore, provide solutions to new emerging applications. They are cheap to manufacture and easy to use with robust design, good sensitivity and selectivity, and amenable to miniaturization. Electrochemical sensors are divided into three main types. Firstly, we have potentiometric sensors that measure changes in voltage/potential under constant current [155-165]. Secondly, there are the Amperometric/Voltammetric ones [166, 167]. These types of sensors are used to measure changes in current at constant or varied potential, and finally, there are the conductometric ones that measure conductivity.

Chemical sensors made of yttria-stabilized zirconia (YSZ) solid electrolyte were studied by G. Fadeyev et al. The researchers used different types of sensing electrodes like silver and electrodes with complex oxides in a perovskite structure. In that way they managed to measure CO and H_2 content in air [168]. In another study, researchers focus on studies from the last three years and analyze the four main different methods that have been explored. They also carry out a thorough study on the mechanism of glucose oxidation over Co, Ni and Cu-Oxides/graphene [151]. Also, other scientists deal with the operating principle and the formatting of various types of solid oxide gas sensors citing at the same time the results of previous studies [154].

2.8.1 LAMBDA SENSORS

From the beginning of the development of internal combustion engines it was necessary to develop oxygen sensors (lambda sensors) to monitor and control combustion efficiency [30, 169, 170]. ROBERT BOSCH first proposed lambda sensors for industrial use back in 1970 that measure the proportion of oxygen in the exhaust gases using a solid yttria-stabilized zirconia (YSZ) electrolyte. This electrolyte is attached to a platinum electrode so that when exposed to oxygen, it produces a potential difference which corresponds to an AFR value given by the formula: AFR=ma/mf (ma is molecular weight of air and mf is molecular weight of fuel). Based on this value, it is possible to control the amount of either air or fuel to make the combustion of hydrocarbons more efficient. The AFR value measured by the lambda sensor is then compared with the stoichiometric AFR=14.7, finally giving the factor λ via the formula $\lambda = AFR_{measured} / AFR_{ideal}$. For $\lambda = 1$ it means that the combustion is perfect in terms of stoichiometry, while for $\lambda<1$ and $\lambda>1$ it means that the combustion is fuel rich and lean respectively. **Figure 2.15 A)** illustrates the lambda sensor currently used in the automotive industry.

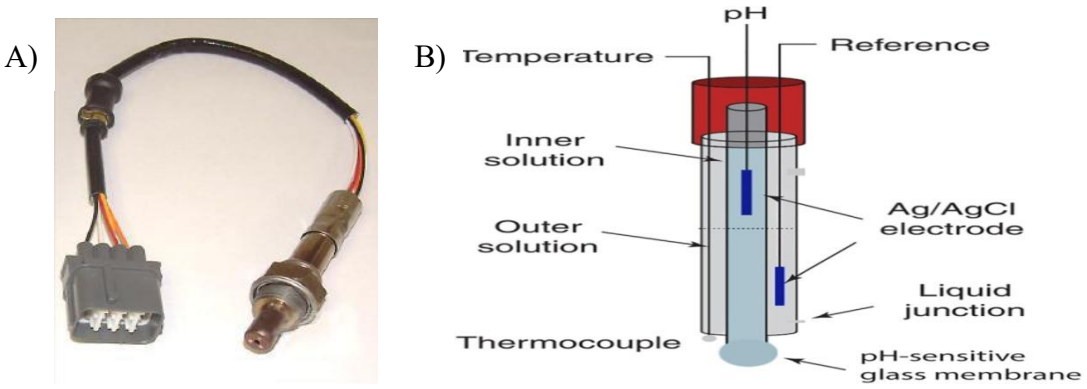

Figure 2.15. A) Lambda sensor and B) pH meter [171, 172].

Lambda sensor is a Nernst-type potentiometric sensor and as mentioned above λ refers to the air-fuel equivalence ratio (AFR). The notation of an electrochemical sensor can be P_{O2} (ref), Pt │ Y_2O_3-ZrO_2 │ Pt, P_{O2} (test), while oxygen is controlled through the following reactions:

Half-cell reactions:

$4e^- + O_{2\ (test)} \rightarrow 2O_2^{2-}$

$2O_2^{2-} \rightarrow 4e^- + O_{2\ (ref)}$

NERST EQUATION: $E = (\frac{RT}{4F}) \ln (\frac{PO2(ref)}{PO2\ (test)})$

2.8.2 pH METER (H^+ IONS SENSOR)

The working principle behind pH meters is potentiometry [173]. A pH meter measures electric potential using 2 electrodes inserted into the liquid to create an electrical circuit and includes a glass membrane that is permeable to protons. The pH-related electrode is glass, while the reference electrode is usually a silver-silver chloride electrode. The glass membrane selectively binds H^+ ions and it might consist of silicon and oxygen bonding together. There is not actually e^- flow, but because of the H^+ ions concentrations difference outside and inside the glass membrane, we have a voltage difference that is measured and converted to pH value. A typical pH meter is illustrated in **Figure 2.15 B)** showing the structure described above.

2.8.3 THREE-ELECTRODE CELL FOR DOPAMINE DETACTION

The three-electrode cell enables the evaluation of one half reaction independent from the other. There are three electrodes that are used [[174], chapter 6]. Firstly, there is the working electrode (WE), the electrode undergoing the studied reaction. In this electrode there is the oxidation or reduction of the species involved. Secondly, the cell has the reference electrode (RE) which is a reference point for the evaluation of other measured parameters. Finally, the cell has the counter electrode (CE) that completes the electric circuit. For the WE, most commonly used in experimental analysis is glassy carbon electrode (GCE) as shown at **Figure 2.16 A)**.

A) B)

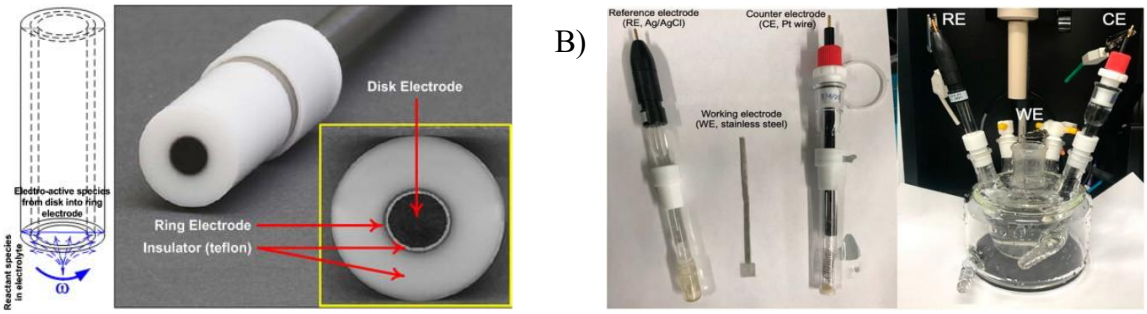

Figure 2.16. A) Working Electrode and B) Three-Electrode Cell [175, 176].

For the CE, platinum wires or meshes are popular. Also, graphite rods due to their large surface area and low prices are used under mild conditions. **Figure 2.16 B)** illustrates the reference electrode, the working electrode and the counter electrode. Also, at the same figure the method of connection in a three-electrode cell is demonstrated.

For the RE, most commonly used in experimental analysis is silver/silver chloride (Ag/AgCl) . The reaction that takes place is quite fast, ensuring the avoidance of any lag in the operating system. The potential of the half-cell reaction shown in equation below is determined by the Cl concentration of the solution, as defined by the Nernst equation.

$AgCl_{(s)} + e^- \leftrightarrow Ag + Cl^-$ / $E_{red}^0 = 0.2224$ vs. SHE (SHE: standard hydrogen electrode)

Chapter 3

HIGH AND LOW TEMPERATURE FUEL CELLS

In this chapter, ethanol fuel in high temperature fuel cells such as the case of NISSAN is first analyzed. In the following, a description of low temperature fuel cells such as PEMFCs and AEMFCs and the potential use of bioethanol in them will be given. Finally, reference will be made to the production process of renewable ethanol, analyzing the steps and the chemical processes involved.

3.1 HIGH TEMPERATURE (THE NISSAN CASE)

SOFC fuel cells are typically composed of a dense yttria-stabilized zirconium oxide electrolyte and porous nickel-based anodes and perovskite-based cathodes. They operate at a fairly high temperature of close to 500 to 850 degrees Celsius and offer an efficiency of over 60% [177-179]. This type of fuel cell has come back into the spotlight, attracting the interest of scientists and investors like NISSAN automotive manufacturer have created the world's first vehicle powered by SOFC with an efficiency of 55% powered with bio-ethanol fuel in June 2016 [180]. This vehicle consists of a SOFC fuel cell system that works in combination with a battery. It also had a bioethanol fuel tank, a reformer and finally the motor. As shown in **Figure 3.1** the fuel was pumped from the tank and added to the reformer. There, hydrogen is obtained from bioethanol which in turn is delivered to the anode of the fuel cells where electricity is generated. This energy is then either delivered directly to the motor to propel the vehicle or stored in the battery. In addition, part of the energy is recovered in the battery through the regenerative braking system, improving overall performance [181].

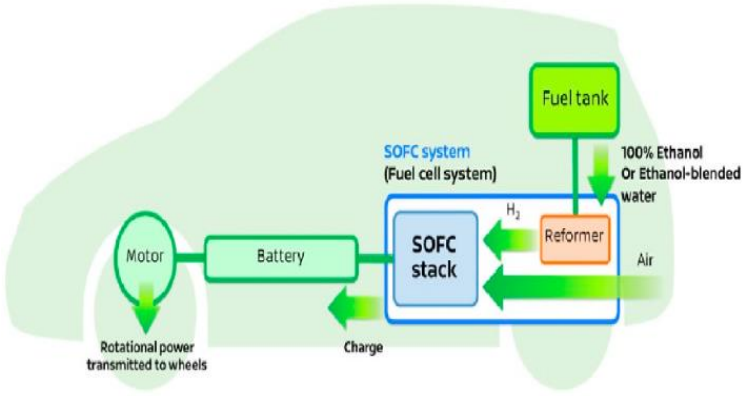

Figure 3.1. Schematic diagram of Nissan SOFC vehicle [182].

NISSAN's vehicle uses entirely ethanol produced from renewable sources and for this reason it was named e-Bio Fuel-Cell Vehicle. Its system is hybrid and consists of a 5kW SOFC system with a 30 L fuel tank and 24 kWh Li-ion battery [181, 182]. Also, its maximum speed is 120 km/h while the

NISSAN x-trail using PEMFC has a speed of 150 km/h. However, it offers a long range of up to 600km and an acceleration time of 14 seconds. The Austrian company Plansee provided NISSAN, with whom it cooperated, with a 5 kW metal-supported SOFC stack that had a specific power of 0.0385 kW/kg and a total weight of 130 kg. This vehicle having a hybrid system has a battery system that besides providing energy during operation helps to start the SOFC system. In particular, it is equipped with a lithium-ion battery pack with an energy capacity of 24 kWh, a weight of 267.5 kg and an energy density of 157Wh/kg. The pack was 290mm x 216mm and consisted of 48 modules, each with 4 cells in turn. Each cell had a voltage rating of 3.75 volts and consisted of lithium manganese oxide-lithium nickel dioxide at the cathode and graphite at the anode. Finally, the motor belongs to the category of synchronous electric motors with 80 kW AC and offers a torque output of 280Nm [181].

Due to their high operating temperature, SOFCs offer great flexibility in terms of the fuel they exploit. The NISSAN as mentioned above in e-bio Fuel Cell vehicle uses entirely ethanol as a fuel source. In particular, the ethanol used comes from a process of extraction of renewable raw materials such as biomass. Through the biomass production process, the carbon dioxide consumed is as much as that produced by using ethanol. Thus, the company promises a CO_2 neutral car with zero additional emissions. However, as will be described at the end of the chapter, ethanol is not fully oxidised to produce $12e^-$ due to the difficulty in breaking the strong C-C bond. In fact it is partially oxidized to produce intermediate compounds while offering only $4e^-$. In order to make better use of the fuel, instead of using ethanol directly for power generation, NISSAN implemented a reformer in the vehicle that converts ethanol into a mixture of substances, mainly hydrogen. Thus, in the SOFC fuel cell system, hydrogen resulting from the reforming of ethanol is used, which is then used to generate electricity through the corresponding reactions. In general, ethanol can be reformed through several possible routes that can be divided into four categories: a) steam ethanol reforming (SER), b) carbon dioxide dry ethanol reforming (DER), c) partial oxidation ethanol reforming (OER) and d) autothermal ethanol reforming (AER). The corresponding reactions describing the above categories are as follows [183, 184]:

a) Steam ethanol reforming:

$C_2H_5OH + H_2O \rightarrow 2CO + 4H_2 \quad \Delta H = +\ 278.5\ kJ\ /\ mol$

Combined with water gas shift reaction:

$2CO + 2H_2O \rightarrow 2CO_2 + 2H_2$

b) Carbon dioxide dry ethanol reforming:

$C_2H_5OH + CO_2 \rightarrow 3CO + 3H_2\ \Delta H = +296.8\ kJ/mol$

c) Partial oxidation ethanol reforming:

$C_2H_5OH + \frac{1}{2}O_2 \rightarrow 2CO + 3H_2\ \Delta H = +30.6\ kJ/mol$

Autothermal ethanol reforming:

$C_2H_5OH + 1.8H_2O + 0.6O_2 \rightarrow 4.8H_2 + 2CO_2$

At the same time, depending on the position of the reformer, the process is divided into external and internal reforming. When the process of reforming ethanol to hydrogen takes place outside the SOFC stack then the process is called external. In contrast, when the reforming occurs inside the SOFC stack then the process is called internal. In the latter case, liquid ethanol is injected into the fuel cell system and the conversion to hydrogen takes place internally in the stack. As for the case of NISSAN, the e-bio vehicle uses the steam ethanol reforming process in combination with water gas shift reaction inside an external reformer as illustrated at **Figure 3.1**. The reactions that take place and described above are the following:

Steam ethanol reforming: $C_2H_5OH + 3H_2O \rightarrow 6H_2 + 2CO_2$

The produced hydrogen is then injected into the SOFC stack where it reacts with the oxygen from the air according to the following reactions. The working principle is illustrated in **Figure 3.2**. As can be seen, during the hydrogen reaction, in addition to electricity, heat is produced, which is not wasted but is used by the reformer to facilitate the conversion of ethanol.

Reactions in the SOFC stack:

ANODE: $H_2 + O^{2-} \rightarrow H_2O + 2e^-$

CATHODE: $\frac{1}{2} O_2 + 2e^- \rightarrow O^{2-}$

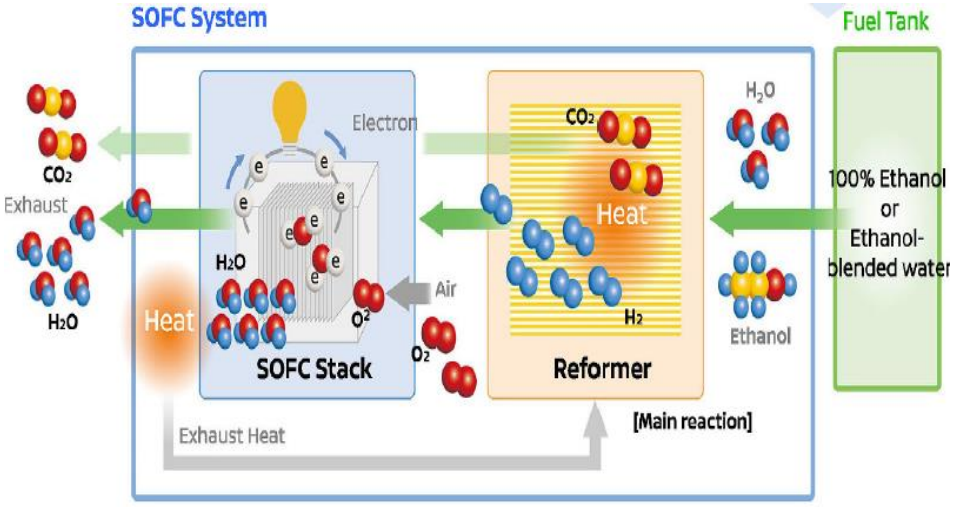

Figure 3.2. Working principle of the e-Bio Fuel Cell system [181].

NISSAN plays an important role in the field of fuel cell vehicle investments, particularly in countries such as Brazil where it can use the large volume of biomass from which it will exploit the bioethanol produced in its vehicles. By continuously optimizing its systems, it is able to create higher-speed vehicles with equivalent performance that are more environmentally friendly. This

will encourage even more companies to follow this path towards a world using carbon-neutral vehicles.

3.2 LOW TEMPERATURE FUEL CELLS

In this section we will go into more depth on low-temperature fuel cells. First, a historical description of PEMFC and AEMFC will be given, citing the evolution of their technology. Next, their operating principles, structure and the components of which they are composed will be discussed and finally an introduction to the potential use of bioethanol by both will be given.

3.2.1 LOW TEMPERATURE PEMFC

Although fuel cell technology has been known for over 150 years PEMFCs were developed near the early 1960s by Thomas Grubb and Leonard Niedrach at General Electric. The company pioneered the first small fuel cell in collaboration with the U.S. Navy's Bureau of Ships (Electronics Division) and the U.S. Army Signal Corps [185]. PEMs operate at low temperatures (around 80 ^{o}C) and quickly proved to be excellent for use in applications such as automotive since they are distinguished by their high-power density, fast start-up times and the fact that the maximum output power of PEM fuel cells ranges from 50W to 75kW.

As mentioned above, with the discovery of this technology, scientists quickly concluded that PEMs can play a big role in the future because of the advantages that come with them. In general, fuel cells present problems regarding their handling, the assembly of their parts and their tightness. PEM fuel cells precisely because they use a solid polymer separator between the electrodes and because of their low operating temperatures seem to overcome these obstacles while at the same time; the electrolyte resupply is not needed. In addition, these cells use a non-corrosive electrolyte so that they can safely use acid and corrosives without risk. Another advantage is that due to its CO_2 tolerance, they can utilize the air offered by the atmosphere without being poisoned by carbon dioxide. Furthermore, PEMFCs have high voltage, current and power density while having the ability to operate at low pressures making them very safe. Finally, they are compact and robust with a simple mechanical design [186]. Despite their advantages, they need to be further optimized in order to overcome any obstacles and make fuel cells widely used. The presence of carbon monoxide as discussed below when it exceeds 10 ppm acts as a poison for PEM fuel cells by reducing the rate of reactions [186, 187]. Additionally, PEMFCs have traditionally used very expensive catalysts [44]. Therefore, it seems necessary to make efforts to get rid of platinum group metals (PGMs). In the following, a description of the operating principles of PEMFCs will be given and at the end, the use of ethanol in them will be analysed.

PEM fuel cells consist of the Membrane Electrode Assembly (MEA) which is synthesized from a proton exchange membrane placed between two electrodes called anode and cathode respectively [19, 21]. Each electrode is plate-shaped on which the gas flow channels (GFC) are grooved. Between each electrode plate and the catalyst layer, there is a Gas Diffusion Layer (GDL). Each electrode is designed to carry out an electrochemical reaction that depends on the fuel used. The reactions take place in the triple phase boundary (TPB). On the anode the TPB is consisted of the electrode, the fuel and the electrolyte while on the cathode TPB is made between the electrode, air and electrolyte. The oxidation reaction of the fuel at a H_2-PEM takes place at the anode electrode, during which protons are produced and are conducted from the membrane and then transported to the cathode [188]. During this reaction, electrons are generated which move through an external circuit to the cathode where the oxygen reduction reaction takes place. The oxygen reduction reaction utilizes the produced electrons and the conducted protons to form eventually water. The reactions described above are the followings:

ANODE: $H_2 \rightarrow 2H^+ + 2e^-$

CATHODE: $2H^+ + ½\ O_2 + 2e^- \rightarrow H_2O$

As mentioned above, the reactions take place on the TPB via a catalyst according to either the Tafel-Volmer reaction or the Heyrovsky-Volmer reaction as follows [189, 190]:

Tafel reaction: $H_2 + 2Pt \leftrightharpoons 2(Pt\text{-}H)$

Heyrovsky reaction: $H_2 + Pt \leftrightharpoons Pt\text{-}H + H^+ + e^-$

Volmer reaction: $Pt\text{-}H \leftrightharpoons Pt + H^+ + e^-$

It has been shown that the presence of carbon monoxide negatively affects the performance of the proton exchange membrane fuel cell. In particular, when the concentration of CO is higher than 10 ppm, the rate of reactions is reduced and the overall catalyst activity is degraded. Carbon monoxide forms stronger bonds with the platinum catalyst compared to the bonds formed by hydrogen, so the CO-Pt bond minimizes the Gibbs free energy. Therefore, as is well known, the CO-Pt bond is preferred. The carbon monoxide poisoning takes place either at vacant platinum sites or at sites already occupied by hydrogen atoms via the linear-bonded or bridge-bonded adsorption mechanism.

Linear-bonded: $Pt + CO \leftrightharpoons Pt - CO$

Bridge-bonded: $2Pt + CO \leftrightharpoons Pt_2 = CO$

According to linear-bonded adsorption, the two poisoning mechanisms are described by the following reactions:

$Pt + CO \leftrightharpoons Pt - CO$

$2(Pt - H) + 2CO \leftrightharpoons 2(Pt - CO) + H_2$

Carbon monoxide negatively affects the performance of the cells by covering the active platinum sites, reducing the rate of the hydrogen oxidation reaction. This creates the need to develop a mechanism to remove CO. The adsorbed CO is removed through oxidation at potentials from 0.6 to 0.9V while HOR occurs at up to 0.2V.

The oxidation of CO is described by the following reactions:

$Pt + H_2O \leftrightharpoons Pt - OH + H^+ + e^-$

$Pt - CO + Pt - OH \leftrightharpoons 2Pt + CO_2 + H^+ + e^-$

The high potential values at which the oxidation of carbon monoxide occurs is firstly due to the strong Pt-CO bond and secondly to the fact that platinum cannot easily form bonds with water and generate hydroxyl species at low potentials where HOR takes place. Because of this difference in potential values, oxidation is very difficult, resulting in severe CO poisoning of the cell. One way of dealing with this is to drive oxidation to lower potential values either by making the Pt-CO bond weaker or by promoting the formation of hydroxyl species. It has been proved that if Pt is combined with another transition metal, the CO tolerance is increased while keeping the HOR activity high. When the two metals act subsidiarily to each other, CO tolerance is increased through two mechanisms: (i) the bifunctional mechanism and (ii) the electronic (or ligand) effect [191]. The electron effect is a mechanism that takes place at lower potentials up to 0.2V where CO adsorption dominates. The combination of Pt with another metal causes the activation of the bifunctional mechanism. This metal in turn enhances the oxidation by shifting it to lower potential values forming M-OH which reacts with Pt-CO and eventually oxidizes CO to CO_2.

The reactions that describe the bifunctional mechanism are shown below:

$Pt + CO \leftrightharpoons Pt - CO$

$M + H_2O \leftrightharpoons M - OH + H^+ + e^-$

$Pt - CO + M - OH \leftrightharpoons Pt + M + CO_2 + H^+ + e^-$

PEM fuel cells have the ability to use ethanol as fuel instead of hydrogen [33, 34, 192]. The typical structure of a direct ethanol proton exchange membrane fuel cell is shown at **Figure 3.3**. In the case of bioethanol, the reactions that take place at the electrodes are as follows [2, 52, 193-195]:

ANODE: $C_2H_5OH + 3H_2O \rightarrow 2CO_2 + 12H+ + 12e^-$

CATHODE: $3O_2 + 12H+ + 12e^- \rightarrow 6H_2O$

TOTAL: $C_2H_5OH + 3O_2 \rightarrow 2CO_2 + 3H_2O$

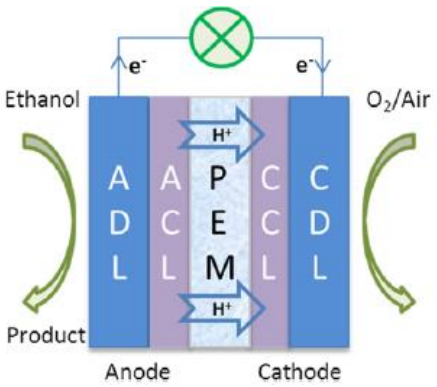

Figure 3.3. The typical structure of a DE-PEMFC [196].

The structure of DE-PEMFCs is similar to that of H2-PEMs. They also include a MEA consisting of a polymer electrolyte membrane based on Nafion [33, 193, 197]. Thus, the choice of catalysts will play an important role in how satisfactory a bioethanol fuel cell will perform. With regard to the cathode, the catalysts studied for direct ethanol PEMFCs are similar to those of H_2-PEMs. However, in addition to the good performance they should have in catalyzing the oxygen reduction reaction, they need to have good resistance to ethanol present in the cathode due to crossover [4]. Song et al. studied ethanol crossover using Nafion -115 [198]. They found that the rate at which ethanol is transferred from anode to cathode through the electrolyte is closely related to the operating temperature of the fuel cell and the concentration of the ethanol aqueous solution. Compared to methanol, ethanol has a lower transport rate due to its larger molecular size [199]. Song et al. found that ethanol crossover may also be caused by the MEA preparation process [200]. Catalysts such as Pt make strong bonds with ethanol which blocks the active sites on the catalyst surface resulting in a decrease in the rate of the oxygen reduction reaction. Many researchers have moved in this direction by creating catalysts that will exhibit enhanced ORR and at the same time ethanol tolerance. Bimetallic materials such as Pt-Co and Pt-Pd/C have been shown to significantly block ethanol adsorption on the catalyst surface showing at the same time great ORR performance [193, 194, 201]. Furthermore, when it comes to anodes, catalyst selection must be done systematically and carefully to ensure optimal utilization of the catalyst to maximize cell performance and fuel efficiency. Ethanol is a heavy molecule that upon its complete oxidation and the breaking of C-C bond 12 electrons are produced. In low temperature fuel cells (<100^{o}C), however, complete oxidation is unable to occur, resulting in the formation of undesirable intermediate compounds. For this reason, catalysts must favor the oxidation of ethanol and at the same time not be poisoned by other compounds [202]. Among the materials studied those that stood out were Pt, the binary Pt-Ru and Pt-Sn and the ternary Pt–Ru based and Pt–Sn based catalysts since they exhibited increased activity of the ethanol oxidation reaction [4, 193, 194, 203-209].

Depending on the potential range for the PtSn/C catalyst, the ethanol oxidation reactions are carried out according to the following [194, 203, 210]:

Lower potential region:

$CH_3CH_2OH \rightarrow CH_3CH_2OH_{ads\ (Pt)}$

$CH_3CH_2OH_{ads\ (Pt)} \rightarrow CH_3CHOH_{ads\ (Pt)} + H^+ + e^-$

$CH_3CHOH_{ads\ (Pt)} \rightarrow CH_3CHO_{ads\ (Pt)} + H^+ + e^-$ receiving CH_3CHO bulk

At higher potentials, water can be activated, and the hydroxyls are used to create oxygenated compounds such as acetic acid:

$H_2O_{\ (Sn)} \rightarrow OH_{ads\ (Sn)} + H^+ + e^-$

$CH_3CH_2OH_{ads\ (Pt)} \rightarrow CH_3CHOH_{ads\ (Pt)} + H^+ + e^-$

$CH_3CHOH_{ads\ (Pt)} \rightarrow CH_3CHO_{ads\ (Pt)} + H^+ + e^-$

$CH_3CHO_{ads\ (Pt)} + OH_{ads} \rightarrow Pt + CH_3COOH + H^+ + e^-$

OVERALL: $CH_3CH_2OH_{ads\ (Pt)} + OH_{ads} \rightarrow CH_3COOH + 3H^+ + 3e^-$

For fuel cells to serve as a competitor to batteries and be applied in various sectors, they must achieve operating times of 2000-3000 hours or more [193]. There are many factors that affect both the performance and lifetime of the fuel cell which are divided into 3 categories: a) chemical, b) mechanical and c) electrochemical. These involve problems such as membrane swelling and softening, catalyst decomposition resulting in reduced reaction rates and membrane drying at high temperatures. Also, as mentioned earlier poisoning phenomena of catalysts reduces their efficiency resulting in wastage and fuel wastage. Also, in applications that involve strong oscillations such as in cars on the road there is a risk of creating cracks in the most vulnerable parts of the cell structure which slowly grow and destroy them. In any case, DE-PEMFCs are very promising for the future especially using bioethanol. However, the various obstacles that prevent their widespread use need to be further studied on the one hand and on the other hand materials that have very good performance, durability and of course at low cost need to be formed.

3.2.2 LOW TEMPERATURE AEMFC

Fuel cells that have an anion exchange membrane in alkaline media are called AEMFCs [18, 67, 211]. More and more scientists have turned their attention to anion exchange membrane fuel cells in the alkaline media due to their higher efficiency, less corrosion and higher kinetics of oxygen reduction reaction compared to lower pH fuel cells, with those fuelled directly from bioethanol being the main research [3, 194].

This type of cells consists of two electrodes, called anode and cathode, and an anion-conducting membrane placed between them, creating a mechanical sandwich. In AEMFCs the MEA consists of the anion exchange membrane, the anode and cathode catalyst layers and the cathode gas diffusion layer (GDL). Finally, there is an external circuit which allows the transfer of electrons from the anode to the cathode. When the anode is supplied with hydrogen it is oxidised through the HOR reaction to form water and produce electrons in the presence of hydroxyl ions. Similarly, in the cathode, the oxygen reduction reaction (ORR) takes place where oxygen is reduced in the presence of water and through electron capture to hydroxyl ions. AEMFCs compared to PEMFCs are more affected by cell operating conditions and require more attention. This is due to the fact that the water produced in the anode by HOR has to diffuse through the membrane to the cathode for the ORR reaction where a larger proportion of it is in liquid form. The reactions described above are the following [212]:

Anode: $2H_2 + 4OH^- \rightarrow 4H_2O + 4e^-$

Cathode: $O_2 + 2H_2O + 4e^- \rightarrow 4OH^-$

When the anode is fed directly with ethanol, it is oxidized in the presence of hydroxyls to CO_2, water and electrons [34, 212, 213]. The electrons are transferred from the anode to the cathode electrode through the external circuit. The cathode is supplied with oxygen, which is reduced to hydroxyl anions in the presence of water and electrons. The hydroxyls are conducted from the anion exchange membrane and driven to the anode, completing the cycle of reactions. The reactions described above are the following [196, 197, 212, 214]:

Anode: $CH_3CH_2OH + 12OH^- \rightarrow 2CO_2 + 9H_2O + 12e^-$	E_a^0 = -0.74 V vs.SHE
Cathode: $3O_2 + 6H_2O + 12e^- \rightarrow 12OH^-$	E_c^0 = 0.40 V vs.SHE
Overall Reaction: $CH_3CH_2OH + 3O_2 \rightarrow 2CO_2 + 3H_2O$	E^0 = + 1.14 V

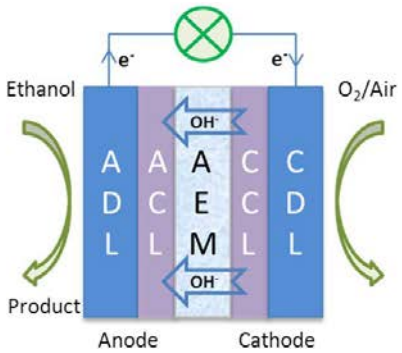

Figure 3.4. Direct ethanol fed AEM fuel cell [196].

Figure 3.4 schematically describes the reactions in an alkaline fuel cell as described above. AEMFCs in general they also consist of a MEA. On the outside, there is a gasket-like material to protect the perimeter. In the anode, the reaction of oxidation of bioethanol to form CO_2 and H_2O

takes place. In contrast, in the cathode the reaction of reduction of oxygen to form hydroxyl ions takes place, which in turn the OH^- passes through the electrolyte from the cathode to the anode. The electrons pass in reverse through an external circuit.

The above reactions are the theoretical operation of alkaline fuel cells. The complete oxidation of bioethanol to CO_2, H_2O and electrons is more of an idealized case and does not represent reality [215]. Bioethanol almost always oxidizes in intermediate stages resulting in the formation of various compounds such as acetate with the production of four electrons according to the following reaction [196]:

$$CH_3CH_2OH + 5OH^- \rightarrow CH_3COO^- + 4H_2O + 4e^-$$

The incomplete oxidation of bioethanol is one of the main disadvantages of this type of fuel cells as it does not allow them to operate at their full potential. As mentioned above, during the theoretical bioethanol oxidation reaction, twelve electrons are produced at the anode electrode and transferred through an external circuit to the cathode. However, in reality, the C-C bond cannot be completely cleaved leading to partial oxidation of bioethanol [214, 216]. Thus, only four electrons are produced with this problem being of dual importance. On the one hand, a significant amount of bioethanol is wasted without yielding the necessary electrons, and on the other hand, due to partial oxidation acetates are formed. The above reaction is the general case of partial oxidation of bioethanol. In fact, the reaction is catalysed in the presence of catalysts in the electrode body. For example, the partial oxidation of bioethanol with catalysts such as palladium and gold is illustrated by the following steps [194, 217, 218]:

$$M + OH^- \rightarrow M - OH_{ads} + e^-$$
$$M + CH_3CH_2OH \rightarrow M\text{-}(CH_3CH_2OH)_{ads}$$
$$M\text{-}(CH_3CH_2OH)_{ads} + 3OH^- \rightarrow M\text{-}(CH_3CO)_{ads} + 3H_2O + 3e^-$$
$$M\text{-}(CH_3CO)_{ads} + M - OH_{ads} \rightarrow M\text{-}CH_3COOH + M$$
$$M\text{-}CH_3COOH + OH^- \rightarrow M + CH_3COO^- + H_2O$$

M = Au or Pd

One of the many advantages of AEMFCs is the use of catalysts other than platinum such as gold and silver that provide high activity. Most AEM fuel cells use palladium as catalyst over platinum since it has been shown to offer better catalyst performance, but this does not make Pt prohibitive. In particular, if Pt is combined with metal oxides such as RuO_2, MnO_2, MoO_2 and IrO_2, it causes an improvement in the overall performance of AEMFCs [67]. For the anode electrode, it has been found that Pd offers very high activity and higher kinetics of the ethanol oxidation reaction, while for the cathode electrode; it is possible to use non-precious metal catalysts such as Fe, Co, Ni, and

Cu [66, 67]. In addition to the ease of catalyst materials, AEMFCs have many advantages over other acid environment fuel cells because they provide better electrochemical kinetics, weaker corrosion, and significantly reduced alcohol crossover.

Significant technological advances have been made regarding the materials and membrane types of AEMFCs that increase their overall performance, operation, robustness, and durability [197]. Yang et al. studied PVA (polyvinyl alcohol) membranes that are distinguished by their low cost, good chemical resistance, high hydrophilicity, non-corrosiveness and formable films [217, 219, 220]. Hou et al. developed a polybenzimidazole (PBI) membrane doped with KOH for high performance alkaline DEFCs [217, 221]. It was found that PBI has excellent resistance to high temperatures and alkaline environments. At present, the predominant membranes for fuel cells in an alkaline environment are Nafion. In direct-fed ethanol AEMGCs, the Nafion membrane is used due to its high electrochemical, thermal, and chemical stability.

To use fuel cells in an alkaline media it is first necessary to overcome certain challenges they present. The oxidation of ethanol is an incomplete reaction forming acetate (CH_3COO^-). Thus the efficiency of the reaction is significantly reduced, creating the need to use very high-activity catalyst materials. In addition, the catalytic activity of catalysts that do not contain Pt in the cathode needs to be enhanced in order to be comparable to those that require Pt. Finally, the conductivity of the membrane to hydroxyl ions should also be significantly enhanced. Overcoming these challenges leads to the realization that there are some unavoidable problems due to the high hydroxyl concentration and the presence of CO_2 in the inlet air [215]. The reaction of OH^- with CO_2 creates carbonate and/or bicarbonate anions that cause problems in the alkaline environment. Also, the presence of CO_2 itself results in a decrease in the efficiency of the membrane and its water content, creating the need for the development of CO_2 removal methods. The reactions to which CO_2 contributes are the following:

$$O_2 + 2H_2O + 4e^- \rightarrow 4OH^-$$
$$CO_2 + OH^- \leftrightharpoons HCO_3^-$$
$$HCO_3^- + OH^- \leftrightharpoons CO_3^{2-} + H_2O$$

As a result, the increased production and accumulation of carbonates in the anode gradually decreases the pH, altering the alkaline conditions of the cell and leading to a decrease in its efficiency and the cell voltage. The cathode due to the presence of OH^- is close to 14 while at the anode it ranges from 8 to 10. At the same time as concerned to the voltage drops if we increase the temperature of the cell and its water content then we manage to reduce the voltage drop to a satisfactory degree. Additionally, these compounds like bicarbonates enter the membrane occupying the positions previously occupied by hydroxyl ions. Thus, the conductivity in the hydroxyls decreases over time and as more carbonates are

produced, fewer hydroxyl anions pass through the membrane from the cathode to the anode. Thus, the efficiency of the ethanol oxidation reaction is reduced by the lack of hydroxyls resulting in reduced electron production. Also, as the carbonates in the membrane increase, they displace water within the membrane and ultimately reduce the efficiency of the overall cell function. To counteract the adverse conditions created by the presence of carbonates, the scientists reduced the thickness of the membrane. It was found that the conductivity of the CO_2 is increased and eventually emitted at a faster rate from the anode. However, if the CO_2 efflux rate increases above a permissible limit then the hydroxyl ions do not have time to enter the membrane due to the presence of CO_2, lowering the overall efficiency of the cell. Another problem with AEMFCs is the cross-linking of ethanol and water. This can be mitigated by reducing the ethanol supply and its concentration.

One gas that also has a negative effect with its presence is CO that is produced as an intermediate from the bioethanol oxidation process. Its effects on the operation of the cell are not as drastic as those due to CO_2, but it is worthy of our attention since it can reduce the efficiency of the cell to a considerable extent. CO forms compounds with the catalyst of the anode electrode, blocking its active sites. The hydroxyl ions passing through the membrane and the ethanol-fed to the anode are both unable to form bonds with the catalyst at 100%, thus rendering the catalyst useless and significantly reducing the efficiency of the alkaline cell. Depending on the catalyst material, some metals bond more easily with carbon monoxide. As mentioned above, Pt is easily poisoned by the CO produced by the ethanol oxidation reaction in low-temperature fuel cells. Thus, the catalysts being studied must have both good performance and enhancement of EOR and very good resistance and tolerance to derivatives of the fuel oxidation reaction. It is shown that doping Pt with other metals such as Ru, Mo, Sn, Re, Os, Rh, Pb and Bi creates synthetic catalysts that can be readily applied with this dual functionality [67].

Overcoming the above-mentioned problems, fuel cells in an alkaline environment perform better than those operating in an acidic media. In particular, in alkaline media, due to the high pH, the ethanol oxidation reaction has higher kinetics than in acidic media. Also, as mentioned earlier in AEMFCs, it is possible to use catalysts made of non-precious metals, making them more economical for commercial use. Furthermore, due to the alkaline environment there is much less corrosion compared to acidic fuel cells. Additionally, there is much less crossover of ethanol leading the AEMFC to better performance. As concerned to the fuel used, researchers are also focusing on cells powered directly by bioethanol, which is supported by its many advantages. As mentioned above, bioethanol is not derived from fossil fuels making it environmentally friendly. Furthermore, it does not contain as toxic substances as gasoline, and those that do are purified during the pre-treatment process. Thus, it does not require different distribution facilities than those already used for gasoline. At the same time, among other alcohols, bioethanol contains a higher energy content, which makes it very efficient as a fuel. Moreover,

at high pH the alcohol oxidation reaction shows higher kinetics than acid fuel cells, thus indicating that AEMFCs can replace PEMFCs and have better performance. However, in order for them to be used on a large scale, the duration of their operation and their good performance during this time need to be taken into account. Hou et al. in their experiment used a modified membrane with 45% PtRu/C in the anode and 40% Pt/C in the cathode electrode. Due to the modified membrane it could operate at higher temperature (90^{o}C) giving better performance for at least 12h of operation but only for 0.2 V and 50 mA cm^{-2} [222]. The same researchers subsequently investigated the same membrane using 40% Pd/C at the anode electrode and 40% MnO2/C at the cathode at 60 ^{o}C. The experiments conducted showed stable performance for 473 h but only at 0.3 V and 25 mA cm^{-2}.

DE-AEMFC fuel cells have the potential to be used in the automotive industry in combination with a reformer. As in the case of NISSAN which used a combined system consisting of a fuel reformer and a SOFC-type fuel cell, an AEMFC-type cell using hydrogen after conversion of ethanol to a reformer can also be applied to a passenger vehicle. The procedure followed differs little from that of NISSAN with SOFC because in AEMFC there is a possibility of serious poisoning of the catalysts by derivatives that arise during the reforming process due to the low operating temperature of this type of fuel cells. First the ethanol is introduced in liquid form into the reformer and then the process of converting it into hydrogen fuel begins. Initially, the first reaction that takes place is steam reforming as shown below [180]:

$CH_3CH_2OH + 3H_2O \Rightarrow 2CO_2 + 6H_2$ $\Delta H= 347$ kJ mol^{-1}

$CH_3CH_2OH + H_2O \Rightarrow 2CO + 4H_2$ $\Delta H= 298$ kJ mol^{-1}

Then, taking advantage of the water gas shift reaction, the carbon monoxide molecules produced by the first step of ethanol reforming are converted into carbon dioxide, producing additional hydrogen fuel and increasing the yield of the original ethanol. The reaction that takes place is the following:

$CO + H_2O \Rightarrow CO_2 + H_2$ $\Delta H= -41.16$ kJ mol^{-1}

Through the water gas shift reaction the concentration of carbon monoxide that was previously at 10% from the first step was now reduced to 0.5-1.5%. Then, in order to further reduce the concentration of CO to less than 10 ppm, the Preferential Oxidation (PROX) reaction is carried out via a catalyst. According to the following reaction, CO reacts with oxygen and eventually carbon dioxide is produced:

$2CO + O_2 \Rightarrow 2CO_2$ $\Delta H= -172.35$ kJ mol^{-1}

The mixture produced then goes through a drying process to evaporate the water and finally the Pressure Switching Adsorption (PSA) technology is applied. The PSA process is used to separate the CO2 molecules from the rest of the mixture and eventually eliminate them. The resulting mixture is then almost pure hydrogen with very little impurities in the exhaust gases and can thus be

used in an AEMFC-type fuel cell that uses hydrogen, eventually providing the motion of the passenger vehicle through energy production.

Considering the above, it is concluded that alkaline direct-fed bioethanol fuel cells can replace the previously compatible and very well designed PEMFCs. However, there are many challenges related to their operation that scientists need to overcome to make AEMFCs a promising power generation technology for the future that will contribute to the transition from internal combustion engines to environmentally friendly technologies.

3.3 BIOETHANOL AS A FUEL FOR FUEL CELLS

Due to international legislation and the total shift away from the use of fossil fuels in both conventional internal combustion engines and fuel cells, bioethanol can play a competitive role in the application of more environmentally friendly fuels [223, 224]. The ethanol extracted after lignocellulosic biomass processing is called bioethanol. Lignocellulosic biomass contains a rich number of sugars that are transformed into bioethanol through a specific technology based on simple steps such as: i) pre-treatment, ii) hydrolysis, iii) fermentation and iv) distillation. One of the disadvantages of bioethanol is the difference in its composition from region to region, the quality and origin of the biomass. Biomass, and by extension bioethanol, is divided into four broad categories depending on its origin. An important source of biomass origin is forest woody sources of either softwood or hardwood. Softwoods are gymnosperms and come from coniferous trees such as pine and fir, while hardwoods are angiosperms and come from oaks, maples, and birches. Another source of lignocellulosic biomass comes from the agricultural waste. Worldwide, agriculture is used to produce plant-based foods, with its residues being one of the main sources of biomass. The available quantity corresponds to an energy value of 47EJ (1EJ = 1 EXAJOULE = 10^18 JOULE) [38, 225]. The biomass quality differs depending on the origin of the crop residues, namely whether they come from corn or corn stalks, rice and wheat straw or sugarcane bagasse. It has been found that biomass derived from agricultural waste includes richer hemicellulosic material than biomass derived from forest sources at rates reaching 25-35% [38]. Thirdly, municipal, and industrial solid waste is an important source of biomass for bioethanol production. However, their use is not very widespread as they have high processing costs and at the same time have a very significant impact on the environment. Finally, perhaps the most efficient source of biomass is that of marine algae. According to Ferrel and Sarisky-Reed, marine algae promises ten times more bioethanol than corn and Harel adds that is a very ecological solution since it consumes huge amounts of CO_2 to grow [38]. However, this technology is at an early stage, but it holds a lot of promise for the near future.

In order to extract ethanol from biomass we can follow two fairly reliable methods, called thermochemical and biochemical conversion [38, 39]. Whichever method is used, the goal is the same, namely the production of lignin, hemicellulose and cellulose fragments through degradation of lignocellulose. These polysaccharides are then hydrolysed into sugars which will give us the desired bioethanol product. According to the thermochemical method, high amounts of thermal energy are required to achieve the gasification of the biomass at a specific temperature and eventually produce carbon monoxide, hydrogen and carbon dioxide. Then, with the addition of MoS_2, the gas mixture is converted into a mixture of alcohols from which ethanol is finally obtained by distillation. The whole process is achieved at high temperatures requiring large amounts of heat, increasing the degree of risk. Therefore, it is not preferred and is mainly used for the treatment of pollutants. In contrast, the most common method of extracting ethanol from biomass is the biochemical route. The biochemical method consists of four simple steps aimed at obtaining bioethanol which are: i) Pre-treatment, ii) Hydrolysis, iii) Fermentation and iv) Distillation.

Pre-treatment is a process that is followed in order to increase the efficiency of hydrolysis and reduce energy consumption. The biomass feedstock contains a significant number of contaminants that need to be addressed in order to obtain the optimal amount of cellulose. Of course, depending on the origin and quality of the biomass, the type of toxic substances it contains will vary. So we have to be particularly careful to choose the appropriate pre-treatment process according to the biomass. For example, Zhu and Pan [226] have stated that it is not wise to use the same pre-treatment process for biomass from woody sources and from agricultural waste since these two varieties differ in their physical and chemical properties. In particular, biomass from woody sources requires larger amounts of energy in order to reduce the size of polysaccharides which will help in more efficient hydrolysis and fermentation process. It also needs to be understood that depending on the nature of the toxic substances and their quantity, the cost and difficulty of pre-treatment is affected.

At the end of pre-treatment, the hydrolysis process starts. The ultimate purpose of hydrolysis is to break down the polymers into smaller sugars which are then converted into bioethanol through fermentation. This process is divided into two broad categories depending on the reactions that take place. If acidic reactions occur, the hydrolysis is called acid hydrolysis, whereas if enzymes are used, it is called enzymatic hydrolysis. Acid hydrolysis does not require strong pretreatment and can easily break down polymers into other simpler chemical compounds. The most common acids are sulfuric acid and hydrochloric acid and depending on their quantity, hydrolysis is divided into dilute hydrolysis and concentrated acid hydrolysis. Dilute hydrolysis is not such an efficient method since in order to break down the structure of polymers, such as cellulose, it is required a temperature close to 200-240 degrees Celsius. Concentrated acid hydrolysis breaks down polysaccharides more

efficiently into simpler ones, producing an overall amount greater than dilute hydrolysis up to 80%. Although this method is seemingly promising, the acids result in the dehydration of the saccharides which in turn create undesirable compounds such as aldehydes. Another way to break down polysaccharides is through the deposition of appropriate enzymes, a process called enzymatic hydrolysis. The main enzymes that are used belong to the class of cellulases, which in turn are divided into three subclasses, namely: a) endoglucanase, b) exoglucanase, c) β-glucosidase.

The third step after pre-treatment and hydrolysis to extract bioethanol from biomass is the fermentation process. Through fermentation, sugars are converted into a mixture of alcohols including bioethanol by appropriate microorganisms. S. cerevisiae is one such microorganism that converts sugars at a temperature of 30 ^{o}C and has a sugar to bioethanol conversion efficiency of 12-17% w/v [38]. Through an anaerobic process carried out at this temperature, bioethanol as the main product and a number of by-products such as CO_2 and other N-based substances are obtained. The fermentation process can take place both during hydrolysis at the same time and separately in a different step through processes called simultaneous saccharification and fermentation (SSF) and separate hydrolysis and fermentation (SHF) processes with the latter being used in most cases. Over the years more and more investments have been made to develop microorganisms that ferment pentose and hexose sugars and endure under inhibitory conditions. Furthermore, the scientists are focusing on the development and optimization of the SSF in order for the hydrolysis and fermentation process to take place in the same reactor reducing the overall cost and at the same time avoiding the accumulation of high amount of inhibitory compounds.

The resulting mixture consists of alcohols and water so that the distillation process is then required in order to obtain a pure bioethanol product. The distillation column at each level is heated to a different temperature resulting in the separation of the components of the mixture depending on the boiling point. Thus, bioethanol with a boiling point of 78.3 degrees Celsius at a pressure of 1 atmosphere is separated from the rest of the mixture. However, the bioethanol concentration is 92%, making it necessary to dehydrate the mixture to obtain 99%. In total, the carbon dioxide produced in the use of bioethanol is the same as that consumed in the production of biomass. Thus, the bioethanol produced through the process described has the advantage of a CO_2-neutral fuel since it comes from renewable energy sources [193, 227-229].

Bioethanol is an efficient and environmentally friendly fuel. A society using mostly bioethanol fuel applications depends both on the supply of raw materials and their quality depending on the region from which they originate and on the performance of the bioprocessing technology. Raw materials such as corn starch and sugar cane lignocellulosic biomass in purely agricultural regions

such as Brazil are offered at quite low prices, reducing the risk of investment. **Table 3** shows different bioethanol sources and their efficiency [193].

Table 3: Different bioethanol sources and their efficiency [193].

Feedstock	Process	Efficiency (bioenergy/biomass energy)
Sugarcane	Pressed, juice fermented to ethanol, bagasse to process heat and power	41% (ethanol only)
Corn grain	Dry milling, fermentation to ethanol, fodder (dried grains plus solubles) for animal feed	62%
Wheat	Similar to corn to ethanol, fodder (dried grains plus solubles)	53-56%
Sugar beet	Crushing, ferment sugar to ethanol and residue	12%
Lignocellulosic materials(wood and straw)	Consolidated bioprocessing	49% for wood and 42% for straw (ethanol)
	Simultaneous saccharification/co-fermentation	39% (ethanol)
Corn stover, switchgrass, bagasse	Simultaneous saccharification/co-fermentation	35% (ethanol)

Alcohols such as bioethanol are highly dependent on the origin and type of biomass. For example, woody biomass contains more lignin than agricultural biomass, which ultimately provides bioethanol of higher energy density. At the same time, bioethanol compared to hydrogen has the potential for easier storage and transport, as it is in the liquid phase at a temperature of 25 degrees Celsius, whereas hydrogen requires cryogenic tanks in order to be stored and transported safely [226]. Bioethanol has been extensively studied and compared with other alcohols to enable it to be used effectively in fuel cells. In most cells the two fuels that have been extensively studied are methanol and ethanol [230]. This was followed by studies on ethylene glycol and glycerol, among other alcohols, while the N-based fuel most commonly tested in AEMFCs is hydrazine. **Figure 3.5**, shows the potential versus current density and power density versus current density plots for the performance of AEMFCs for fuels other than hydrogen like ethanol, methanol, ethylene glycol, glycerol, borohydride, hydrazine, glucose, ammonia and ammonia borane [3]. Fuel cells using hydrogen differ little from those using other fuels in the fact that in the latter case there is an addition of liquid electrolyte to the fuel inlet. Thus, in order for the AEMFC fuel cell to perform efficiently, metal OH^- salts are added to the fuel supply at the anode.

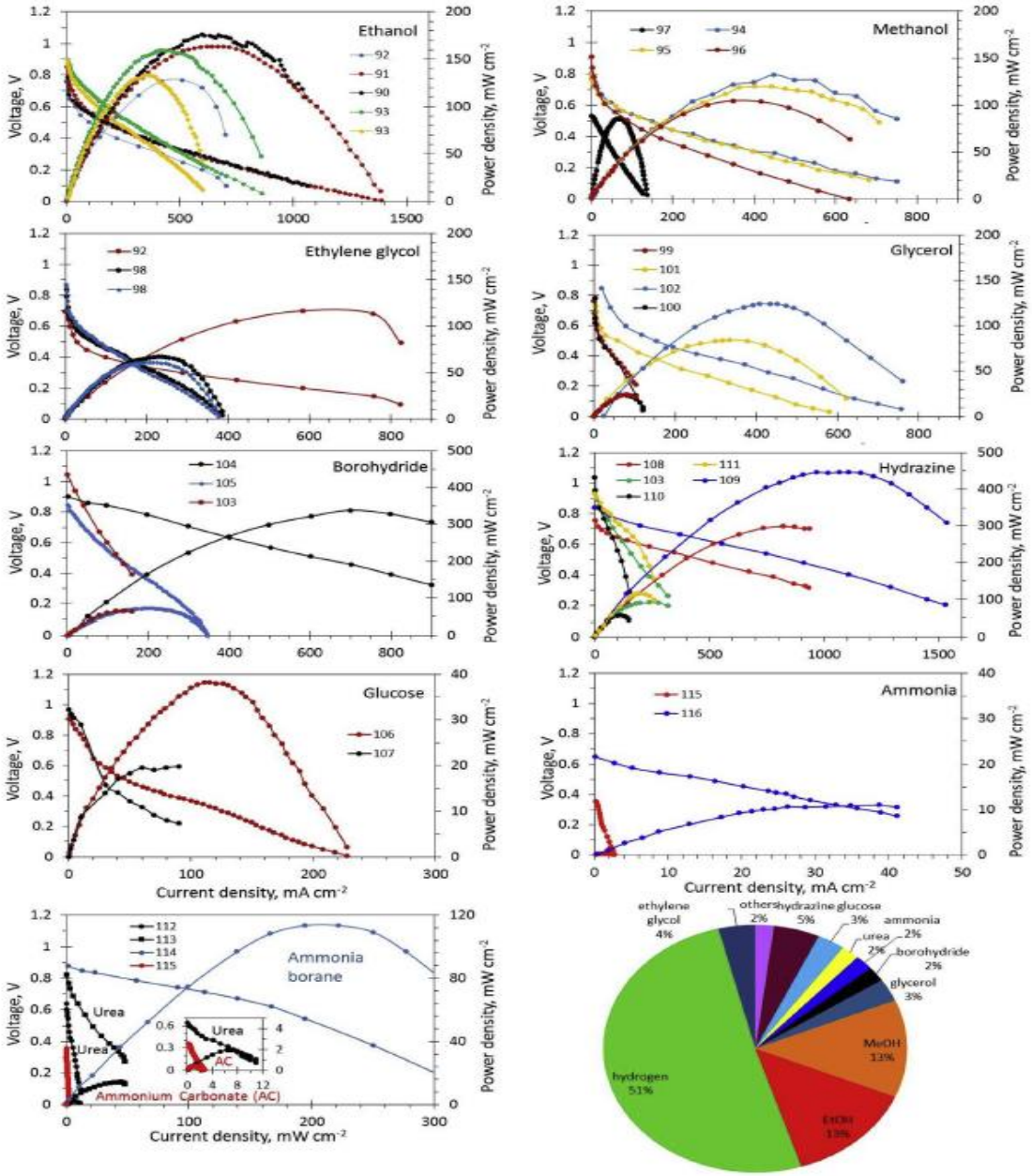

Figure 3.5. Potential versus current density and power density versus current density plots for the performance of direct fueled AEMFCs with fuels other than hydrogen [3].

Consequently, for AEM fuel cell performance tests with direct liquid fuel supply, KOH (or NaOH) is added to the liquid solution fuel. At **Figure 3.5** it can be easily seen that for direct liquid fuel AEMFCs the open circuit voltage (OCV) values range between 0.75-0.95V, the exception being borohydride, while the OCVs in H2-AEMFCs have been reported to be higher than 1.0 V [3]. Also as illustrated good performance was achieved by methanol, ethanol and hydrazine. In particular in direct liquid fuel-AEMFCs reached peak power densities of 130 mW cm^{-2}, 180 mW cm^{-2} and 450 mW cm^{-2}, measured at current densities of 450 mA cm^{-2}, 650 mA cm^{-2}, and 1300 mA cm^{-2}, respectively [3].

Chapter 4

CATALYSTS FOR EOR IN ALKALINE FUEL CELLS

Bioethanol fuel cells for electricity generation are a very promising technology with alkaline fuel cells having an advantage. Fuel cells fueled with ethanol have an advantage over those fuelled with methanol and acidic PEM-type fuel cells since they are able to break the C-C bond more easily [46, 193, 217, 231, 232]. It is shown that the C-C bond cleavage occurs more easily in an alkaline environment than in an acidic one, enhancing both the efficiency and the electrokinetics of the reaction. Another important point is that anion exchange membrane fuel cells (AEMFCs) do not require the use of noble metals. Thus they have the potential to operate with lower cost metals without much reduction in their performance [233-236]. Scientists had carried out several studies on the catalysis of reactions in PEMFCs, concluding that platinum could fulfill its intended purpose to a satisfactory degree. In view of the above, the first studies on the technology of AEMFCs started with platinum as a catalyst assuming that it would cause similarly satisfactory results. However, it was quickly understood that palladium could replace platinum since in an alkaline environment it performs better in the corresponding reactions. The whole technology is still in infant steps, requiring the improvement of palladium's function by enhancing its activity, durability and resistance to an alkaline environment. In general, the properties and catalytic activity of non-Pt catalysts like gold and silver that provide high activity need to be improved. Most AEM fuel cells use palladium as catalyst over platinum since it has been shown to offer better catalyst performance, but this does not make Pt prohibitive. In particular, if Pt is combined with metal oxides such as RuO_2, MnO_2, MoO_2 and IrO_2, it causes an improvement in the overall performance of AEMFCs [67]. For the anode electrode, it has been found that Pd offers very high activity and higher kinetics of the ethanol oxidation reaction, while for the cathode electrode; it is possible to use non-precious metal catalysts such as Fe, Co, Ni, and Cu [66, 67]. In addition to the ease of catalyst materials, AEMFCs have many advantages over other acid environment fuel cells as they provide better electrochemical kinetics, weaker corrosion, and significantly reduced alcohol crossover. Significant technological advances have been also made regarding the materials and membrane types of AEMFCs that increase their overall performance, operation, robustness, and durability. Yang et al. studied polyvinyl alcohol (PVA) membranes [217, 219, 220]. PVA membranes are distinguished by their low cost, good chemical resistance, high hydrophilicity, non-corrosiveness and formable films. Scientists conducted experiments using a novel PVA/Hydroxyapatite (HAP) composite polymer membrane in alkaline (KOH) fuel solutions achieving good performances [220, 237]. Hou et al. on the other side developed a polybenzimidazole (PBI) membrane doped with KOH for high performance

alkaline DEFCs [217, 221] and it was found that PBI has excellent resistance to high temperatures and alkaline environments. At present, the predominant membranes in direct-fed ethanol AEMFCs, the Nafion membrane is used due to its high electrochemical, thermal, and chemical stability.

Most studies concluded that palladium offers better properties in terms of strength, speed of reactions and resistance to alkaline environments. As time went on and more studies and experiments were conducted, new combinations of metals were created. In particular, Salma Jadali et al. conducted experiments with bimetallic PtPd and found that Pt_3Pd_2 nanoparticles had the best electrocatalytic activity and resistance to poisoning [238]. Zhiyong Zhang et al. created carbon-supported Pd-Ni nanoparticles with different compositions and then conducted experiments presenting their results [239]. Pd-based catalysts cleave the C-C bond more easily than Pt-based ones while at the same time, they report that hydroxyls facilitate dehydrogenation and enhance EOR in Pd-based catalysts. M.A.F. Akhairi and S.K. Kamarudin in their research thoroughly analyze platinum and palladium catalysts dividing them into monometallic, bimetallic and trimetallic [233]. They compare these two catalysts while giving an understanding of how the emerging gold catalyst also affects them. R. Carrera-Cerritos et al. in their report analyze through their experiments the performance and stability of palladium nanoparticles describing their function [240]. Yixuan Wang in his book presents extensive research by first analyzing the effects of platinum and palladium on the ethanol oxidation reaction and then proceeds to study catalysts such as Au and Pt/Au [209]. In this article, motivated by the aforementioned researchers and based on their work, an attempt will be made to understand the principles of operation and the usefulness of developing high-tech catalysts that will contribute to increasing the efficiency of fuel cells in an alkaline environment.

As mentioned above, palladium catalysts compared to platinum exhibit higher electrocatalytic activity and better stability for alcohol oxidation in alkaline environment. Thus, although in acidic media palladium is the least reactive catalyst, in alkaline media it is a better solution than platinum. According to the research of Zhang et al. Pd exhibited almost four times higher of the maximum peak in the cyclic voltammetry test of ethanol compared to Pt under the same conditions [239]. Also, Ma et al. in their study comparing platinum with palladium found that the highest peak for Pd in the CV test of ethanol is two and a half times higher than Pt for 2M EtOH as shown in **Figure 4.1** [241]. **Figure 4.1 a)** illustrates the CVs for various ethanol solutions on Pt/C where for example for 2M EtOH concentration it shows a mass current density close to 600 mA mg^{-1}. As shown in **Figure 4.1 b)** for the same ethanol concentration on Pd/C, the mass current density is about 1500 mA mg^{-1} which is 2.5 times higher than that of Pt/C.

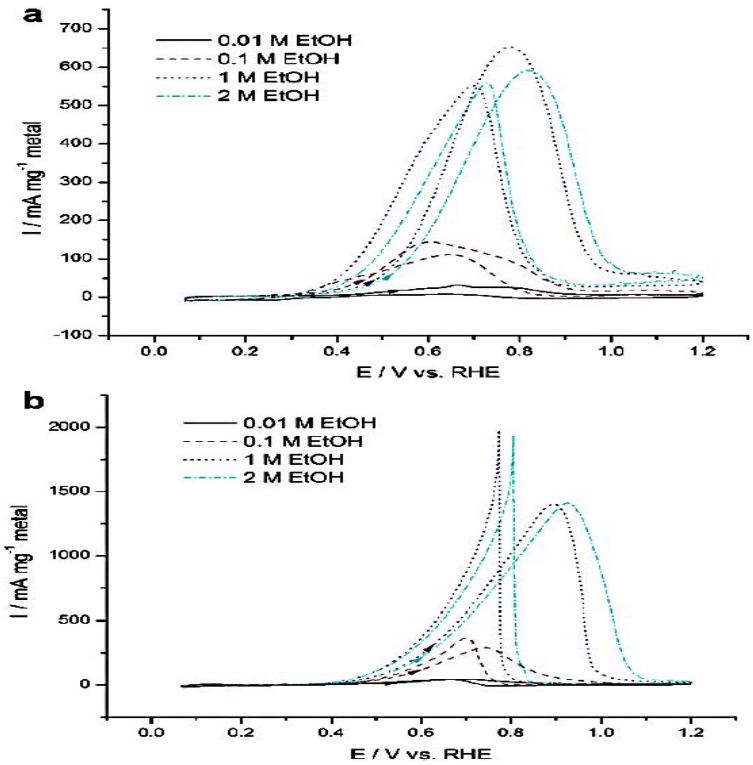

Figure 4.1. The CVs of electrodes in a 1 M NaOH + ethanol solution, (a) Pt/C, and (b) Pd/C. Scanning rate: 10 mV s^{-1} [241].

Although palladium performs better as a monometallic catalyst than platinum, because the study of its use in alkaline media is in its early stages, scientists are focusing their study on Pd-based bimetallic and trimetallic catalysts [218]. With the addition of a second or third element, a composite catalyst is created that combines the desired properties of both Pd and the accessory metals. As mentioned above, CO is a gas that may not poison to the same extent as CO_2 in anion exchange membrane fuel cells, but its presence as an intermediate compound from the ethanol oxidation process can significantly reduce cell performance. CO blocks the active sites of the catalyst by forming high-energy bonds with Pd, preventing ethanol from oxidizing to the extent possible. The addition of a synergistic metal will help to weaken this bond and reduce the rate of CO adsorption. As far as the choice of co-catalysts is concerned, factors such as their cost on the one hand and the properties they must possess on the other hand have a significant influence. In alkaline cells due to the less corrosive conditions it is possible to use lower cost catalysts such as Ni metals as co-catalysts for Pd [242, 243]. Shen et al. in their study found that the bimetallic catalyst Pd_2Ni_3/C showed excellent resistance to poisoning by intermediate compounds by weakening the bonds [242]. As an alternative to Ni, other elements such as Ag [235], Ru [234, 244], Sn [245] and Bi [246] were studied to be used as co-catalysts to increase Pd poison tolerance and promote the oxidation of ethanol. Scientists, seeing the better properties of the composite catalysts, wanted to add a third element to them, creating trimetallic catalysts. The formation of trimetallic catalysts aims at the same function as bimetallic catalysts such as enhancing the tolerance from intermediates that can block the active sites of the catalyst and enhance the ethanol oxidation rate. Su et

al. through their research found that the addition of Ni provided adsorption sites for the hydroxyl ions to oxidize CO_{ads} to CO_2 and that the addition of Au to the Pd lattice structure prevented the formation of bonds between Pd and CO_{ads} [247]. However, the addition of Au and Ni to palladium and the formation of PdAuNi trimetallic catalyst showed lower maximum peak voltage. This may be because although both Au and Ni are compatible with Pd, they may form an aggregate between them that affects the performance of EOR. Despite their lower performance at this time compared to bimetallic catalysts, trimetallic catalysts perform better than monometallic catalysts. With the development of materials constantly advancing, trimetallic catalysts are expected to significantly improve the ethanol oxidation rate and thus surpass the bimetallic catalysts. In the following, some of the most basic composite catalysts such as PtPd, PdNi, and other Pd-based catalysts are discussed.

Salma Jadali et al. report that there is controversy over the best choice between platinum and palladium with studies disagreeing on which metal has the best characteristics. They proceed to a comparison of the two catalysts for EOR by conducting experiments with monometallic and bimetallic nanoparticles Pt:Pd in different ratios at the same conditions and illustrate their results with a water-in-oil microemulsion method [238]. All experiments were performed on a standard three-electrode cell system with the working, counter and reference electrodes being respectively a modified glassy carbon electrode (2 mm in diameter, GCE), Pt wire and a saturated Ag/AgCl. The researchers proceeded to synthesize particles, which were subsequently named Pt, Pt_4Pd, Pt_3Pd_2, Pt_2Pd_3, $PtPd_4$ and Pd corresponding to theoretical Pt:Pd ratios of 100:0, 80:20, 60:40, 40:60, 20:80 and 0:100 respectively. They were able through the transmission electron microscopy (TEM) process to image the nanoparticles as shown at **Figure 4.2** [238].

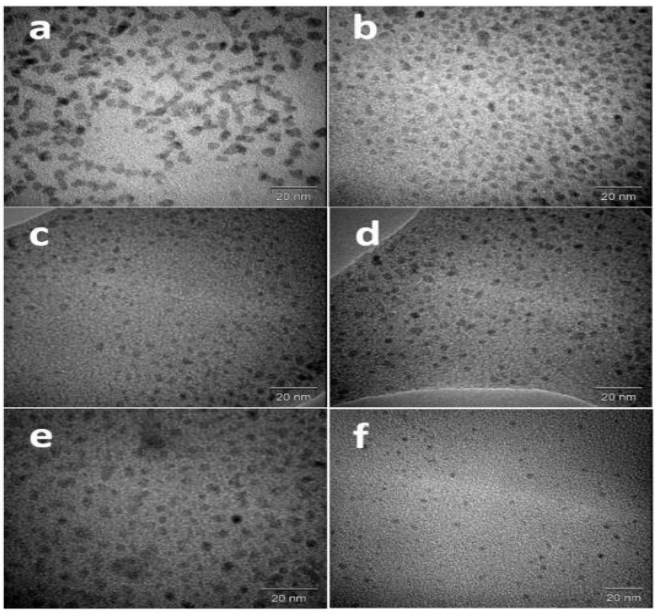

Figure 4.2. Representative transmission electron microscopy (TEM) micrographs of Pt (a), Pt_4Pd (b), Pt_3Pd_2 (c), Pt_2Pd_3 (d), $PtPd_4$ (e), and Pd (f) nanoparticles [238].

In particular, the size of the nanoparticles is plotted on a 20 nm scale starting from **Figure 4.2 a)** where monometallic Pt is shown and ending with monometallic Pd in **Figure 4.2 f).** The platinum and palladium complex catalysts are shown in the accompanying figures. All nanoparticles are below 5 nm in diameter while the average diameter of a set of 200 nanoparticles for Pt is 4.5nm, for Pt_4Pd is 3.5nm, for Pt_3Pd_2 is 3.4nm, for Pt_2Pd_3 is 4.1nm, for $PtPd_4$ 3.4nm and finally for Pd is 1.6nm.

Subsequently, cyclic voltammetry was performed for the electrochemical characterization of the nanoparticles in a 0.1 M NaOH solution at a scan rate of 0.05 V s^{-1} with the results illustrated at **Figure 4.3** [238]. The signals observed refer to hydrogen ad(b)sorption-desorption ($H_{ad(b)s}$-H_{des}), OH adsorption (OH_{ads}), metal oxidation, and reduction processes whose position depends on the type of nanoparticles being tested. In particular, the **Figure 4.3 a)** describes pure Pt in which the two peaks a1 and a2 correspond to the H desorption at the active positions of pure Pt. On the other hand, the adsorption of H is characterized by symmetric peaks at negative values of a1' and a2' respectively [238, 248-250]. **Figure 4.3 f)** shows the corresponding graph for Pd where desorption of the H_{abs} and H_{ads} occurs at the positive peaks b1 and b2 while their formation occurs at a single peak in the negative potential sweep b1' [238, 251-255]. In the composite catalysts as the Pd ratio increases the two formation peaks of H_{abs} and H_{ads} merge into a single one. Regarding the adsorption of hydroxyls, the oxidation of Pt-OH to Pt-O and the reduction of PtO to Pt on the platinum surface in **Figure 4.3 a)** correspond to a3, a4 and a4' respectively. While, concerning the palladium surface the adsorption of OH is not well distinguished and the oxidation of Pd-OH to Pd-O and the reduction of Pd-O to Pd are characterized by the b3 and b3' respectively. It can be easily seen that the reduction of PtO (a4') occurs at a more positive potential than that of PdO (b3'). The researchers list the values for the corresponding nanoparticles while providing the possibility to compare the two pure particles in the **Table 4** below.

Table 4: Values of the reduction peak of the Pt-Pd oxide for all the nanoparticles [238].

Nanoparticles	Q/μC	Width at Half Height/V	E_{peak}/V
Pt	120.4	0.24	0.72
Pt_4Pd	83.5	0.24	0.72
Pt_3Pd_2	305.5	0.22	0.70
Pt_2Pd_3	377.8	0.15	0.70
$PtPd_4$	64.1	0.15	0.70
Pd	25.0	0.10	0.67

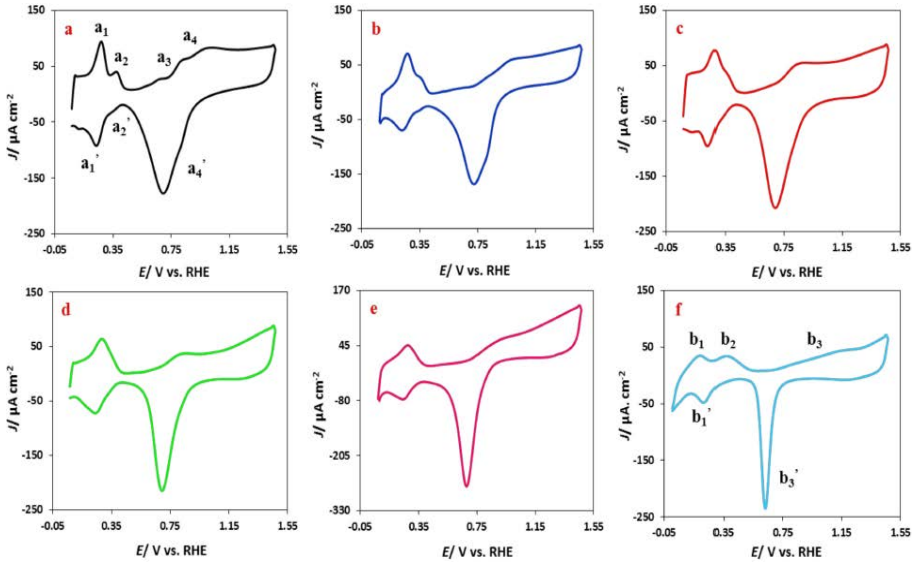

Figure 4.3. Voltammetric profile of the modified glassy carbon electrode (GCE) with (a) Pt, (b) Pt_4Pd, (c) Pt_3Pd_2, (d) Pt_2Pd_3, (e) $PtPd_4$, and (f) Pd nanoparticles in 0.1 M NaOH solution at the scan rate of 0.05 V s^{-1} [238].

According to the **Table 4**, the fourth column compares the peaks of the reduction reactions of PtO and PdO oxides that are also illustrated at **Figure 4.3**. As indicated in **Table 4** the reduction of PtO oxides occurs at a peak at 0.72 V while for Pd nanoparticles the reduction of PdO oxides occurs at a peak at 0.67 V. At the same time, **Figure 4.3 a)** shows that the reduction of PtO occurs at a broader peak while for PdO in **Figure 4.3 f)** it occurs at a sharper peak and by measuring the width at half height of the peak it is possible to compare these values in the third column at **Table 4**. Finally, the same figure shows that the oxidation peaks of PtOH to PtO and PdOH to PdO and reduction peaks of PtO to Pt and PdO to Pd respectively do not occur at the same potential values which proves that these reactions are irreversible.

Subsequently, Salma Jadali et al. proceeded with voltammetry experiments to investigate the oxidation of bioethanol in a solution of 0.1 M NaOH and 0.1 M ethanol by applying the respective catalysts each time as presented by them at **Figure 4.4**. The research mainly aims according to them to address four issues as listed. Initially it aims to compare between Pt and Pd catalysts in terms of properties such as their catalytic activity on bioethanol oxidation. Second, it examines the effect of the electron structure of the PtPd nanoparticles on the ethanol oxidation reaction activity. Thirdly, it tests to what extent the new synthesized nanoparticles affect the deactivation of the catalyst. Last but not least the research studies the effect of intermediate species on poisoning and current reduction upon cycling. As can be easily seen in **Figure 4.4**, the peaks presented in **Figure 4.3** concerning the desorption and the absorption-adsorption of H are no longer present as a result of the ethoxy species such as $(CH_3CO)_{ads}$ that block the electroactive sites. On the contrary, two peaks are distinguished with one in the positive direction and one in the negative direction during the scan. According to the researchers'

results, the maximum activity in the nanoparticles occurs at 0.8 V and then decreases as the scanning progresses. This decrease is due to the fact that there is a gradual formation of oxides of catalysts, binding them and not allowing at the same time the catalysis of the reactions to the maximum extent. Based on their findings at 1.2 V, the surface of the nanoparticles is now completely covered with the oxides of the Pd and Pt, making the bioethanol oxidation process prohibitive, and the current density becomes almost equal to that previously recorded without the addition of bioethanol. The peak that appears during the negative scan is due to the recovery of the catalyst after the amount of oxides has decreased. However, their amount has not been completely removed and therefore the peak reaches a lower height. Furthermore, throughout the EOR, acetaldehydes are gradually produced due to the partial oxidation that occurs. Thus, the catalyst is gradually poisoned, resulting in a lower peak in the negative scan than initially. In contrast, at the onset of the ethanol oxidation reaction at potential values from 0.4 V to about 0.6 V it appears that the currents in the negative scan direction are higher than in the positive sweep direction. This demonstrates that in the positive scanning direction the surface of the catalysts on the electrodes is blocked by some ethoxy adsorbed species. In any case, as illustrated in the **Figure 4.4**, the bimetallic catalysts studied performed significantly better than the platinum and palladium monometallic catalysts. The best performance was achieved by the Pt:Pd combination with a ratio of 60:40 corresponding to the red curve. In particular, the curve corresponding to Pt during the positive scan direction shows a peak current at about 1600 μA cm^{-2}. In the same scan direction for the Pt_3Pd_2 catalyst, a peak current is depicted at 4800 μA cm^{-2}, which is three times higher than before.

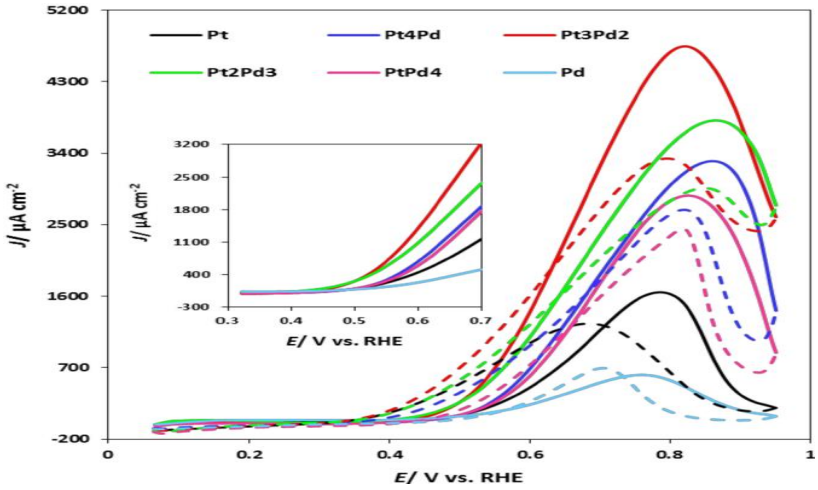

Figure 4.4. Cyclic voltammograms of the synthesized nanoparticles in a 0.1 M NaOH solution containing 0.1 M EtOH at a scan rate of 0.05 V s^{-1} [238].

Then, in order to obtain a characterization of the stability of the electrocatalytic activity, the researchers performed 20 scans with the results presented in **Figure 4.5**. This figure shows the performance of the catalysts on the first and the twentieth scan in the same diagrams. In **Figure 4.5 a)** the peak current for Pt in the first cycle is approximately 1600 μA cm^{-2}. After twenty cycles are completed, the peak current drops to 295 μA cm^{-2} which represents 18.4 % of the first cycle. In

contrast, the bimetallic catalyst Pt_3Pd_2 at **Figure 4.5 c)** after twenty cycles maintains a very good performance with a current peak of 65% of the first cycle having the highest resistance to poisoning. In the first cycle, it exhibits a peak current at 4800 μA cm^{-2} which decreases around 3140 μA cm^{-2}. As shown in **Figure 4.5**, Pt_3Pd_2 retains most of its initial performance making it the most suitable in this experiment. Then, to evaluate the stability of the catalysts with time, chronoamperometric experiments were applied at a constant potential of 0.56 V vs. RHE in 0.1 M NaOH solution with 0.1 M EtOH.

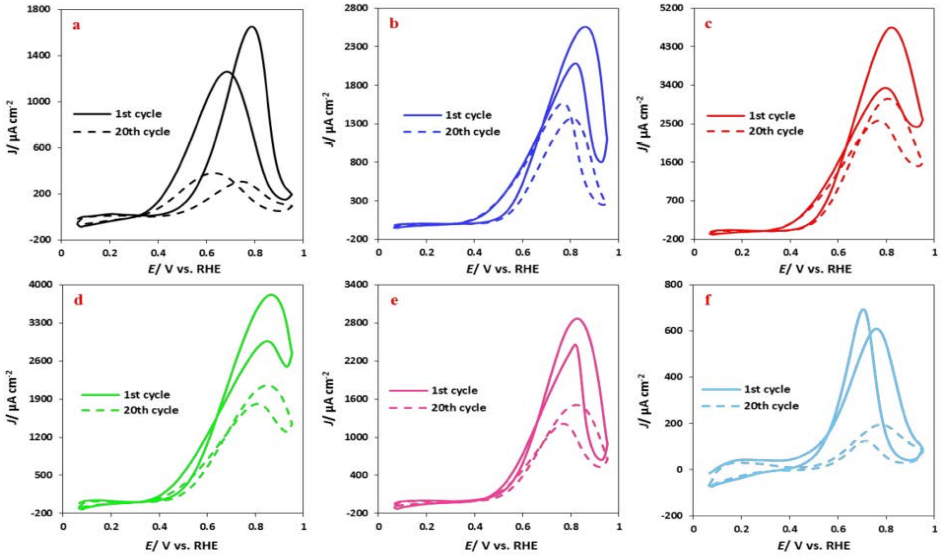

Figure 4.5. 1st and 20th cyclic voltammograms for EOR in 0.1M EtOH + 0.1M NaOH solution for a)Pt, b)Pt_4Pd, c)Pt_3Pd_2, d)Pt_2Pd_3, e)$PtPd_4$ and f) Pd at a scan rate of 50mV s^{-1} [238].

As illustrated in **Figure 4.6** in the first minute there is a sharp decrease in the current and then for 1000 seconds all the transients are in a steady state. The highest current density during 1000 seconds is detected by the red curve corresponding to the Pt_3Pd_2 catalyst while the lowest corresponds to the blue curve of the palladium monometallic catalyst.

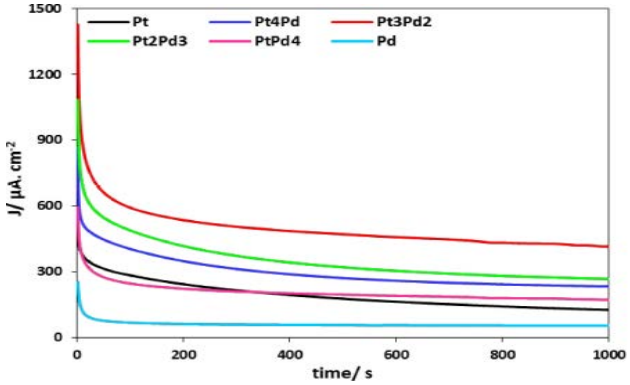

Figure 4.6. Chronoamperometric curves for the various Pt_xPd_y catalysts in 0.1M NaOH solution with 0.1M EtOH at 0.56V [238].

Bimetallic catalysts utilize a second element to further weaken the bond of the intermediates, formed during the oxidation of ethanol, with the catalyst. Ni is a promising choice as a co-catalyst due to its

good properties for the purpose mentioned above and its lower cost compared to platinum. S.Y. Shen et al. proceeded to synthesize PdNi/C catalysts with different Pd/Ni atomic ratios [242]. The size of the nanoparticles was determined through the TEM process where the monometallic Pd/C had a diameter of 3.8 nm while the catalyst Pd_2Ni_3/C had a diameter of 3.7 nm. Then experiments were conducted and the designed catalysts were compared with the monometallic Pd/C in terms of the ethanol oxidation reaction. The TEM images are shown at **Figure 4.7 a)** for Pd/C and **Figure 4.7 b)** for Pd_2Ni_3/C. As can be seen, both catalysts have a spherical shape and resemble each other.

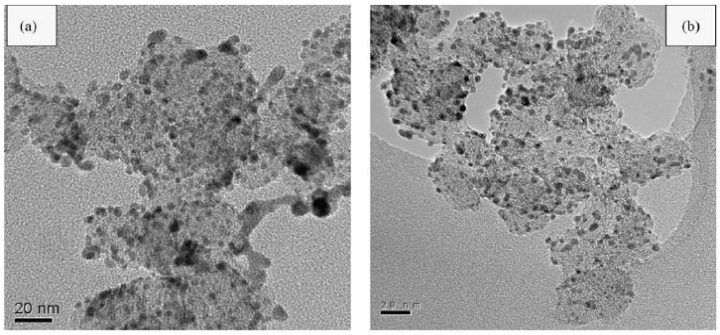

Figure 4.7. TEM images for a) Pd/C and b) Pd_2Ni_3/C catalysts [242].

Next, as shown in **Figure 4.8**, the CV curves of EOR on Pd/C and PdNi/C catalysts in 1M KOH solution with 1M EtOH at potential values from -0.926 to 0.274 V were compared. In particular, as can be seen in comparison with the monometallic Pd/C catalyst, as the percentage of Ni increases, the activity of the Pd catalyst increases. The Pd/C catalyst shows a peak current of 114 mA cm^{-2} while for Pd_2Ni_3/C is at 217 mA cm^{-2}. For the Pd_1Ni_1/C the peak current as shown at the same figure is about at 200 mA cm^{-2}. However, even though if we slightly increase the Ni content the catalyst activity increases, by increasing the Ni excessively the properties of the bimetallic catalyst become worse reducing the catalyst activity as shown by Pd_2Ni_5/C where the peak current is close to 150 mA cm^{-2} lower than the other two bimetallic catalysts.

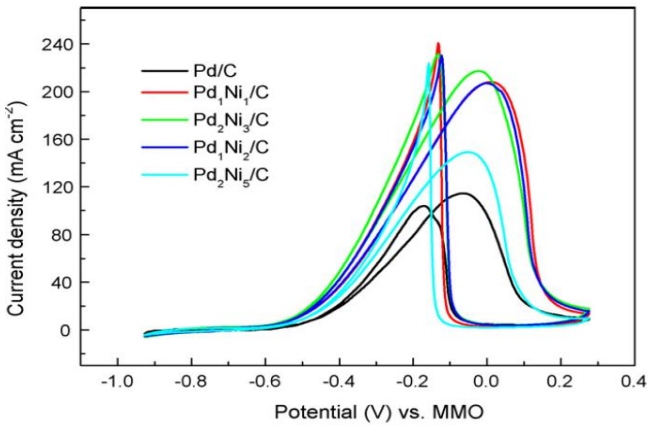

Figure 4.8. CV curves of EOR on Pd/C and PdNi/C catalysts [242].

As shown in **Figure 4.8** the Pd_2Ni_3/C catalyst has the best activity as far as ethanol oxidation is concerned and at the same time the reaction starts earlier compared to the simple palladium catalyst where for Pd_2Ni_3/C the onset potential is -0.65 V while for Pd/C the onset potential is -0.55 V.

Then, to test the stability of the catalyst, the researchers applied 20mA cm^{-2} for twelve hours straight. Between Pd_2Ni_3/C and Pd/C the former is more stable as shown by the red curve in **Figure 4.9** that illustrates the chronopotentiometric curves. The slope of the red curve with time is only 0.0069 which is almost half of the slope of the black curve for which the slope is 0.0129. Through this observation it is established that the bimetallic catalyst is more resistant to poisoning by intermediates caused during the oxidation of alcohol.

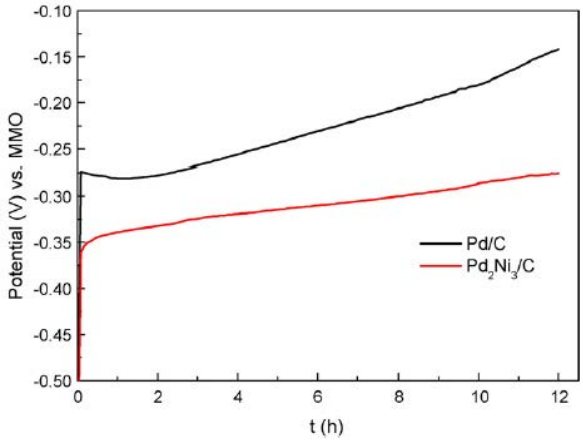

Figure 4.9. Chronopotentiometric curves of EOR on Pd/C and Pd_2Ni_3/C catalysts at 20mA cm^{-2} [242].

Qinggang Hea et al. created Pd_4Au/C and $Pd_{2.5}Sn$/C catalysts and compared them with the commercial Pt/C catalyst [256]. In their experiments they found that both bimetallic catalysts showed better properties with enhanced activity compared to the monometallic catalyst. **Figure 4.10** shows the voltammetric responses of the catalysts in ethanol oxidation where the upper bimetallic catalysts are distinguished, with the Au-containing catalyst having a slightly higher peak current and an earlier anodic onset potential.

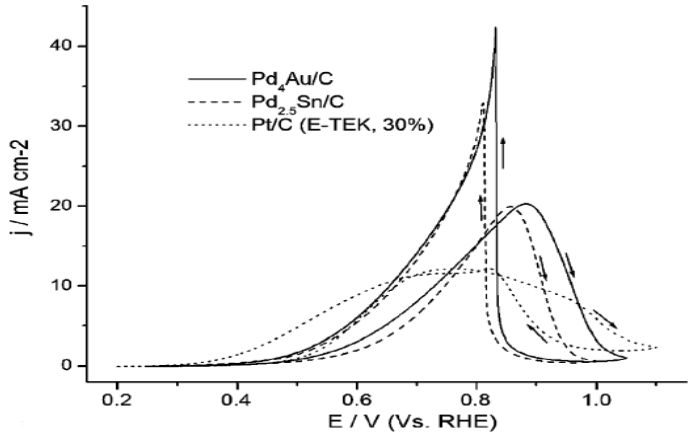

Figure 4.10. Voltammetric responses of the catalysts in ethanol oxidation [256].

In terms of resistance to poisoning as illustrated in **Figure 4.11**, bimetallic catalysts have a smaller current drop over time.

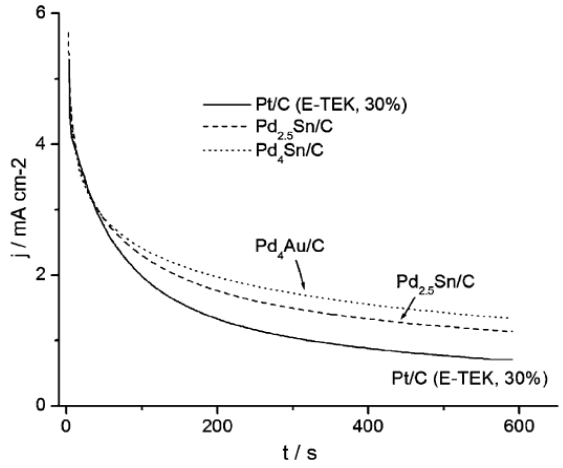

Figure 4.11. Chronoamperometric profiles of Pt/C, $Pd_{2.5}Sn/C$ and Pd_4Au/C [256].

Au and Sn have been studied by many scientists as co-catalysts in direct ethanol anion exchange membrane fuel cells. L.D. Zhu et al. created bimetallic catalysts of palladium and gold in various contents and conducted experiments in 1M ethanol+1M KOH [257]. As shown in **Figure 4.12** according to the researchers the Pd@Au/C ratio of 1:4 shows the highest peak current while from the 1:4 to 1:1 ratio the catalyst activity gradually decreases. For the 1:4 ratio, it is also illustrated to have a lower onset potential for ethanol oxidation. In the same picture for the 1:6 ratio the activity seems to be higher than in Pd/C starting at the same time from more negative potentials. However, the effect is not as good with such a high Au content as the 1:4 ratio.

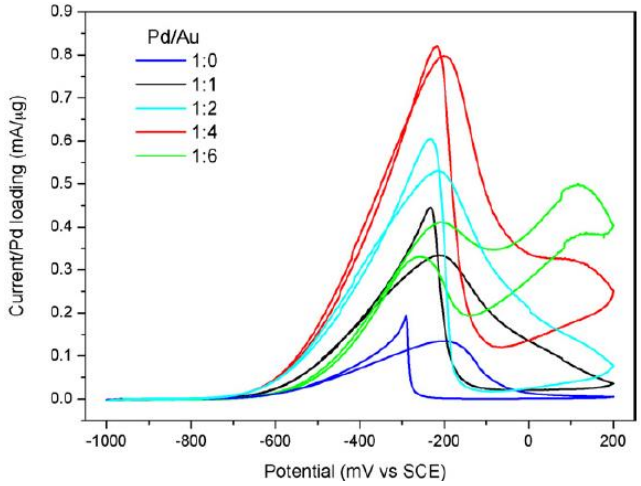

Figure 4.12. Cyclic voltammograms of Pd/C and Pd@Au/C in 1M ethanol+1M KOH at scan rate of 50 mVs^{-1} [257].

The optimization of the Pd catalyst with the addition of Au is shown in their experiment by the chronoamperograms of Pd/C and Pd@Au/C at **Figure 4.13** where the composite catalysts have higher stability with time.

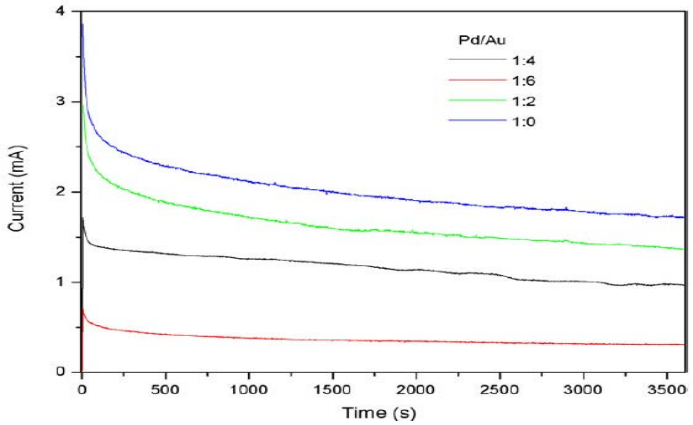

Figure 4.13. Chronoamperograms of Pd/C and Pd@Au/C in 1M ethanol+1M KOH at -0.4V [257].

However, the addition of Au is not yet significantly supported by experimental evidence that it improves the activity of the palladium sufficiently but is a promising option because of the stability it offers if the right content is found. Shuiyun Shen et al. also created a series of Pd_xAu_y/C electrocatalysts and conducted experiments [258]. However, more studies are still needed in order to optimize Pd@Au/C bimetallic catalysts and to analyze sluggish kinetics and catalyst degradation problems. Shuiyun Shen et al. created Pd@Au/C 1:0, 5:1, 3:1, 1:1, and 1:3 ratios. According to **Figure 4.14** the green curve corresponding to a 1:1 ratio is shown with the highest current peak while the onset of ethanol oxidation starts at a more negative potential at -0.58 V. The peak current is found to be 84.16mA cm^{-2} while that of the monometallic Pd/C catalyst is 59.73mA cm^{-2}. The lowest peak current is of the catalyst with a ratio of 1:3 at 54.56mA cm^{-2} while it also shows the slowest onset of ethanol oxidation at a potential of -0.48 V. The second peak current corresponds to the Pd_3Au/C catalyst at 63.90 mA cm^{-2} with the onset of ethanol oxidation at a potential of -0.58 V.

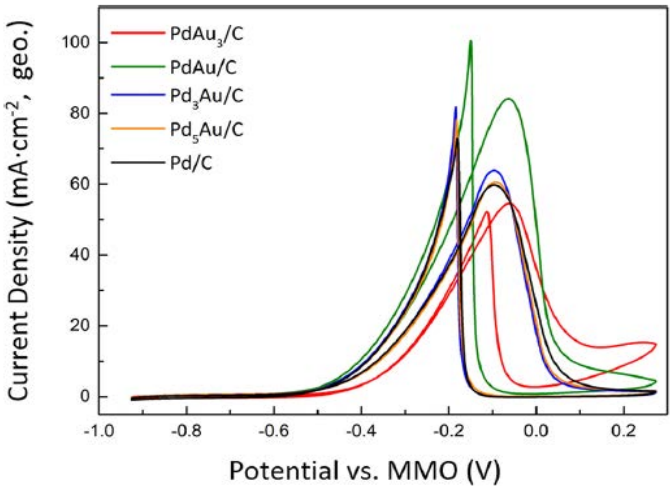

Figure 4.14. Cyclic voltammograms of Pd_xAu_y/C in 1M ethanol + 1M KOH [258].

In the same study, in order to investigate the degradation rates of the catalysts over time, their performance was compared at the 40th cycle and after 3000 cycles. As shown at **Figure 4.15**, the 1:1 ratio has the smallest drop in catalyst performance. Specifically for the PdAu/C catalyst the degradation

is by 12% going from 84.16 mA cm^{-2} at 40 cycles to 74.06mA cm^{-2} at 3000 cycles. In contrast, for monometallic Pd/C the most severe degradation of 66.8% is observed, going from 59.73 mA cm^{-2} to 19.83 mA cm^{-2}. This also demonstrates the improvement in the stability of the catalyst.

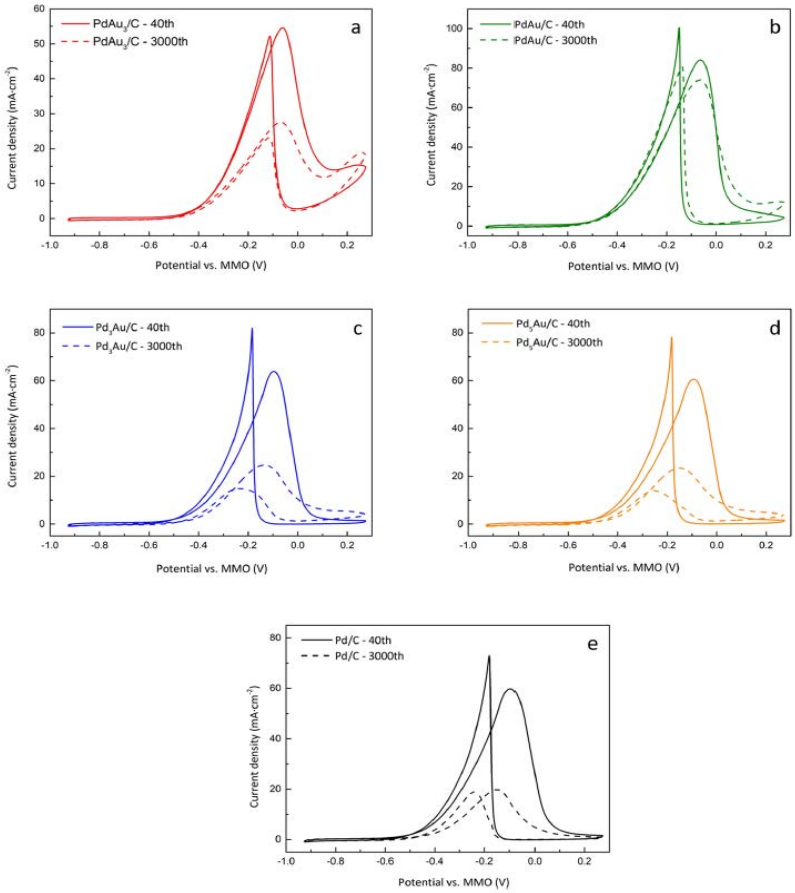

Figure 4.15. 40th and 3000th cyclic voltammograms of EOR at various Pd_xAu_y/C contents in 1M ethanol+1M KOH at scan rate 50mV s^{-1} [258].

Pt-Sn catalysts have been extensively tested in acid electrolytes, showing excellent performance. However, there have not been many corresponding studies on Pd-Sn catalysts in alkaline electrolytes. Thus, the appropriate tin content is still being investigated with many researchers proposing corresponding Pd:Sn ratios [259-262]. Wenxin Du et al. formed various bimetallic Pd-Sn/C catalysts with different contents. From their results, they concluded that the catalyst with 14% tin content showed the best performance in the ethanol oxidation reaction [262]. The researchers first carried out cyclic voltammetry measurements in 0.5M KOH aqueous solution. As shown in **Figure 4.16 a)** the curves detected are similar in shape to those presented in **Figure 4.3** for the Pt-Pd alloy catalysts. In particular, region A corresponds to the oxidation of Pd-OH and the formation of Pd-O. The peak of negative values detected during the negative scan direction in region B corresponds to the reduction of Pd-O to Pd. Finally, regions C and D correspond to the absorption and desorption of hydrogen respectively. Then, 0.5 M ethanol was added to the 0.5 M KOH solution and cyclic voltammetry measurements were taken with respect to EOR as illustrated in **Figure 4.16 b)**. As illustrated the

$Pd_{86}Sn_{14}$/C catalyst shows the highest peak current density for the EOR while the commercial catalyst Pd/C shows the lowest one between all the synthesized catalysts. At the same time, all palladium-tin catalyst alloys show the onset of ethanol oxidation at more negative potentials while the Pd/C catalyst shows the slowest onset of ethanol oxidation at more positive potentials.

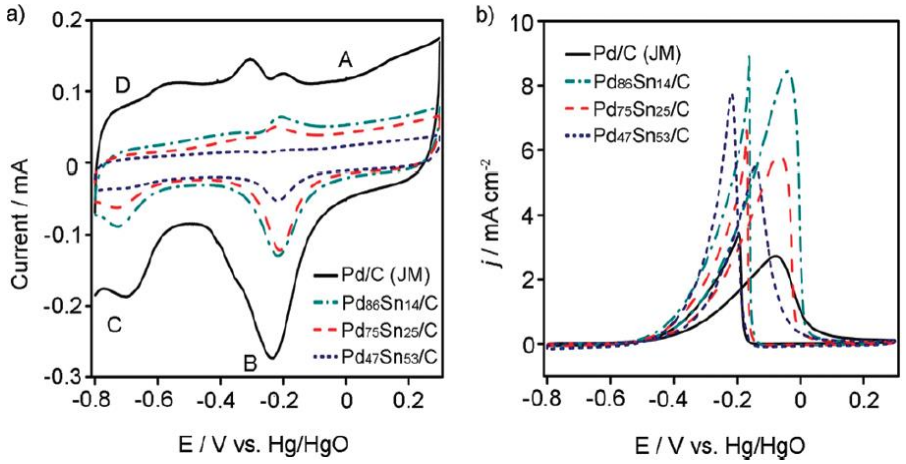

Figure 4.16. Cyclic voltammetric measurements for various Pd_xSn_y/C catalysts in a) 0.5M KOH solution and b) 0.5M KOH + 0.5M ethanol solution [262].

However, to make a complete scientific approach for the catalyst fidelity the researchers applied chronoamperometry in a solution of 0.5 M KOH and 0.5 M ethanol at a constant potential of -0.1 V to determine its stability. As illustrated in **Figure 4.17**, during the first 15 minutes there is a rapid drop in current density, which subsequently reaches a nearly steady state over a period of two hours. The initial drop is probably due to the fact that the active sites of the catalyst are blocked by the accumulation of intermediates. The $Pd_{86}Sn_{14}$ catalyst shows the highest activity after the passage of two hours. The catalysts $Pd_{75}Sn_{25}$ and Pd show similar variation with respect to time, while the worst activity is detected by the catalyst $Pd_{47}Sn_{53}$. For the $Pd_{86}Sn_{14}$ catalyst the current density at two hours is 0.07 mA cm^{-2} which is 1.4 times higher than that of Pd/C.

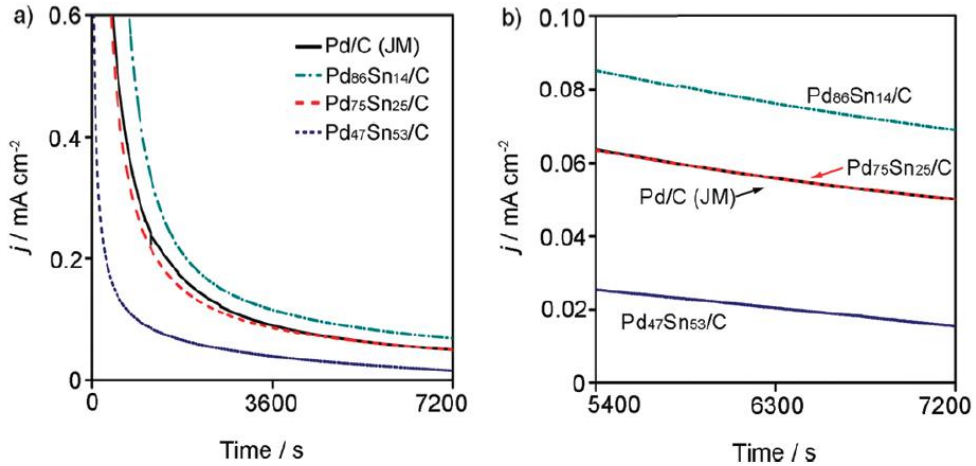

Figure 4.17. Chronoamperometric measurements of various Pd_xSn_y/C contents in 0.5M KOH+0.5M EtOH solution for 2h [262].

Ruthenium has been studied by various researchers as a co-catalyst with palladium [244, 263, 264]. According to the results of their experiments the addition of Ru leads to lower EOR onset potential in the cyclic voltammetry curves compared to the palladium monocatalyst. Junsong Guo et al. in their research compared the Pd/C and Pd_2Ru/C catalysts and obtained useful information about both the peak currents and the potentials at which they occur [265]. **Figure 4.18** shows the CV curves in 1.0 M NaOH + 1.0 M ethanol at a scan rate of 20 mV s^{-1}. With respect to Pd/C during positive scan direction the ethanol oxidation starts at about -0.6 V while the reaction peak occurs at 0.04 V. After the peak and as the potential values increase the ethanol oxidation current drops due to the formation of palladium oxides. During the negative scan direction, the reduction of Pd oxides starts, resulting in the recovery of the active sites of the catalyst and thus improving its activity in ethanol oxidation, again displaying a peak current. On the other hand, the curve concerning Pd_2Ru/C shows two oxidation processes in both positive and negative potential scans. The current values start to increase slightly at lower potential values at -0.80 V compared to the palladium monometallic catalyst and then remain relatively stable until the potential value of -0.40 V. There the main part of ethanol oxidation begins, showing a peak current near potential -0.10 V. This agrees with the earlier studies that showed Pd_xRu_y/C catalysts have lower EOR onset potential and also lower peak potential than the Pd/C catalyst. Additionally, the peak current referred to the EOR on Pd_xRu_y/C is an order smaller than that on Pd/C.

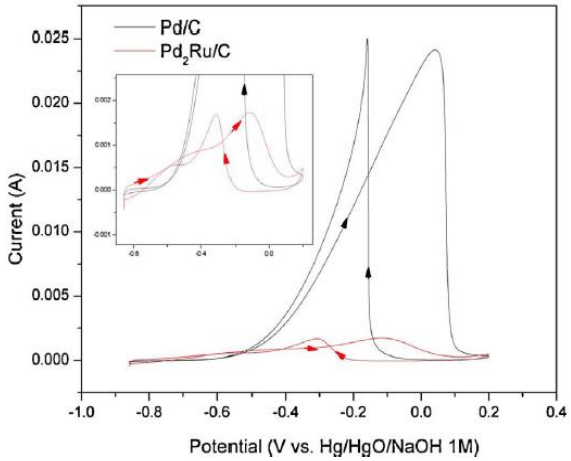

Figure 4.18. CV curves of Pd/C and Pd_2Ru/c catalysts in 1M NaOH+1M EtOH at a scan rate of 20mV s^{-1} [265].

Liang Ma et al. prepared Pd:Ru catalysts with various content ratios and a monometallic Pd/C catalyst in order to investigate their performance in the ethanol oxidation reaction in alkaline media [244]. After creating the catalysts, the researchers measured the particle size of Pd_3Ru/C and Pd/C using transmission electron microscopy. From the TEM images obtained, one hundred particles were randomly selected and it was found that with respect to Pd/C the particle size ranged from 2.2

nm to 5.2 nm while the average particle size was 3.4 nm [244]. In contrast, for the Pd_3Ru/C catalyst the particle size ranges from 1.5 nm to 4.4 nm with the average size being 2.8 nm. As it turns out the average particle size for Pd_3Ru/C is smaller than that of Pd/C. The researchers then proceeded to generate the cyclic voltammograms with respect to Ru/C, Pd_3Ru/C and Pd/C catalysts in an Ar-saturated 1M NaOH solution. As illustrated in **Figure 4.19** for the monometallic Pd/C catalyst the adsorption of hydroxyls takes place immediately after hydrogen desorption showing a small peak at a potential of 0.49 V. As for Ru/C, a broad peak in the positive scan direction from 0.2 V to 0.8 V due to RuO_xH_y formation is shown. For potential values higher than 0.9 V the oxidation of RuO_xH_y and the formation of bulk RuO_2 or high valence Ru oxides takes place [244, 266, 267]. During the negative scan direction for potential values higher than 0.9 V the reduction of RuO_2 is carried out [244, 266]. Then between 0.2 V and 0.8 V the reduction of RuO_x is carried out. As illustrated in **Figure 4.19** for the Pd_3Ru/C catalyst, the regions involving the hydrogen adsorption and desorption processes as well as the oxidation of Pd-OH to form PdO and the reduction of PdO oxides to Pd coincide with the oxidation of RuO_xH_y species to form Ru oxides and their reduction, giving a broad peak in the potential region below 0.8 V.

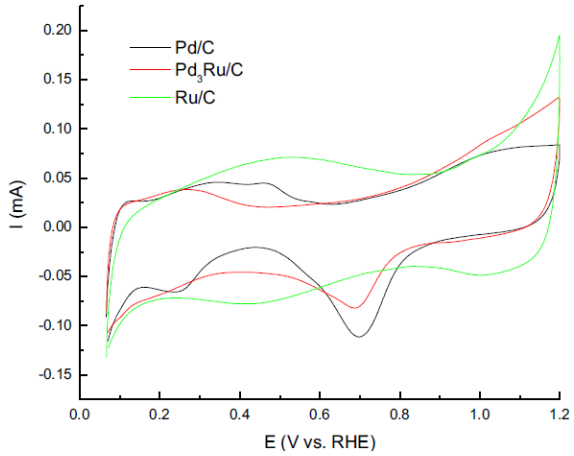

Figure 4.19. The CVs of Pd/C, Ru/C and Pd3Ru/C electrocatalysts in an Ar-saturated 1M NaOH solution at a scanning rate of 10 mV s^{-1} [244].

Subsequently, the scientists generated the CVs in 1M NaOH solution with 1M EtOH and at a scanning rate of 10 mV s^{-1}. They compared the performance of the catalysts they created with different Pd:Ru contents, with Pd/C and commercial Pd/C-ETEK as illustrated at **Figure 4.20**. As shown in the black curve concerning Pd/C during the positive scan direction, a peak current concerning the EOR appears near 0.9 V. In contrast, during the negative scan direction, a sharp peak appears around 0.76 V. In the same figure, as shown by all CV curves referred to the Pd_xRu_y/C bimetallic catalysts of different contents, one peak current appears for the ethanol oxidation reaction in the positive scan direction and two peak currents in the negative scan direction respectively. During the negative scan, one peak current is sharp and occurs at higher potentials while the second

one is a broad peak current and occurs at lower potentials. In addition, the ratio of the peak current in the positive scan direction to that in the negative scan direction is smaller compared to the corresponding ratio for Pd/C. This demonstrates that the palladium surface is more severely poisoned by the intermediates resulting from the partial oxidation of ethanol on the PdxRuy/C catalyst than on the Pd/C. As mentioned above, ethanol is usually not fully oxidized due to the strong C-C bond and thus does not break the bond completely [268]. Therefore, intermediate compounds are formed which adsorb on the surface of the palladium covering its active sites and poisoning it. As illustrated in **Figure 4.20** and in association with what has been mentioned above, from the ratios of the peak currents on the positive and negative scan direction it can be concluded that the Pd_xRu_y/C catalysts are more prone to poisoning.

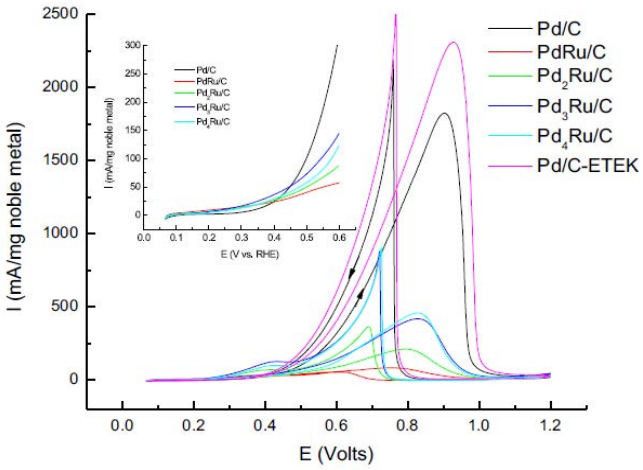

Figure 4.20. The CVs of Pd_xRu_y/C , Pd/C and commercial Pd/C-ETEK catalysts in an Ar-saturated 1M NaOH + 1M EtOH solution at a scanning rate of 10mV s^{-1} [244].

The scientists, later on, measured the quasi-steady-state currents by chronoamperometry (CA) to get a more complete understanding of the performance of the catalysts of various contents of Pd:Ru and Pd/C as shown in **Figure 4.21**. As can be noticed, the currents for Pd/C decreased slightly at the beginning with time, reaching a nearly steady state after 15 minutes. In contrast, for the Pd_xRu_y/C bimetallic catalysts, the currents in the first 0-200 seconds increase giving a peak and then begin to slowly decrease over time. As illustrated in **Figure 4.21**, as the potential increases, these spikes become more pronounced and sharper, giving higher current values. These peaks at the beginning of the time axis are most likely due to i) instantaneous oxidation of the H_{upd} (hydrogen underpotential deposition) adlayer, ii) simultaneous dissociative adsorption of ethanol and iii) pseudocapacitive currents [244, 269]. Then, as already mentioned above, the partial oxidation of ethanol creates intermediates such as CO and other hydrocarbon residues which adsorb strongly on the surface of the Pd_xRu_y/C catalysts resulting in a gradual decrease of the currents over time as shown in all the diagrams in **Figure 4.21**. For the potential 0.45 V, all Pd_xRu_y/C catalysts showed

higher steady currents for ethanol oxidation reaction compared to the monometallic Pd/C catalyst from 140 seconds onwards. In particular, the highest values correspond to the catalyst Pd_3Ru/ C while the lower ones of the bimetallic catalysts correspond to Pd_4Ru/C. In diagrams of **Figure 4.21 b)** and **Figure 4.21 c)** as the potential increases the constant current increases for all catalysts as shown by the curves. However, even though for the potential of 0.5 V, all the current versus time curves of the Pd_xRu_y/C catalysts were at higher values than Pd/C, for the potential of 0.55 V the PdRu/C and Pd_2Ru/C catalysts showed lower steady currents than the monometallic catalyst. **Figure 4.21** shows the chronoamperometry curves of electrodes in an Ar-saturated 1M NaOH with 1M ethanol solution for three different potential values: a) 0.45 V, b) 0.5 V and c) 0.55 V.

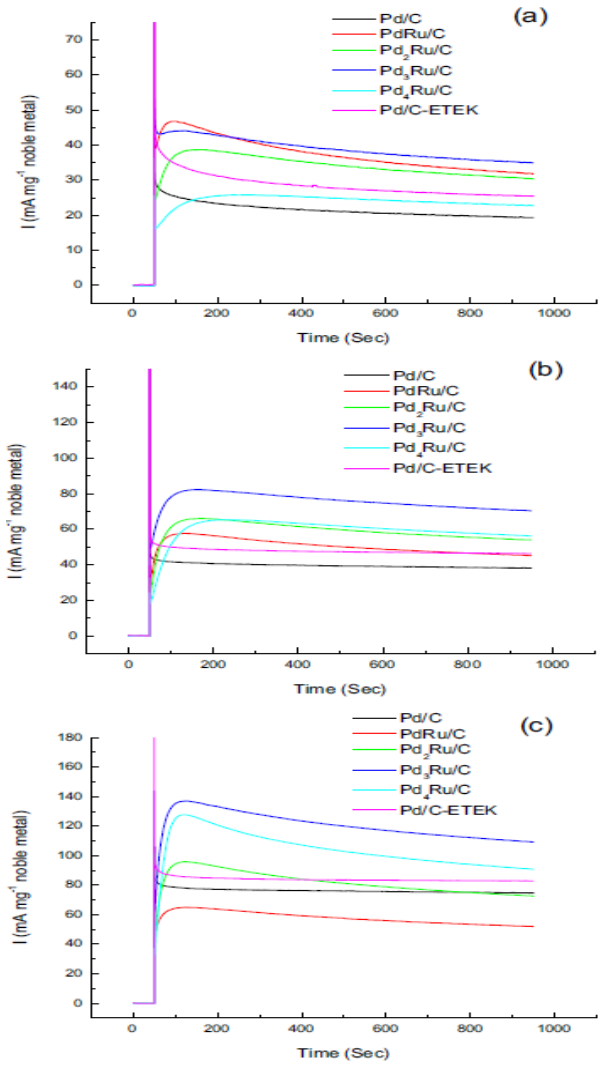

Figure 4.21. The CAs of electrodes in an Ar-saturated 1M NaOH+1M EtOH solution at potential of a) 0.45 V, b) 0.5V and c) 0.55 V [244].

In conclusion, Pd_3Ru/C and Pd_4Ru/C catalysts showed similar cyclic voltammetry curves as reflected in **Figure 4.20** while also Pd_3Ru/C catalyst showed the highest steady current according to **Figure 4.21** for all three potential values. The addition of a second metal by creating alloys with

palladium helps to increase the performance of the catalyst by making it more resistant to the intermediates that block its active sites and reduce the EOR performance. Earlier in this chapter, various bimetallic catalysts investigated by scientists in recent years were analysed. Subsequently, several researchers added a third metal to form trimetallic catalyst alloys. In the following, some experimental results of trimetallic catalysts are given to investigate their performance in the ethanol oxidation reaction. First, scientists Ahmed Elsheikh and James McGregor prepared two trimetallic $Pd_xAg_yNi_z/C$ catalysts which they then tested for both EOR performance and durability over time [270]. The resulting composite catalysts were $Pd_4Ag_2Ni_1/C$ and PdAgNi/C with the theoretical Pd:Ag:Ni molar ratio being 57:28:15 and 34:33:33, respectively. Then using the micrographs they created using the transmission electron microscopy technique they measured the average particle size of the catalysts. **Figure 4.22** shows the TEM micrographs (A, C, E) of Pd/C, Pd4Ag2Ni1/C, and PdAgNi/C with the corresponding particle size distribution plots (B, D, F).

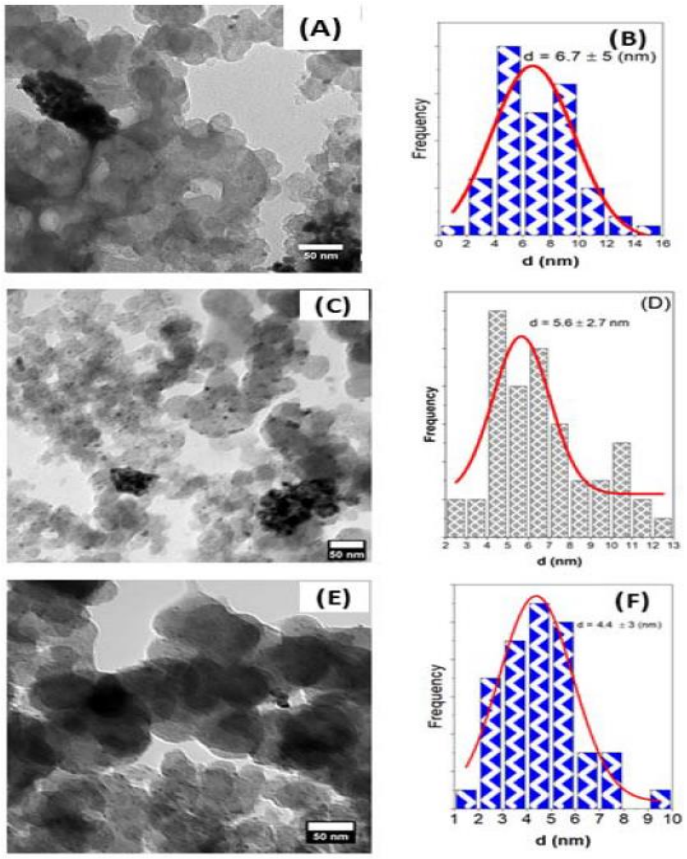

Figure 4.22. TEM micrographs and the corresponding particle size distribution of Pd/C (A,B), Pd4Ag2Ni1/C (C,D), and PdAgNi/C (E,F) [270].

As illustrated in **Figure 4.22**, the Pd nanoparticles are dispersed in larger carbon aggregates forming some condensates as well. The average size of Pd/C particles is 6.7 nm with a standard deviation of 5 nm. On the other hand, the average particle size of $Pd_4Ag_2Ni_1/C$ is 5.6 nm with a corresponding standard deviation of 2.7 nm. The smaller average particle size of the trimetallic catalyst compared to

Pd/C is probably due to the fact that the preparation of polymetallic samples leads to smaller particle sizes due to different attraction and repulsion forces [247, 271-274]. Also, regarding the PdAgNi/C catalyst, the average particle size is 4.4 nm which is also smaller than Pd/C and with a standard deviation of 3 nm. The scientists then proceeded to perform cyclic voltammetry in 1M KOH solution at 50 mV s^{-1} with the cyclic voltammograms of Pd/C, PdAgNi/C, and $Pd_4Ag_2Ni_1/C$ shown in **Figure 4.23**. As presented in previous analyses of catalyst materials, Pd has the property of absorbing hydrogen within its bulk at the lowest potentials of the cyclic voltammetry curves. However, in **Figure 4.23** the $H_{abs/ads}$ peak during the forward scan at -600 mV is not present. In contrast, according to the black and red curve corresponding to the trimetallic catalysts, the $H_{abs/ads}$ peak is more prominent due to the addition of Ag. On the other hand, the hydroxyl adsorption peak at potentials from -400 mV to -200 mV is more pronounced for the palladium monometallic catalyst than for the trimetallic catalysts. Also, according to **Figure 4.23** the oxidation of Pd is observed at a potential of 0.0 mV vs. NHE while for Ag and Ni the surface oxidation is observed at 470 mV and 600 mV respectively. As for the PdAgNi/C catalyst with theoretical Pd:Ag:Ni molar ratio 34:33:33 the oxidation peaks of both Ag and Ni are more prominent compared to the $Pd_4Ag_2Ni_1/C$ catalyst with theoretical Pd:Ag:Ni molar ratio 57:28:15 due to the higher content of Ag and Ni. Finally, in the negative scan direction three reduction peaks are observed for Ni, Ag and Pd at potential values of 450 mV, 220 mV and -200 mV respectively.

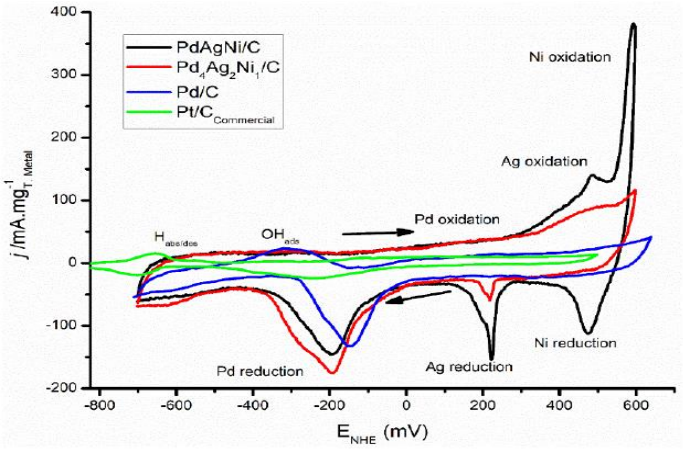

Figure 4.23. CV voltammograms of Pd/C, $Pd_4Ag_2Ni_1/C$, and PdAgNi/C in 1M KOH at 50 mV s^{-1} [270].

Subsequently, Ahmed Elsheikh et al. in order to test the performance of the catalysts in the ethanol oxidation reaction re-performed cyclic voltammetry in a solution of 1M KOH with 1M EtOH at a scanning rate of 50 mV s^{-1}. **Figure 4.24** shows the cyclic voltammetry curves of Pd/C, $Pd_4Ag_2Ni_1/C$, and PdAgNi/C, with the highest peak current corresponding to the PdAgNi/C catalyst and the lowest to Pd/C. Once the adsorption of the hydroxyls begins, the oxidation of the adsorbed ethoxy species starts releasing the Pd sites for further ethanol oxidation. As the scanning continues in the positive direction and as the adsorbed OH increases, there is an increase in current due to ethanol oxidation. Subsequently, the active sites of the catalyst are blocked by various intermediates causing a drop in current. As for Pd/C the onset

oxidation potential is located at -390 mV while for PdAgNi/C and $Pd_4Ag_2Ni_1$/C catalysts it is at a lower potential at -500 mV which means that the oxidation reaction starts earlier. Also as mentioned above the PdAgNi/C catalyst showed the highest peak current at a value close to 2700 mA/mg_{Pd} while for the $Pd_4Ag_2Ni_1$/C catalyst is 2300 mA/mg_{Pd}. The Pd/C catalyst showed the lowest value at 1800 mA/mg_{Pd}. Furthermore, for the PdAgNi/C catalyst a small shoulder peak appears in the current at a potential value of 200 mV which is most likely due to the oxidation of ethoxy intermediates on Pd. At the same time, from **Figure 4.24** for the same catalyst in the positive scan direction at potentials close to 600 mV a sudden sharp peak due to Ni oxidation is observed. Finally, in the negative scan direction and for all curves there is a sharp peak which is explained by the removal of the intermediates produced by the incomplete oxidation of ethanol. Compared to other bimetallic catalyst materials analyzed earlier, the peak current for all curves in the positive scan direction is higher than the corresponding one in the negative scan direction. This suggests that these catalysts have greater tolerance to the presence of poisoning species such as CO.

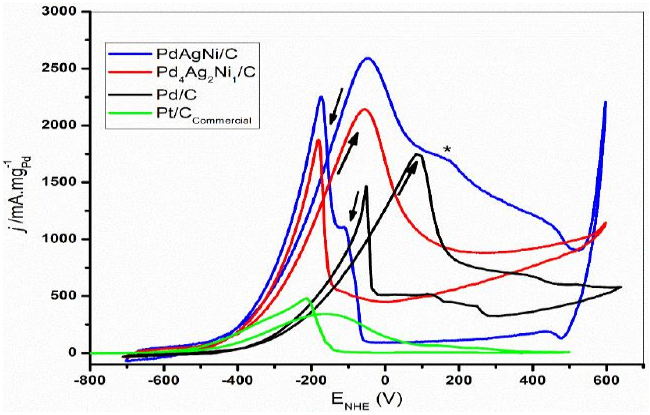

Figure 4.24. CV voltammograms of Pd/C, PdAgNi/C and $Pd_4Ag_2Ni_1$/C in a 1M KOH + EtOH solution at 50 mV s^{-1} [270].

Thereafter, to investigate the stability of the catalysts over time chronoamperometry was applied at two different potential values of -0.3 V and +0.1 V vs. NHE with the chronoamperometric scans depicted in **Figure 4.25**. The potential value -0.3 V was chosen because this is where OH adsorption occurs which triggers the oxidation and removal of ethoxy species from the Pd surface. On the contrary, the value of +0.1 V was chosen because it is slightly higher than the potential at which the Pd surface oxidation starts. As can be seen, the PdAgNi/C catalyst for a potential of -0.3 V maintains a higher current density compared to the $Pd_4Ag_2Ni_1$/C catalyst for duration of 1750 seconds. On the contrary, for potential +0.1 V the current density of PdAgNi/C decays more rapidly and thus drops below that of $Pd_4Ag_2Ni_1$/C catalyst at the end of the CA duration. At higher potentials due to incomplete oxidation of ethanol, the resulting intermediates adhere to the palladium and poison the catalyst. Thus, since the $Pd_4Ag_2Ni_1$/C catalyst contains a higher Pd content it also offers more active Pd sites making it more tolerant to CO species. As a result during the chronoamperometric scans the $Pd_4Ag_2Ni_1$/C catalyst provides a steadier CA current density than PdAgNi/C at +0.1 V.

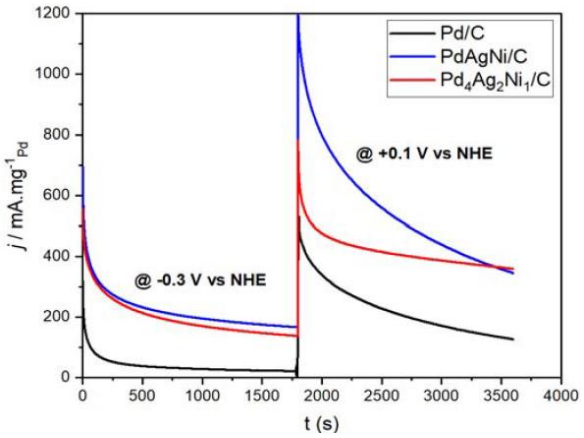

Figure 4.25. Chronoamperometric (CA) scans of Pd/C, Pd4Ag2Ni1/C and PdAgNi/C at -0.3 V and +0.1 V vs. NHE [270].

Scientists Abhijit Dutta and Jayati Datta formed a trimetallic catalyst consisting of Pd, Au and Ni. They then proceeded to cyclic voltammetry both without and in the presence of ethanol and compared the trimetallic catalyst with the bimetallic catalysts Pd:Ni and Pd:Au and with the monometallic catalyst Pd/C [274]. The bimetallic catalysts they created had atomic compositions $Pd_{58}Ni_{42}$/C and $Pd_{53}Au_{47}$/C while the trimetallic catalyst had $Pd_{41}Au_{29}Ni_{30}$/C. According to TEM technology through a set of 200 particles, it was calculated that for the ternary catalyst the particle size distribution ranges from 1 to 8 nm while the average size is 3.1 nm. Subsequently, they performed cyclic voltammetry in 0.5 M NaOH at a scan rate of 50 mV s^{-1} over a potential region between -1000 and 800 mV for the catalysts Pd/C, $Pd_{58}Ni_{42}$/C, $Pd_{53}Au_{47}$/C, and $Pd_{41}Au_{29}Ni_{30}$/C as shown in **Figure 4.26**. Due to the high hydrogen penetration into Pd, the desorption region is slightly depressed. In contrast, the hydrogen region is more prominent in the trimetallic and Au-containing catalyst. On the other hand, as shown in **Figure 4.26 b)** Ni-based catalysts do not contribute significantly to the corresponding region. In the same image, the area of oxide reduction peaks is shown in magnification.

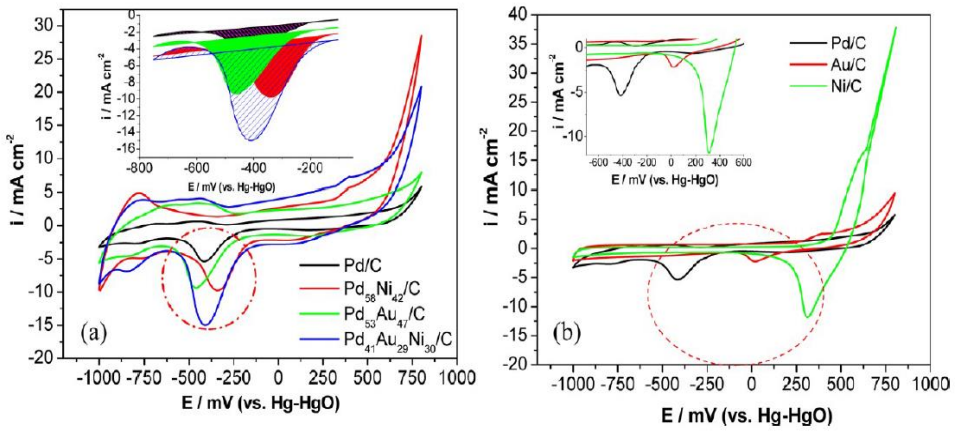

Figure 4.26. Cyclic voltammograms of Pd/C, $Pd_{58}Ni_{42}$/C, $Pd_{53}Au_{47}$/C, and $Pd_{41}Au_{29}Ni_{30}$/C and (b) Pd/C, Au/C, and Ni/C catalysts in 0.5 M NaOH at a scanning rate of 50 mV s^{-1} [274].

Thereafter, in order to examine the performance of the catalysts generated towards the ethanol oxidation reaction, cyclic voltammetry was performed again in the presence of 1M EtOH. As illustrated in **Figure 4.27**, the curves corresponding to the bimetallic catalysts $Pd_{58}Ni_{42}/C$ and $Pd_{53}Au_{47}/C$ are higher than those of the monometallic catalysts Pd/C and Au/C. This demonstrates that the bimetallic catalysts show superior activity to the corresponding monometallic ones. The curve for Ni/C is omitted because it shows no characteristics in the fuel cell potential range of -0.1 to 0.8 V. Furthermore, the curve corresponding to the trimetallic catalyst Pd:Au:Ni is higher than all the others having the highest peak current with a considerable difference from the second one of the bimetallic catalyst with Au. At the same time, for the $Pd_{41}Au_{29}Ni_{30}/C$ catalyst according to **Figure 4.27 b)** the oxidation reaction starts earlier with the onset potential being respectively the lowest at -903 V. In contrast, the corresponding values for the bimetallic catalysts $Pd_{53}Au_{47}/C$ and $Pd_{58}Ni_{42}/C$ are -773 mV and -689 mV while concerning Pd/C the onset potential of the reaction is -519 V. These values are illustrated in **Figure 4.27** in diagram **c)**, where the above values are recorded at a current output of 3 mA cm^{-2}. Finally, the order of activity of the catalysts in the same figure based on the peak current in the curves is $Pd_{41}Au_{29}Ni_{30}/C > Pd_{53}Au_{47}/C > Pd_{58}Ni_{42}/C > Pd$.

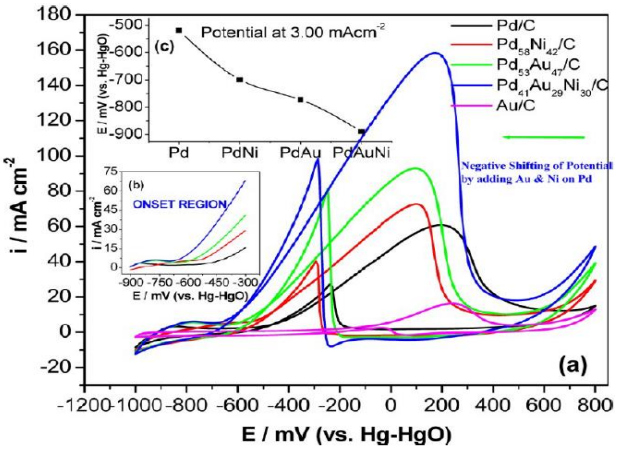

Figure 4.27. Cyclic voltammograms a) for the EOR on monometallic, bimetallic and trimetallic catalysts, b) onset potential region and c) onset potential values at 3.00 mA cm^{-2} in 0.5 M NaOH + 1 M EtOH at room temperature at a scanning rate of 50 mV s^{-1} [274].

Then, due to the fact that the electrode kinetics are significantly affected by temperature in the trimetallic catalyst, they proceeded to generate cyclic voltammetry diagrams for EOR in 0.5 M NaOH and 1.0 M ethanol at 40 °C for all catalysts and from 20-80 °C for the $Pd_{41}Au_{29}Ni_{30}/C$ catalyst as illustrated in **Figure 4.28 a)** and **b)** respectively. As it turns out, as the temperature increases from 20°C to 80 °C, the corresponding catalyst performance for the ethanol oxidation reaction also increases. At the same time, according to the researchers, this increase in the performance of $Pd_{41}Au_{29}Ni_{30}/C$ is much greater than the corresponding increase in the bimetallic alloys PdAu/C and PdNi/C with increasing temperature.

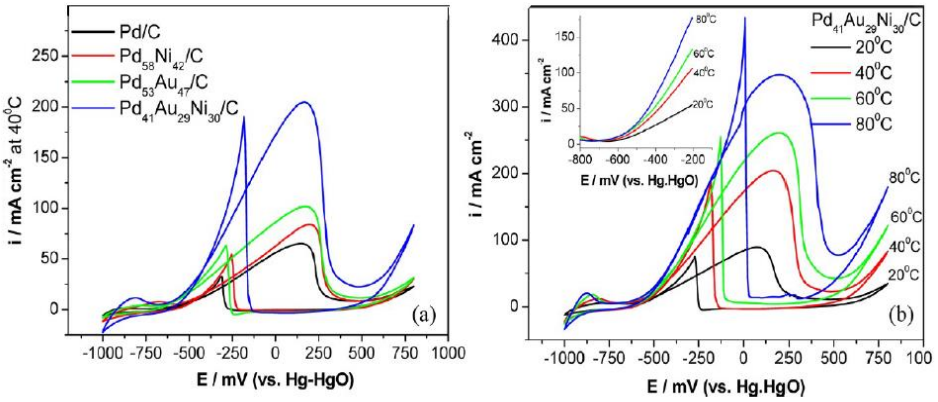

Figure 4.28. Cyclic voltammograms for EOR in 0.5 M NaOH + 1 M EtOH on a) Pd/C, $Pd_{58}Ni_{42}$/C, $Pd_{53}Au_{47}$/C and $Pd_{41}Au_{29}Ni_{30}$/C at 40 °C and b) $Pd_{41}Au_{29}Ni_{30}$/C at 20-80 °C [274].

Then, to compare the stability of the catalysts in EOR, they proceeded to create chronoamperometry curves in 0.5 M NaOH containing 1.0 M EtOH. The variation curves of the ethanol oxidation current with time are shown in **Figure 4.29** at potential -300 mV over a period of 3600 s. As illustrated for all the composite catalysts there is a sharp decrease in current density at the beginning of the plot and then the Pd41Au29Ni30/C catalyst has the best performance. Second in order is the bimetallic catalyst with Au since as discussed earlier the addition of Au gives good stability over time. Finally, the worst performer was the binary catalyst containing Ni.

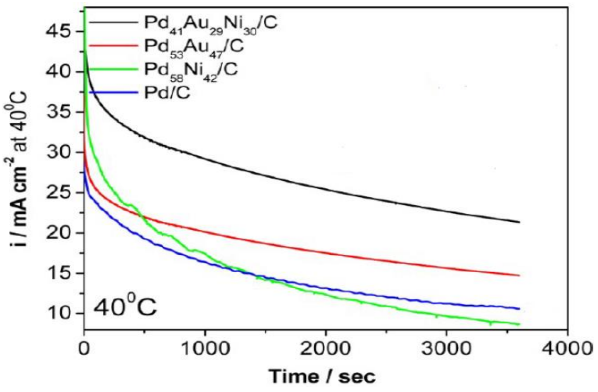

Figure 4.29. Chronoamperograms of Pd/C, $Pd_{58}Ni_{42}$/C, $Pd_{53}Au_{47}$/C and $Pd_{41}Au_{29}Ni_{30}$/C in a solution of 0.5 M NaOH + 1 M EtOH at -300 mV (vs. Hg/HgO) and at 40 °C [274].

Pd has shown a fairly good performance in the ethanol oxidation reaction. However, to make the catalyst more resistant to the presence of intermediates such as CO resulting from the incomplete ethanol oxidation reaction, two strategies are used [275]. One way is to add second or third metals such as Ru, Au, Ag, Cu, Sn and Ni to create alloys with palladium. The second strategy is the addition of hydroxides or oxide components such as $Bi(OH)_3$, $Ni(OH)_2$, CeO_2 and SnO_2 [245, 276]. The addition of tin oxide (SnO_2) can improve the catalytic activity. In addition to its application in fuel cell catalysts, it is also used as the anode in lithium-ion batteries and gas sensors. Scientists Hongmin Mao et al. prepared PdSn-SnO_2/C and PdSn/C catalysts which they tested for ethanol oxidation and compared their

performance with that of Pd/C and SnO_2/C. Subsequently, the size of the prepared catalysts was measured via a TEM procedure with the images presented in **Figure 4.30**. As shown by the particle size histogram, the average diameter of PdSn-SnO_2 particles was 4.25 nm. **Figure 4.30 C)** shows the TEM image for the SnO_2 nanoparticles, where, as it turns out, the average size was very small at about 1.8 nm, which is why they are not very distinct in the TEM image of SnO_2/C in **Figure 4.30 D)**.

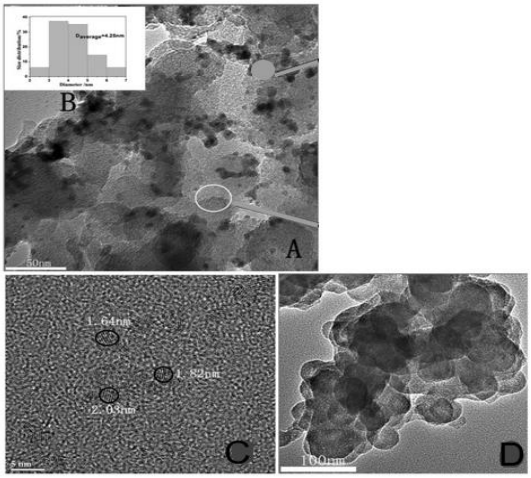

Figure 4.30. TEM images of the PdSn-SnO_2/C A), SnO_2 C) and SnO_2/C D); the size distribution histogram of PdSn-SnO_2/C particles B) [245].

Thereafter, the researchers generated the cyclic voltammogram curves for PdSn-SnO_2/C, Pd/C, PdSn/C and SnO_2/C in N_2-saturated 1.0 M KOH solution and are given in **Figure 4.31**. There the hydrogen adsorption and desorption region range in potential values from -1.1 V to -0.7 V. Immediately after the hydrogen desorption region the adsorption of hydroxyls and the formation of Pd-OH takes place. The small peaks that appear at potentials above -0.25 V are due to the fact that the Pd-OH are oxidized to form palladium oxides (PdO) on the surface of the catalyst. Finally during the negative scan direction the peaks that appear at a potential close to -0.4 V are due to the reduction reaction of these palladium oxides.

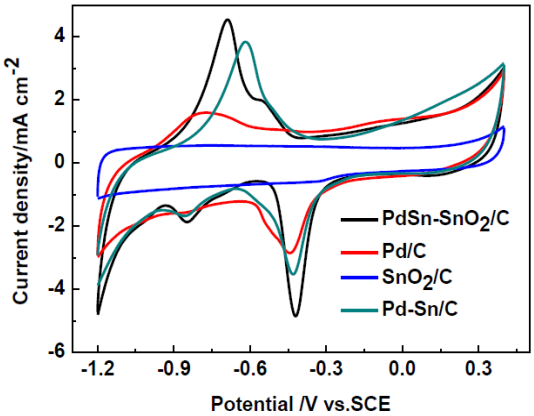

Figure 4.31. Cyclic voltammogram curves of PdSn-SnO2/C, Pd/C, SnO2/C and PdSn/C in N2-saturated 1M KOH solution at a scanning rate of 50 mV s^{-1} [245].

Then, in order to test the performance of the PdSn-SnO_2/C catalyst in the ethanol oxidation reaction, the cyclic voltammogram curves were re-generated in 1 M KOH and 1 M C_2H_5OH aqueous solution at

a scanning rate of 50 mV s^{-1}. **Figure 4.32** shows that the PdSn-SnO_2/C catalyst performed very well in terms of EOR compared to Pd/C, SnO_2/C and PdSn/C. The peak current (a) in the positive scan direction refers to the oxidation of ethanol after its adsorption. The current peak (b) during the negative scan direction occurs more due to the removal of intermediates formed during the incomplete ethanol oxidation reaction in the positive scan direction and less due to the oxidation of freshly chemisorbed species derived from ethanol adsorption. Also, the PdSn-SnO_2/C catalyst exhibited the best performance, yielding the highest peak current as shown in **Figure 4.32** at 68.71 mA cm^{-2}. In contrast, the second most influential catalyst was PdSn/C with a peak current of 37.86 mA cm^{-2} while the third was Pd/C showing a corresponding value of 28.8 mA cm^{-2}. Bare SnO_2 nanoparticles without Pd showed no signal towards ethanol oxidation as evidenced by the same figure.

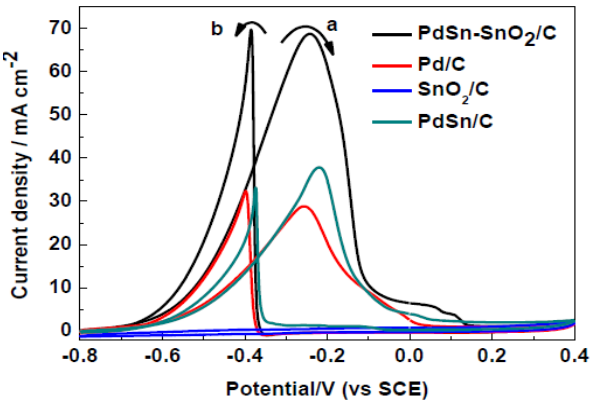

Figure 4.32. Cyclic voltammogram curves of the PdSn-SnO_2/C, Pd/C, SnO_2/C and PdSn/C in 1 M KOH + 1 M EtOH aqueous solution at a scanning rate of 50 mV s^{-1} [245].

After checking the performance of PdSn-SnO_2/C catalyst towards the ethanol oxidation reaction, the researchers presented the chronoamperometry curves for ethanol oxidation in 1.0 M KOH and 1.0 M C_2H_5OH on PdSn-SnO_2/C, Pd/C, PdSn/C and SnO_2/C catalysts at a constant potential of -0.3 V to examine its stability. As illustrated in **Figure 4.33**, all catalysts show a decrease in current density in the first 15 minutes and with more time they reach a nearly steady state.

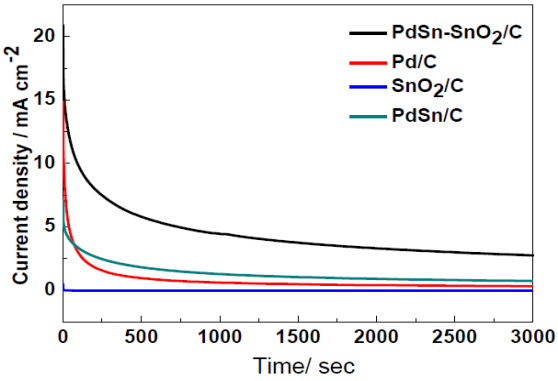

Figure 4.33. Chronoamperometry curves for ethanol oxidation in 1 M KOH + 1 M EtOH on PdSn-SnO_2/C, Pd/C, PdSn/C and SnO_2/C catalysts at -0.3 V [245].

After the passage of 3000 seconds the PdSn-SnO_2/C catalyst showed quite good stability having the highest energy density value of 4.45 mA cm^{-2}. According to **Figure 4.33**, the PdSn/C and Pd/C catalysts had a lower current density than the PdSn-SnO_2/C catalyst after the end of 3000 seconds. This demonstrates that the PdSn-SnO_2/C composite significantly increased the catalytic activity for the ethanol oxidation reaction.

To develop catalysts that can promote the oxidation of intermediate compounds such as CO and CH_3CO_{ads} resulting from the incomplete ethanol oxidation reaction and at the same time to be durable, Jiatai Zhong et al. developed the Pd/$Ni(OH)_2$ catalyst. **Figure 4.34** shows the TEM images where **A)** and **B)** indicate that Pd is uniformly distributed on the $Ni(OH)_2$ sheets. Also as illustrated in the same figure from **C)** and **D)** the average size of the Pd nanoparticles is about 30 nm.

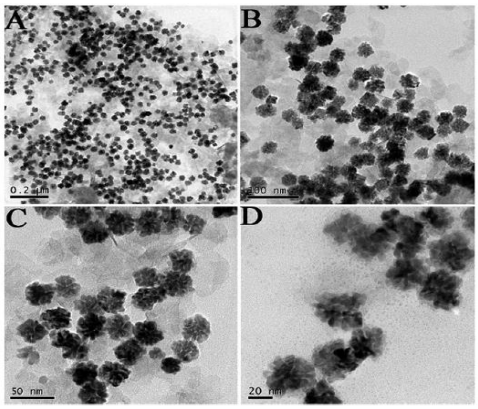

Figure 4.34. TEM images of Pd/$Ni(OH)_2$ with different magnification [277].

They then performed circular voltammetry in an alkaline medium of 1M KOH solution with a potential range from -0.8V to 0.3V at a scan rate of 50 mV s^{-1} and the extracted curves are shown in **Figure 4.35**. For both Pd/$Ni(OH)_2$ and the commercial Pd/C catalyst, a peak occurs in the negative scan direction at -0.31 V vs. SCE which is due as previously reported to the reduction of palladium oxides.

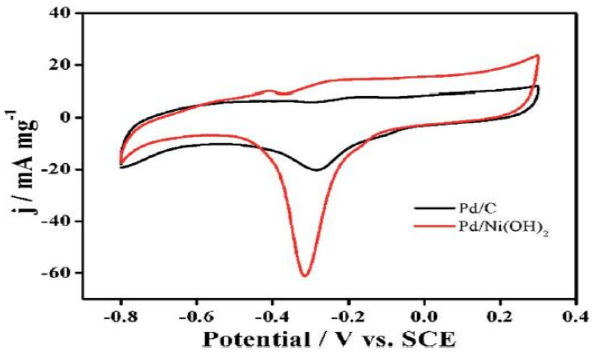

Figure 4.35. CVs of commercial Pd/C and Pd/$Ni(OH)_2$ catalysts in 1 M KOH solution at a scanning rate of 50 mV s^{-1} [277].

In order to investigate the catalytic activity of Pd/$Ni(OH)_2$, cyclic voltammetry was repeated in a solution containing 1 M KOH and 1 M C_2H_5OH at the scan rate of 50 mV s^{-1} and the

performance was compared with commercial Pd/C as illustrated at **Figure 4.36**. The peak current that occurs in the positive scan direction is due to the oxidation of the adsorbed ethanol while the peak in the negative scan direction is due to the removal of the intermediates that block the active sites of the catalyst. According to the same figure, the onset potential of the Pd/Ni(OH)$_2$ catalyst is about -0.62 V. In contrast, for the commercial Pd/C catalyst the corresponding value is -0.52 V, 100 mV more positive. This demonstrates that ethanol oxidation is more easily initiated on the Pd/Ni(OH)$_2$ catalyst than Pd/C at lower potential values. Moreover, the Pd/Ni(OH)$_2$ catalyst has the highest peak current at 2532.72 mA mg^{-1} demonstrating better performance with the addition of Ni(OH)$_2$. Similarly, the value for Pd/C is at 572.31 mA mg^{-1} which is approximately 4.4 times lower from that of the synthesized catalyst. The enhancement of ethanol oxidation is due to the fact that the addition of hydroxide facilitates the removal of intermediates and releases the active sites of the catalyst.

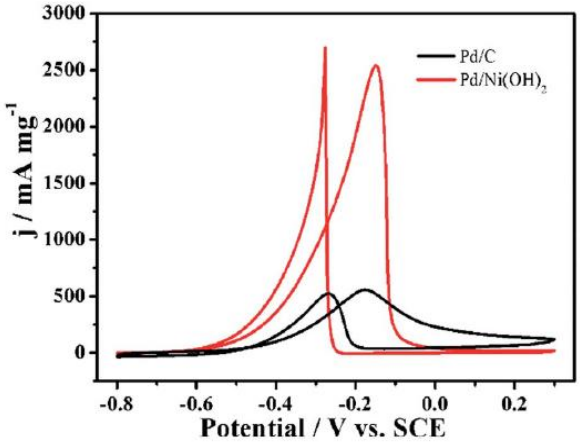

Figure 4.36. CV curves of commercial Pd/C and Pd/Ni(OH)$_2$ catalysts in solution 1M KOH+ 1M EtOH at a scanning rate of 50 mV s^{-1} [277].

CA curves were then formed in order to compare the Pd/Ni(OH)$_2$ catalyst in terms of long-term stability and durability with the commercial Pd/C catalyst in a 1M KOH + 1M EtOH solution at -0.25 V (vs. SCE) for 3600 s as illustrated in **Figure 4.37**. As can be seen, in the first 400 seconds the current density drops rapidly in both curves for both catalysts due to the accumulation of intermediates such as CO and CH_3CO_{ads} that poison the catalyst and are caused by the incomplete oxidation reaction. Thereafter, from 400 and until the end of 3600 seconds a smaller decrease occurs, resulting in an almost constant current density. Furthermore, as shown in **Figure 4.37 A)** the Pd/Ni(OH)$_2$ catalyst maintained a higher current density throughout the 3600 seconds indicating the best performance. Thereafter, to examine the long-term stability of the Pd/Ni(OH)$_2$ catalyst, the researchers performed the CVs scans of 500 cycles on the catalysts in an alkaline medium containing 1 M KOH + 1 M EtOH at a scanning rate of 50 mV s^{-1}.

Figure 4.37 B) shows the diagram of the variation of the peak current density with the corresponding cycle number.

As illustrated for the $Pd/Ni(OH)_2$ catalyst there is a rapid increase in the initial cycles with the maximum peak current density finally occurring after the first 20 cycles. From 20 to 160 cycles the current density drops while after 160 cycles it is maintained almost constant indicating good long-term stability towards ethanol oxidation. Throughout the 500 cycles, it maintains a much higher current density in contrast to the commercial catalyst exhibiting better performance in the studied reaction. According to the scientists, the conservation rate of the peak current density for the $Pd/Ni(OH)_2$ catalyst is about 48.33% of the maximum value observed. In contrast, the corresponding conservation rate for the commercial Pd/C catalyst is 9.62% of the maximum value of the peak current density.

According to what has been reported, the researchers conclude that the addition of $Ni(OH)_2$ contributes to the excellent stability towards ethanol oxidation after the passage of several cycles and the enhanced tolerance of intermediates making the $Pd/Ni(OH)_2$ catalyst very promising.

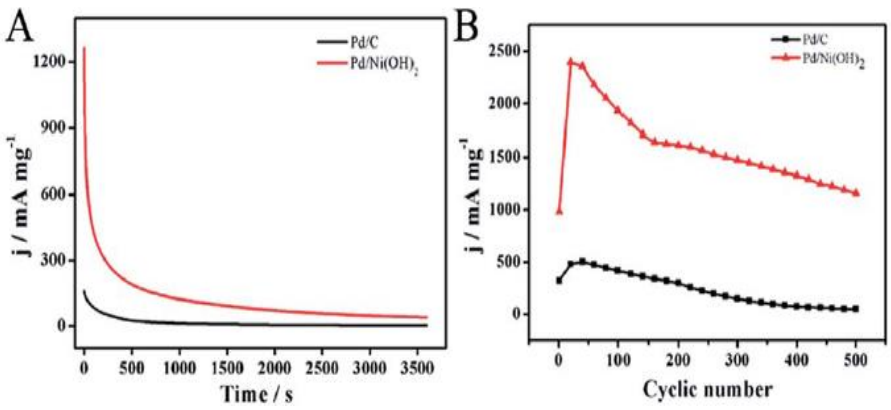

Figure 4.37. A) CA curves on Pd/C and $Pd/Ni(OH)_2$ catalysts at -0.25 V in 1M KOH+1M EtOH. B) The variation of the maximum specific peak current density with increasing cycle number for the Pd/C and $Pd/Ni(OH)_2$ [277].

Finally, to get a more complete understanding of CO tolerance, the researchers created the CVs of $Pd/Ni(OH)_2$ and commercial Pd/C catalysts at a potential range of -0.8 to 0.3 V at a scanning rate of 50 mV s^{-1} in CO-saturated solution of 1 M KOH. As shown in **Figure 4.38 A)** during the positive scan direction of the first cycle, a CO oxidation peak appears caused by the good oxidation activity for CO on the $Pd/Ni(OH)_2$ catalyst. In contrast, in the negative scan direction, this peak no longer exists. This means that during the first scan, there was complete oxidation of CO. Regarding the commercial catalyst, according to **Figure 4.38 B)** the CO oxidation peak appears in both the first and second scans indicating that not all CO was fully oxidized in the first scan.

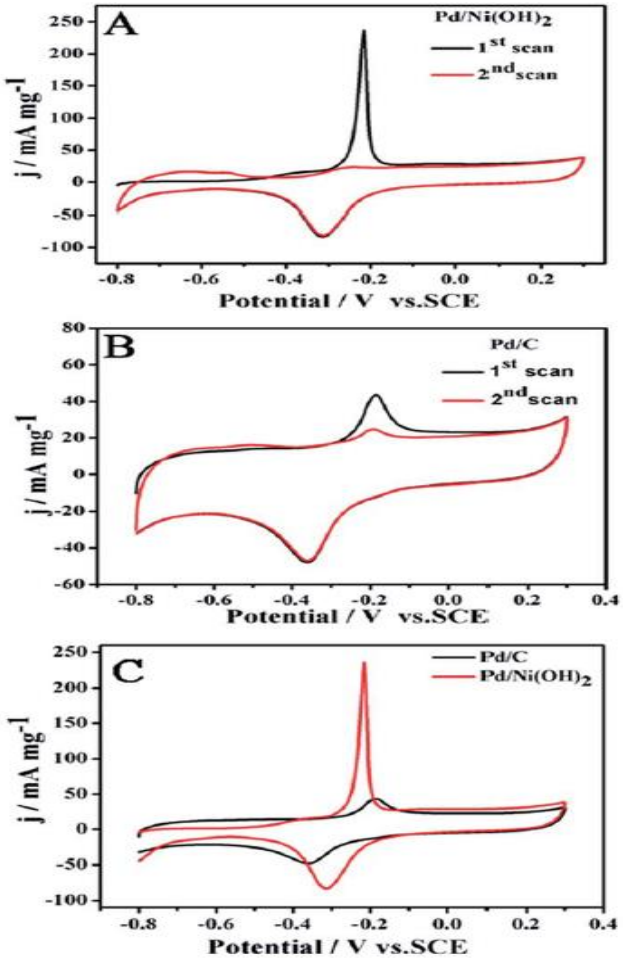

Figure 4.38. CO stripping curves on A) Pd/Ni(OH)2, B) Pd/C in 1M KOH solution at a scanning rate of 50 mV s-1, C) the comparison of CO stripping voltammograms of the Pd/Ni(OH)2 and Pd/C catalysts [277].

Finally, as shown in **Figure 4.38 C)** in which the first scans in the positive direction are compared, the onset potential of carbon monoxide oxidation for the Pd/Ni(OH)2 catalyst is -0.43 V which is more negative than the corresponding value for the commercial catalyst which is -0.31 V.

Chapter 5

CONCLUSION

The greenhouse effect is getting worse over time due to the presence of pollutants in the atmosphere produced by human activities. Many of our daily activities such as our personal transportation use energy conversion machines such as internal combustion engines. As a result, the European Union and other global organizations are moving rapidly to make it possible to get rid of fossil fuels for many processes as far as possible. Hydrogen is a good alternative to fossil fuels because it does not produce CO, CO_2 and SO_2 during combustion but only water. In particular, when the water electrolysis electricity is wisely supplied by renewable energy sources, such as wind turbines In particular, when hydrogen is a product of water electrolysis with the electricity for electrolysis being provided by renewable energy sources such as wind turbines, then hydrogen is considered a green fuel. Ethanol can also be considered an environmentally friendly fuel when derived from biomass. The process of extraction from biomass involves the use of enzymes to convert sugars into alcohols including ethanol. Depending on the region of origin of the biomass and its composition, its quality can be significantly affected. The resulting ethanol is called bioethanol and can be used in fuel cells in order to produce electricity to power a vehicle through the corresponding reactions.

The scientific community is called upon to design and build the best, most efficient and safest possible machines for widespread use. Energy storage, conversion and supply devices such as batteries have been extensively studied to be used in everyday appliances as the main energy systems or in combination with other devices such as fuel cells. Lithium-ion batteries are currently the most widespread because of their very good characteristics such as high energy density and high power density. Others equally important are lithium-air and metal-air batteries.

Fuel cells are electrochemical cells that can use fuels such as ethanol and hydrogen and convert the chemical energy into electricity which in turn can be used to power passenger vehicles. Therefore, if the ethanol comes from renewable sources such as biomass, then they can operate with a renewable and more environmentally friendly fuel since bioethanol is CO_2-neutral. Fuel cells can be divided according to operating temperature into high and low temperature fuel cells. Also depending on the membrane they use, they can be divided into proton exchange membrane fuel cells and anion exchange membrane fuel cells.

In order to improve fuel cells and enable their widespread use in everyday applications, it is necessary to study materials that will enhance the rate and performance of the reactions. In proton

exchange membrane fuel cells more study has been done and it has been shown that platinum-based catalysts are ideal both in performance and in the stability they offer over time. In contrast, in direct-ethanol anion exchange membrane fuel cells, there are few reports on the most ideal catalyst materials that improve ethanol oxidation reaction performance, stability and enhance tolerance to intermediates caused by incomplete ethanol oxidation reaction. In an alkaline medium palladium-based catalysts show better properties in contrast to acidic cells where platinum-based catalysts were better. These catalysts can be divided into monometallic, bimetallic and trimetallic catalysts depending on the number of elements they contain. In this thesis, an attempt was made to understand the basic principles of operation of the most important catalysts currently being studied.

First, an attempt was made to compare Pd with Pt by citing important studies by other researchers. As it turned out, in alkaline media, palladium showed better properties exhibiting higher activity towards the ethanol oxidation reaction. Various bimetallic catalysts were then examined for their main characteristics by investigating the most important factors, such as their performance in terms of EOR and the stability they impart over time and significant results were obtained. In particular, concerning the Pt:Pd composite catalysts all the studied contents showed better activity towards EOR while at the same time, the Pt_3Pd_2 catalyst retained most of its initial performance after the passage of 20 cycles demonstrating that it exhibits the highest resistance to poisoning for the specific Pt:Pd catalysts. Next, Pd:Ni catalysts were analyzed where all studied contents showed better performance in terms of alcohol reaction with Pd_2Ni_3/C catalyst having the highest peak current and a more negative onset potential compared to Pd/C exhibiting also greater stability. Next, Pd:Au catalysts were described where investigations showed that they did not show a significant improvement in terms of activity. However, the stability they added to the reaction makes them a good alternative. Regarding the class of bimetallic catalysts, Pd:Sn and Pd:Ru were also examined. The first catalyst showed an improvement in activity in terms of EOR but also improved its stability. In contrast, the addition of Ru leads to lower peaks of current while the reaction starts from more negative potentials. Also, as analysed, it can be concluded that the studied Pd_xRu_y/C catalysts are more prone to poisoning. Then some trimetallic catalysts such as Pd:Ag:Ni and Pd:Au:Ni were investigated. As the results showed, the former exhibited better EOR performance, maintained higher current density and had more negative onset potential than Pd/C. Also, for the second trimetallic catalyst both the performance in terms of ethanol oxidation reaction and current density was better. Finally, the catalysts PdSn-SnO_2/C and Pd/$Ni(OH)_2$ were studied for the same characteristics and important information was extracted. Each catalyst improved both performance and stability compared to Pd/C.

As the time passed and the ongoing evolution of technology, better catalytic materials with enhanced stability and EOR activity are being developed. Therefore, in the future, fuel cells are expected to play the role of a regulator of energy management and supply in everyday applications.

REFERENCES

[1] Z. Qi, Proton exchange membrane fuel cells, CRC Press 2013.

[2] G.M. Andreadis, A.K.M. Podias, P.E. Tsiakaras, The effect of the parasitic current on the Direct Ethanol PEM Fuel Cell Operation, Journal of Power Sources, 181 (2008) 214-227.

[3] D.R. Dekel, Review of cell performance in anion exchange membrane fuel cells, Journal of Power Sources, 375 (2018) 158-169.

[4] E. Antolini, Catalysts for direct ethanol fuel cells, Journal of Power Sources, 170 (2007) 1-12.

[5] M. Shao, Electrocatalysis in Fuel Cells, Mdpi AG2018.

[6] A. Lavacchi, H. Miller, F. Vizza, Nanotechnology in electrocatalysis for energy, Springer2013.

[7] Y. Shi, N. Cai, T. Cao, J. Zhang, High-temperature electrochemical energy conversion and storage: fundamentals and applications, CRC Press2017.

[8] Y. Wu, R. Holze, Electrochemical energy conversion and storage, John Wiley & Sons2021.

[9] V. Neburchilov, J. Zhang, Metal-air and metal-sulfur batteries: fundamentals and applications, CRC Press2016.

[10] Y. Wu, Lithium-ion batteries: Fundamentals and Applications, CRC press2015.

[11] L. An, R. Chen, Y. Li, Flow Cells for Electrochemical Energy Systems: Fundamentals and Applications, Springer International Publishing2023.

[12] V.S. Bagotsky, Fundamentals of Electrochemistry, Wiley2005.

[13] A. Braun, Electrochemical Energy Systems: Foundations, Energy Storage and Conversion, De Gruyter2018.

[14] B. Zhu, R. Raza, L. Fan, C. Sun, Solid Oxide Fuel Cells: From Electrolyte-Based to Electrolyte-Free Devices, Wiley2020.

[15] K. Kendall, M. Kendall, High-Temperature Solid Oxide Fuel Cells for the 21st Century: Fundamentals, Design and Applications, Elsevier Science2015.

[16] A. Albarbar, M. Alrweq, Proton Exchange Membrane Fuel Cells: Design, Modelling and Performance Assessment Techniques, Springer International Publishing2017.

[17] T. Taner, Proton Exchange Membrane Fuel Cell, IntechOpen2018.

[18] J. Thomas, A. Schechter, F. Grynszpan, B. Francis, S. Thomas, Alkaline Anion Exchange Membranes for Fuel Cells: From Tailored Materials to Novel Applications, Wiley2024.

[19] D.P. Wilkinson, J. Zhang, R. Hui, J. Fergus, X. Li, Proton Exchange Membrane Fuel Cells: Materials Properties and Performance, CRC Press2009.

[20] K. Huang, J.B. Goodenough, Solid Oxide Fuel Cell Technology: Principles, Performance and Operations, Elsevier Science2009.

[21] R. O'Hayre, S.W. Cha, W. Colella, F.B. Prinz, Fuel Cell Fundamentals, Wiley2016.

[22] L. Zhang, H. Zhao, D.P. Wilkinson, X. Sun, J. Zhang, Electrochemical water electrolysis: fundamentals and technologies, CRC Press2020.

[23] A. Iulianelli, A. Basile, Advances in hydrogen production, storage and distribution, Elsevier2014.

[24] T.R. Crompton, Battery reference book, Newnes2000.

[25] R. Korthauer, Lithium-ion batteries: basics and applications, Springer2018.

[26] H. Zhang, X. Li, J. Zhang, Redox flow batteries: fundamentals and applications, CRC Press2017.

[27] P.K. Shen, C.Y. Wang, S.P. Jiang, X. Sun, J. Zhang, Electrochemical Energy: Advanced Materials and Technologies, CRC Press2018.

[28] S. Sun, X. Sun, Z. Chen, Y. Liu, D.P. Wilkinson, J. Zhang, Carbon Nanomaterials for Electrochemical Energy Technologies: Fundamentals and Applications, CRC Press2017.

[29] C. Breitkopf, K. Swider-Lyons, Springer Handbook of Electrochemical Energy, Springer Berlin Heidelberg2016.

[30] S. Zhuiykov, Electrochemistry of Zirconia Gas Sensors, CRC Press2007.

[31] L.M. Moretto, K. Kalcher, Environmental analysis by electrochemical sensors and biosensors, Springer2014.

[32] J. Fraden, J. King, Handbook of modern sensors: physics, designs, and applications, Springer2010.

[33] R.G. Akay, A.B. Yurtcan, Direct Liquid Fuel Cells: Fundamentals, Advances and Future, Academic Press2020.

[34] F. Şen, Nanomaterials for Direct Alcohol Fuel Cells: Characterization, Design, and Electrocatalysis, Elsevier Science2021.

[35] Y. Chen, M. Bellini, M. Bevilacqua, P. Fornasiero, A. Lavacchi, H.A. Miller, L. Wang, F. Vizza, Direct Alcohol Fuel Cells: Toward the Power Densities of Hydrogen-Fed Proton Exchange Membrane Fuel Cells, ChemSusChem, 8 (2015) 524-533.

[36] B. Volynets, F. Ein-Mozaffari, Y. Dahman, Biomass processing into ethanol: pretreatment, enzymatic hydrolysis, fermentation, rheology, and mixing, 6 (2017) 1-22.

[37] A. Sharma, V. Pareek, D. Zhang, Biomass pyrolysis—A review of modelling, process parameters and catalytic studies, Renewable and Sustainable Energy Reviews, 50 (2015) 1081-1096.

[38] S. Achinas, G.J.W. Euverink, Consolidated briefing of biochemical ethanol production from lignocellulosic biomass, Electronic Journal of Biotechnology, 23 (2016) 44-53.

[39] A. Devi, A. Singh, S. Bajar, D. Pant, Z.U. Din, Ethanol from lignocellulosic biomass: An in-depth analysis of pre-treatment methods, fermentation approaches and detoxification processes, Journal of Environmental Chemical Engineering, 9 (2021) 105798.

[40] Y. Yun, Alcohol fuels: current status and future direction, Alcohol Fuels-Current Technologies and Future Prospect, (2020).

[41] C.G. Vayenas, S. Bebelis, I.V. Yentekakis, P. Tsiakaras, H. Karasali, Non-Faradaic Electrochemical Modification of Catalytic Activity, Platinum Metals Review, 34 (1990) 122-130.

[42] P. Tsiakaras, C. Athanasiou, G. Marnellos, M. Stoukides, J.E. ten Elshof, H.J.M. Bouwmeester, Methane activation on a La0.6Sr0.4Co0.8Fe0.2O3 perovskite: Catalytic and electrocatalytic results, Applied Catalysis A: General, 169 (1998) 249-261.

[43] P. Tsiakaras, C.G. Vayenas, Oxidative Coupling of CH4 on Ag Catalyst-Electrodes Deposited on ZrO2 (8 mol% Y2O3), Journal of Catalysis, 144 (1993) 333-347.

[44] R. Wu, P. Tsiakaras, P.K. Shen, Facile synthesis of bimetallic Pt-Pd symmetry-broken concave nanocubes and their enhanced activity toward oxygen reduction reaction, Applied Catalysis B: Environmental, 251 (2019) 49-56.

[45] F.J. Rodríguez Varela, O. Savadogo, Ethanol-tolerant Pt-alloy cathodes for direct ethanol fuel cell (DEFC) applications, Asia-Pacific Journal of Chemical Engineering, 4 (2009) 17-24.

[46] A.O. Neto, M. Linardi, D.M. dos Anjos, G. Tremiliosi-Filho, E.V. Spinacé, Electro-oxidation of ethanol on PtSn/CeO2–C electrocatalyst, Journal of Applied Electrochemistry, 39 (2009) 1153-1156.

[47] J.S. Dordick, Biocatalysts for Industry, Springer US2013.

[48] G. de Gonzalo, P.D. de María, Biocatalysis: An Industrial Perspective, Royal Society of Chemistry2017.

[49] C.F. Zinola, Electrocatalysis: Computational, Experimental, and Industrial Aspects, CRC Press2010.

[50] A. Ray, I. Mukhopadhyay, R.K. Pati, Electrocatalysts for Fuel Cells and Hydrogen Evolution: Theory to Design, IntechOpen2018.

[51] V. Sproat, D. LaHurd, Fuel Cell Balance-of-Plant Reliability Testbed Project, Stark State College of Technology, North Canton, OH (United States), 2016.

[52] A.M. Pinto, V.S. Oliveira, D.S.C. Falcão, Direct alcohol fuel cells for portable applications: fundamentals, engineering and advances, Academic Press2018.

[53] K. Matsuoka, Y. Iriyama, T. Abe, M. Matsuoka, Z. Ogumi, Alkaline direct alcohol fuel cells using an anion exchange membrane, Journal of Power Sources, 150 (2005) 27-31.

[54] P. Tsiakaras, A. Demin, Thermodynamic analysis of a solid oxide fuel cell system fuelled by ethanol, Journal of Power Sources, 102 (2001) 210-217.

[55] S.L. Douvartzides, F.A. Coutelieris, P.E. Tsiakaras, On the systematic optimization of ethanol fed SOFC-based electricity generating systems in terms of energy and exergy, Journal of Power Sources, 114 (2003) 203-212.

[56] S. Dwivedi, Solid oxide fuel cell: Materials for anode, cathode and electrolyte, International Journal of Hydrogen Energy, 45 (2020) 23988-24013.

[57] M. Kiani, X.Q. Tian, W. Zhang, Non-precious metal electrocatalysts design for oxygen reduction reaction in polymer electrolyte membrane fuel cells: Recent advances, challenges and future perspectives, Coordination Chemistry Reviews, 441 (2021) 213954.

[58] S.M. Jamil, M.H.D. Othman, M.A. Rahman, J. Jaafar, A.F. Ismail, K. Li, Recent fabrication techniques for micro-tubular solid oxide fuel cell support: A review, Journal of the European Ceramic Society, 35 (2015) 1-22.

[59] S. He, Y. Zou, K. Chen, S.P. Jiang, A critical review of key materials and issues in solid oxide cells, Interdisciplinary Materials, 2 (2023) 111-136.

[60] M.A. Peña, J.L.G. Fierro, Chemical Structures and Performance of Perovskite Oxides, Chemical Reviews, 101 (2001) 1981-2018.

[61] S. Afroze, A. Karim, Q. Cheok, S. Eriksson, A.K. Azad, Latest development of double perovskite electrode materials for solid oxide fuel cells: a review, Frontiers in Energy, 13 (2019) 770-797.

[62] A. Alaswad, A. Omran, J.R. Sodre, T. Wilberforce, G. Pignatelli, M. Dassisti, A. Baroutaji, A.G. Olabi, Technical and Commercial Challenges of Proton-Exchange Membrane (PEM) Fuel Cells, Energies, 2021.

[63] S. Mekhilef, R. Saidur, A. Safari, Comparative study of different fuel cell technologies, Renewable and Sustainable Energy Reviews, 16 (2012) 981-989.

[64] T. Wilberforce, Z. El-Hassan, F. Khatib, A. Al Makky, J. Mooney, A. Barouaji, J.G. Carton, A.-G. Olabi, Development of Bi-polar plate design of PEM fuel cell using CFD techniques, International Journal of Hydrogen Energy, 42 (2017) 25663-25685.

[65] T. Wilberforce, Z. El-Hassan, F.N. Khatib, A. Al Makky, A. Baroutaji, J.G. Carton, A.G. Olabi, Developments of electric cars and fuel cell hydrogen electric cars, International Journal of Hydrogen Energy, 42 (2017) 25695-25734.

[66] L. Osmieri, L. Pezzolato, S. Specchia, Recent trends on the application of PGM-free catalysts at the cathode of anion exchange membrane fuel cells, Current Opinion in Electrochemistry, 9 (2018) 240-256.

[67] M. Hren, M. Božič, D. Fakin, K.S. Kleinschek, S. Gorgieva, Alkaline membrane fuel cells: anion exchange membranes and fuels, Sustainable Energy & Fuels, 5 (2021) 604-637.

[68] H.A. Firouzjaie, W.E. Mustain, Catalytic Advantages, Challenges, and Priorities in Alkaline Membrane Fuel Cells, ACS Catalysis, 10 (2020) 225-234.

[69] M.R. Gerhardt, L.M. Pant, A.Z. Weber, Along-the-Channel Impacts of Water Management and Carbon-Dioxide Contamination in Hydroxide-Exchange-Membrane Fuel Cells: A Modeling Study, Journal of The Electrochemical Society, 166 (2019) F3180.

[70] N. Ziv, W.E. Mustain, D.R. Dekel, The Effect of Ambient Carbon Dioxide on Anion-Exchange Membrane Fuel Cells, ChemSusChem, 11 (2018) 1136-1150.

[71] Y. Zheng, T.J. Omasta, X. Peng, L. Wang, J.R. Varcoe, B.S. Pivovar, W.E. Mustain, Quantifying and elucidating the effect of CO2 on the thermodynamics, kinetics and charge transport of AEMFCs, Energy & Environmental Science, 12 (2019) 2806-2819.

[72] Y. Mun, M.J. Kim, S.-A. Park, E. Lee, Y. Ye, S. Lee, Y.-T. Kim, S. Kim, O.-H. Kim, Y.-H. Cho, Y.-E. Sung, J. Lee, Soft-template synthesis of mesoporous non-precious metal catalyst with Fe-Nx/C active sites for oxygen reduction reaction in fuel cells, Applied Catalysis B: Environmental, 222 (2018) 191-199.

[73] M. Piana, M. Boccia, A. Filpi, E. Flammia, H.A. Miller, M. Orsini, F. Salusti, S. Santiccioli, F. Ciardelli, A. Pucci, H2/air alkaline membrane fuel cell performance and durability, using novel ionomer and non-platinum group metal cathode catalyst, Journal of Power Sources, 195 (2010) 5875-5881.

[74] X. Li, B.N. Popov, T. Kawahara, H. Yanagi, Non-precious metal catalysts synthesized from precursors of carbon, nitrogen, and transition metal for oxygen reduction in alkaline fuel cells, Journal of Power Sources, 196 (2011) 1717-1722.

[75] M.M. Hossen, K. Artyushkova, P. Atanassov, A. Serov, Synthesis and characterization of high performing Fe-N-C catalyst for oxygen reduction reaction (ORR) in Alkaline Exchange Membrane Fuel Cells, Journal of Power Sources, 375 (2018) 214-221.

[76] E. Zoulias, E. Varkaraki, N. Lymberopoulos, C.N. Christodoulou, G.N. Karagiorgis, A review on water electrolysis, Tcjst, 4 (2004) 41-71.

[77] L. Zhang, J. Lu, S. Yin, L. Luo, S. Jing, A. Brouzgou, J. Chen, P.K. Shen, P. Tsiakaras, One-pot synthesized boron-doped RhFe alloy with enhanced catalytic performance for hydrogen evolution reaction, Applied Catalysis B: Environmental, 230 (2018) 58-64.

[78] J. Lu, Z. Tang, L. Luo, S. Yin, P. Kang Shen, P. Tsiakaras, Worm-like S-doped RhNi alloys as highly efficient electrocatalysts for hydrogen evolution reaction, Applied Catalysis B: Environmental, 255 (2019) 117737.

[79] S. Jing, D. Wang, S. Yin, J. Lu, P.K. Shen, P. Tsiakaras, P-doped CNTs encapsulated nickel hybrids with flower-like structure as efficient catalysts for hydrogen evolution reaction, Electrochimica Acta, 298 (2019) 142-149.

[80] C. Yu, J. Lu, L. Luo, F. Xu, P.K. Shen, P. Tsiakaras, S. Yin, Bifunctional catalysts for overall water splitting: CoNi oxyhydroxide nanosheets electrodeposited on titanium sheets, Electrochimica Acta, 301 (2019) 449-457.

[81] Z. Xie, Z. Song, J. Zhao, Y. Li, X. Cai, D. Liu, J. Shen, P. Tsiakaras, CuZr Metal Glass Powder as Electrocatalysts for Hydrogen and Oxygen Evolution Reactions, Catalysts, 2022.

[82] A. Saad, D. Liu, Y. Wu, Z. Song, Y. Li, T. Najam, K. Zong, P. Tsiakaras, X. Cai, Ag nanoparticles modified crumpled borophene supported Co3O4 catalyst showing superior oxygen evolution reaction (OER) performance, Applied Catalysis B: Environmental, 298 (2021) 120529.

[83] S. Peng, F. Gong, L. Li, D. Yu, D. Ji, T. Zhang, Z. Hu, Z. Zhang, S. Chou, Y. Du, S. Ramakrishna, Necklace-like Multishelled Hollow Spinel Oxides with Oxygen Vacancies for Efficient Water Electrolysis, Journal of the American Chemical Society, 140 (2018) 13644-13653.

[84] C. Hu, L. Zhang, J. Gong, Recent progress made in the mechanism comprehension and design of electrocatalysts for alkaline water splitting, Energy & Environmental Science, 12 (2019) 2620-2645.

[85] S. Jiao, X. Fu, S. Wang, Y. Zhao, Perfecting electrocatalysts via imperfections: towards the large-scale deployment of water electrolysis technology, Energy & Environmental Science, 14 (2021) 1722-1770.

[86] Y. Yan, B.Y. Xia, B. Zhao, X. Wang, A review on noble-metal-free bifunctional heterogeneous catalysts for overall electrochemical water splitting, Journal of Materials Chemistry A, 4 (2016) 17587-17603.

[87] M. Carmo, R.C. Sekol, S. Ding, G. Kumar, J. Schroers, A.D. Taylor, Bulk Metallic Glass Nanowire Architecture for Electrochemical Applications, ACS Nano, 5 (2011) 2979-2983.

[88] M.A. Zeeshan, D. Esqué-De Los Ojos, P. Castro-Hartmann, M. Guerrero, J. Nogués, S. Suriñach, M.D. Baró, B.J. Nelson, S. Pané, E. Pellicer, J. Sort, Electrochemically synthesized amorphous and crystalline nanowires: Dissimilar nanomechanical behavior in comparison with homologous flat films, Nanoscale, 8 (2016) 1344-1351.

[89] Y. Liu, J. Liu, S. Sohn, Y. Li, J.J. Cha, J. Schroers, Metallic glass nanostructures of tunable shape and composition, Nature Communications, 6 (2015).

[90] S. Wang, C. Zhang, H. Li, L. Liu, Enhanced electro-catalytic performance of Pd-based amorphous nanoporous structure synthesized by dealloying Pd32Ni48P20 metallic glass, Intermetallics, 87 (2017) 6-12.

[91] S. Mukherjee, R.C. Sekol, M. Carmo, E.I. Altman, A.D. Taylor, J. Schroers, Tunable Hierarchical Metallic-Glass Nanostructures, Advanced Functional Materials, 23 (2013) 2708-2713.

[92] Z. Jia, Q. Wang, L. Sun, L.C. Zhang, G. Wu, J.H. Luan, Z.B. Jiao, A. Wang, S.X. Liang, M. Gu, J. Lu, Attractive In Situ Self-Reconstructed Hierarchical Gradient Structure of Metallic Glass for High Efficiency and Remarkable Stability in Catalytic Performance, Advanced Functional Materials, 29 (2019).

[93] Z. Wang, P. Liu, J. Han, C. Cheng, S. Ning, A. Hirata, T. Fujita, M. Chen, Engineering the internal surfaces of three-dimensional nanoporous catalysts by surfactant-modified dealloying, Nature Communications, 8 (2017).

[94] M.-X. Li, S.-F. Zhao, Z. Lu, A. Hirata, P. Wen, H.-Y. Bai, M. Chen, J. Schroers, Y. Liu, W.-H. Wang, High-temperature bulk metallic glasses developed by combinatorial methods, Nature, 569 (2019) 99-103.

[95] F. Dawood, M. Anda, G.M. Shafiullah, Hydrogen production for energy: An overview, International Journal of Hydrogen Energy, 45 (2020) 3847-3869.

[96] E.S. López-Alonso Conty, A proposed methodology for passive autocatalytic recombiners sizing and location in LWR containments, Industriales, 2016.

[97] I. Vincent, D. Bessarabov, Low cost hydrogen production by anion exchange membrane electrolysis: A review, Renewable and Sustainable Energy Reviews, 81 (2018) 1690-1704.

[98] J. Liu, X. Duan, Z. Yuan, Q. Liu, Q. Tang, Experimental study on the performance, combustion and emission characteristics of a high compression ratio heavy-duty spark-ignition engine fuelled with liquefied methane gas and hydrogen blend, Applied Thermal Engineering, 124 (2017) 585-594.

[99] D. Parra, X. Zhang, C. Bauer, M.K. Patel, An integrated techno-economic and life cycle environmental assessment of power-to-gas systems, Applied Energy, 193 (2017) 440-454.

[100] S.A. Sherif, F. Barbir, T.N. Veziroglu, Wind energy and the hydrogen economy—review of the technology, Solar Energy, 78 (2005) 647-660.

[101] I.P. Jain, Hydrogen the fuel for 21st century, International Journal of Hydrogen Energy, 34 (2009) 7368-7378.

[102] W.G. Colella, M.Z. Jacobson, D.M. Golden, Switching to a U.S. hydrogen fuel cell vehicle fleet: The resultant change in emissions, energy use, and greenhouse gases, Journal of Power Sources, 150 (2005) 150-181.

[103] C. Coutanceau, S. Baranton, Electrochemical conversion of alcohols for hydrogen production: a short overview, WIREs Energy and Environment, 5 (2016) 388-400.

[104] R. Kothari, D. Buddhi, R.L. Sawhney, Comparison of environmental and economic aspects of various hydrogen production methods, Renewable and Sustainable Energy Reviews, 12 (2008) 553-563.

[105] D.B. Myers, G.D. Ariff, B.D. James, J.S. Lettow, C. Thomas, R.C. Kuhn, Cost and performance comparison of stationary hydrogen fueling appliances, The Hydrogen Program Office, (2002) 1-8.

[106] W.G. Colella, Design considerations for effective control of an afterburner sub-system in a combined heat and power (CHP) fuel cell system (FCS), Journal of Power Sources, 118 (2003) 118-128.

[107] W.G. Colella, Modelling results for the thermal management sub-system of a combined heat and power (CHP) fuel cell system (FCS), Journal of Power Sources, 118 (2003) 129-149.

[108] M.Z. Jacobson, G.M. Masters, Exploiting wind versus coal, American Association for the Advancement of Science, 2001, pp. 1438-1438.

[109] G.M. Masters, Renewable and efficient electric power systems, John Wiley & Sons2013.

[110] A.K. Gupta, S. Ibrahim, A. Al Shoaibi, Advances in sulfur chemistry for treatment of acid gases, Progress in Energy and Combustion Science, 54 (2016) 65-92.

[111] J. Huang, I. Dincer, Parametric analysis and assessment of a coal gasification plant for hydrogen production, International Journal of Hydrogen Energy, 39 (2014) 3294-3303.

[112] I. Staffell, D. Scamman, A. Velazquez Abad, P. Balcombe, P.E. Dodds, P. Ekins, N. Shah, K.R. Ward, The role of hydrogen and fuel cells in the global energy system, Energy & Environmental Science, 12 (2019) 463-491.

[113] Y. Manoharan, S.E. Hosseini, B. Butler, H. Alzhahrani, B.T. Senior, T. Ashuri, J. Krohn, Hydrogen Fuel Cell Vehicles; Current Status and Future Prospect, Applied Sciences, 2019.

[114] J.O. Abe, A.P.I. Popoola, E. Ajenifuja, O.M. Popoola, Hydrogen energy, economy and storage: Review and recommendation, International Journal of Hydrogen Energy, 44 (2019) 15072-15086.

[115] J. Ren, N.M. Musyoka, H.W. Langmi, M. Mathe, S. Liao, Current research trends and perspectives on materials-based hydrogen storage solutions: A critical review, International Journal of Hydrogen Energy, 42 (2017) 289-311.

[116] R. Prabhukhot Prachi, M. Wagh Mahesh, C. Gangal Aneesh, A review on solid state hydrogen storage material, Adv. Energy Power, 4 (2016).

[117] P.P. Edwards, V.L. Kuznetsov, W.I.F. David, Hydrogen energy, Philosophical Transactions of the Royal Society A: Mathematical, Physical and Engineering Sciences, 365 (2007) 1043-1056.

[118] Y. Jia, C. Sun, S. Shen, J. Zou, S.S. Mao, X. Yao, Combination of nanosizing and interfacial effect: Future perspective for designing Mg-based nanomaterials for hydrogen storage, Renewable and Sustainable Energy Reviews, 44 (2015) 289-303.

[119] A. Eftekhari, B. Fang, Electrochemical hydrogen storage: Opportunities for fuel storage, batteries, fuel cells, and supercapacitors, International Journal of Hydrogen Energy, 42 (2017) 25143-25165.

[120] Y. Wang, R. Huang, Z. Liu, The Relationship between Structural Intensity and Sound Field Characteristics of Cylindrical Shells, Procedia Engineering, 214 (2017) 41-49.

[121] X. Shan, J.H. Payer, W.D. Jennings, Mechanism of increased performance and durability of Pd-treated metal hydriding alloys, International Journal of Hydrogen Energy, 34 (2009) 363-369.

[122] G.J. Stiegel, M. Ramezan, Hydrogen from coal gasification: An economical pathway to a sustainable energy future, International Journal of Coal Geology, 65 (2006) 173-190.

[123] H. Liang, L. Jia, F. Chen, S. Jing, P. Tsiakaras, A novel efficient electrocatalyst for oxygen reduction and oxygen evolution reaction in Li-O2 batteries: Co/CoSe embedded N, Se co-doped carbon, Applied Catalysis B: Environmental, 317 (2022) 121698.

[124] S. Jing, Y. Zhang, F. Chen, H. Liang, S. Yin, P. Tsiakaras, Novel and highly efficient cathodes for Li-O2 batteries: 3D self-standing NiFe@NC-functionalized N-doped carbon nanonet derived from Prussian blue analogues/biomass composites, Applied Catalysis B: Environmental, 245 (2019) 721-732.

[125] H. Liang, F. Chen, M. Zhang, S. Jing, B. Shen, S. Yin, P. Tsiakaras, Highly performing free standing cathodic electrocatalysts for Li-O2 batteries: CoNiO2 nanoneedle arrays supported on N-doped carbon nanonet, Applied Catalysis A: General, 574 (2019) 114-121.

[126] T. Kim, W. Song, D.-Y. Son, L.K. Ono, Y. Qi, Lithium-ion batteries: outlook on present, future, and hybridized technologies, Journal of Materials Chemistry A, 7 (2019) 2942-2964.

[127] F. Cheng, J. Chen, Metal–air batteries: from oxygen reduction electrochemistry to cathode catalysts, Chemical Society Reviews, 41 (2012) 2172-2192.

[128] S. Jing, Z. Gai, M. Li, S. Tang, S. Ji, H. Liang, F. Chen, S. Yin, P. Tsiakaras, Enhanced electrochemical performance of a Li-O2 battery using Co and N co-doped biochar cathode prepared in molten salt medium, Electrochimica Acta, 410 (2022) 140002.

[129] Y. Yao, F. Wu, Naturally derived nanostructured materials from biomass for rechargeable lithium/sodium batteries, Nano Energy, 17 (2015) 91-103.

[130] X. Zeng, L. Leng, F. Liu, G. Wang, Y. Dong, L. Du, L. Liu, S. Liao, Enhanced Li-O2 battery performance, using graphene-like nori-derived carbon as the cathode and adding LiI in the electrolyte as a promoter, Electrochimica Acta, 200 (2016) 231-238.

[131] G. Zhang, Y. Shi, H. Wang, L. Jiang, X. Yu, S. Jing, S. Xing, P. Tsiakaras, A facile route to achieve ultrafine Fe2O3 nanorods anchored on graphene oxide for application in lithium-ion battery, Journal of Power Sources, 416 (2019) 118-124.

[132] L. Lu, X. Han, J. Li, J. Hua, M. Ouyang, A review on the key issues for lithium-ion battery management in electric vehicles, Journal of Power Sources, 226 (2013) 272-288.

[133] Z. Yadi, J. Jiangmin, Y. An, L. Wu, H. Dou, J. Zhang, Y. Zhang, S. Wu, X. Zhang, M. Dong, Z. Guo, Sodium-ion capacitors: Materials, Mechanism, and Challenges, ChemSusChem, 13 (2020).

[134] X. Chen, W. Shen, T.T. Vo, Z. Cao, A. Kapoor, An overview of lithium-ion batteries for electric vehicles, 2012 10th International Power & Energy Conference (IPEC), 2012, pp. 230-235.

[135] X. Wu, K. Song, X. Zhang, N. Hu, L. Li, W. Li, L. Zhang, H. Zhang, Safety Issues in Lithium Ion Batteries: Materials and Cell Design, Frontiers in Energy Research, 7 (2019).

[136] R. Schröder, M. Aydemir, G. Seliger, Comparatively Assessing different Shapes of Lithium-ion Battery Cells, Procedia Manufacturing, 8 (2017) 104-111.

[137] T. Najam, S.S.A. Shah, L. Peng, M.S. Javed, M. Imran, M.-Q. Zhao, P. Tsiakaras, Synthesis and nano-engineering of MXenes for energy conversion and storage applications: Recent advances and perspectives, Coordination Chemistry Reviews, 454 (2022) 214339.

[138] X. Jiang, Y. Chen, X. Meng, W. Cao, C. Liu, Q. Huang, N. Naik, V. Murugadoss, M. Huang, Z. Guo, The impact of electrode with carbon materials on safety performance of lithium-ion batteries: A review, Carbon, 191 (2022) 448-470.

[139] K.E. Aifantis, S.A. Hackney, R.V. Kumar, High energy density lithium batteries, Wiley Online Library2010.

[140] D. Lyu, S. Yao, A. Ali, Z.Q. Tian, P. Tsiakaras, P.K. Shen, N, S Codoped Carbon Matrix-Encapsulated Co9S8 Nanoparticles as a Highly Efficient and Durable Bifunctional Oxygen Redox Electrocatalyst for Rechargeable Zn–Air Batteries, Advanced Energy Materials, 11 (2021) 2101249.

[141] Y. Wang, Y. Song, Y. Xia, Electrochemical capacitors: mechanism, materials, systems, characterization and applications, Chemical Society Reviews, 45 (2016) 5925-5950.

[142] P. Simon, Y. Gogotsi, Perspectives for electrochemical capacitors and related devices, Nature Materials, 19 (2020) 1151-1163.

[143] R.K. Gupta, Pseudocapacitors: Fundamentals to High Performance Energy Storage Devices, Springer2024.

[144] A. Yu, V. Chabot, J. Zhang, Electrochemical Supercapacitors for Energy Storage and Delivery: Fundamentals and Applications, 2017.

[145] A. Pramitha, Y. Raviprakash, Recent developments and viable approaches for high-performance supercapacitors using transition metal-based electrode materials, Journal of Energy Storage, 49 (2022) 104120.

[146] N. Ma, D. Yang, S. Riaz, L. Wang, K. Wang, Aging Mechanism and Models of Supercapacitors: A Review, Technologies, 2023.

[147] K.K. Kar, Handbook of Nanocomposite Supercapacitor Materials III: Selection, Springer International Publishing2021.

[148] P. Thounthong, S. Raël, B. Davat, Supercapacitors as an energy storage for fuel cell automotive hybrid electrical system, Int. J. Electrical Eng. Transportation, 1 (2005).

[149] T.P. Sumangala, M.S. Sreekanth, A. Rahaman, Applications of Supercapacitors, in: K.K. Kar (Ed.) Handbook of Nanocomposite Supercapacitor Materials III: Selection, Springer International Publishing, Cham, 2021, pp. 367-393.

[150] Y. Liu, S.P. Jiang, Z. Shao, Intercalation pseudocapacitance in electrochemical energy storage: recent advances in fundamental understanding and materials development, Materials Today Advances, 7 (2020) 100072.

[151] E. Gorbova, G. Balkourani, C. Molochas, D. Sidiropoulos, A. Brouzgou, A. Demin, P. Tsiakaras, Brief Review on High-Temperature Electrochemical Hydrogen Sensors, Catalysts, 2022.

[152] A. Kalyakin, A.K. Demin, E. Gorbova, A. Volkov, P.E. Tsiakaras, Sensor Based on a Solid Oxide Electrolyte for Measuring the Water-Vapor and Hydrogen Content in Air, Catalysts, 2022.

[153] G. Balkourani, A. Brouzgou, C.L. Vecchio, A.S. Aricò, V. Baglio, P. Tsiakaras, Selective electro-oxidation of dopamine on Co or Fe supported onto N-doped ketjenblack, Electrochimica Acta, 409 (2022) 139943.

[154] E. Gorbova, F. Tzorbatzoglou, C. Molochas, D. Chloros, A. Demin, P. Tsiakaras, Fundamentals and Principles of Solid-State Electrochemical Sensors for High Temperature Gas Detection, Catalysts, 2022.

[155] J. Fouletier, Gas analysis with potentiometric sensors. a review, Sensors and Actuators, 3 (1982) 295-314.

[156] W.C. Maskell, B.C.H. Steele, Solid state potentiometric oxygen gas sensors, Journal of Applied Electrochemistry, 16 (1986) 475-489.

[157] W.C. Maskell, Inorganic solid state chemically sensitive devices: electrochemical oxygen gas sensors, Journal of Physics E: Scientific Instruments, 20 (1987) 1156.

[158] T. Takeuchi, Oxygen sensors, Sensors and Actuators, 14 (1988) 109-124.

[159] W. Göpel, G. Reinhardt, M. Rösch, Trends in the development of solid state amperometric and potentiometric high temperature sensors, Solid State Ionics, 136-137 (2000) 519-531.

[160] R. Ramamoorthy, P.K. Dutta, S.A. Akbar, Oxygen sensors: Materials, methods, designs and applications, Journal of Materials Science, 38 (2003) 4271-4282.

[161] R. Ramamoorthy, S.A. Akbar, P.K. Dutta, Dependence of potentiometric oxygen sensing characteristics on the nature of electrodes, Sensors and Actuators B: Chemical, 113 (2006) 162-168.

[162] S. Akbar, P. Dutta, C. Lee, High-Temperature Ceramic Gas Sensors: A Review, International Journal of Applied Ceramic Technology, 3 (2006) 302-311.

[163] U. Guth, W. Vonau, J. Zosel, Recent developments in electrochemical sensor application and technology—a review, Measurement Science and Technology, 20 (2009) 042002.

[164] Y. Liu, J. Parisi, X. Sun, Y. Lei, Solid-state gas sensors for high temperature applications – a review, Journal of Materials Chemistry A, 2 (2014) 9919-9943.

[165] T. Liu, X. Zhang, L. Yuan, J. Yu, A review of high-temperature electrochemical sensors based on stabilized zirconia, Solid State Ionics, 283 (2015) 91-102.

[166] A. Kalyakin, A. Volkov, A. Demin, E. Gorbova, P. Tsiakaras, Determination of nitrous oxide concentration using a solid-electrolyte amperometric sensor, Sensors and Actuators B: Chemical, 297 (2019) 126750.

[167] G. Fadeyev, A. Kalyakin, E. Gorbova, A. Brouzgou, A. Demin, A. Volkov, P. Tsiakaras, A simple and low-cost amperometric sensor for measuring H2, CO, and CH4, Sensors and Actuators B: Chemical, 221 (2015) 879-883.

[168] G. Fadeyev, A. Kalakin, A. Demin, A. Volkov, A. Brouzgou, P. Tsiakaras, Electrodes for solid electrolyte sensors for the measurement of CO and H2 content in air, International Journal of Hydrogen Energy, 38 (2013) 13484-13490.

[169] P. Mohankumar, J. Ajayan, R. Yasodharan, P. Devendran, R. Sambasivam, A review of micromachined sensors for automotive applications, Measurement, 140 (2019) 305-322.

[170] N.V. Krishna Prasad, K. Venkata Prasad, S. Ramesh, S.V. Phanidhar, K. Venkata Ratnam, S. Janardhan, H. Manjunatha, M.S.S.R.K.N. Sarma, K. Srinivas, Ceramic Sensors: A mini-review of their applications, Frontiers in Materials, 7 (2020).

[171] S. Aravind, P. Ragupathi, D.S. Kumar, G. Vignesh, A Numerical Investigation of Automotive Lambda Sensor to Improve the Life Span of the Sensor using CFD, IOP Conference Series: Materials Science and Engineering, 923 (2020) 012003.

[172] Y. Villasana, N. Moradi, C. Navas-Cárdenas, G.S. Patience, Experimental methods in chemical engineering: pH, The Canadian Journal of Chemical Engineering, 100 (2022) 1703-1717.

[173] O. Smutok, E. Katz, Electroanalytical instrumentation—how it all started: history of electrochemical instrumentation, Journal of Solid State Electrochemistry, (2023).

[174] O.N. de Oliveira, F.L.G. Marystela, F. de Lima Leite, A.L. Da Róz, Nanoscience and its Applications, Elsevier Science2016.

[175] H.-L. Chou, B.-J. Hwang, C.-L. Sun, Chapter 9 - Catalysis in Fuel Cells and Hydrogen Production, in: S.L. Suib (Ed.) New and Future Developments in Catalysis, Elsevier, Amsterdam, 2013, pp. 217-270.

[176] E.B. Creel, X. Lyu, G. McCool, R.J. Ouimet, A. Serov, Protocol for Screening Water Oxidation or Reduction Electrocatalyst Activity in a Three-Electrode Cell for Alkaline Exchange Membrane Electrolysis, Frontiers in Energy Research, 10 (2022).

[177] T. Krummrein, M. Henke, P. Kutne, M. Aigner, Numerical analysis of operating range and SOFC-off-gas combustor requirements of a biogas powered SOFC-MGT hybrid power plant, Applied Energy, 232 (2018) 598-606.

[178] Y. Lu, Y. Cai, L. Souamy, X. Song, L. Zhang, J. Wang, Solid oxide fuel cell technology for sustainable development in China: An over-view, International Journal of Hydrogen Energy, 43 (2018) 12870-12891.

[179] T. Lan, K. Strunz, Multiphysics Transients Modeling of Solid Oxide Fuel Cells: Methodology of Circuit Equivalents and Use in EMTP-Type Power System Simulation, IEEE Transactions on Energy Conversion, 32 (2017) 1309-1321.

[180] Z. Dimitrova, Fuel cell electric vehicles. Investigation of the energy balance for optimal reforming process of bio-ethanol, IOP Conference Series: Materials Science and Engineering, 1002 (2020) 012025.

[181] S. Ma, M. Lin, T.-E. Lin, T. Lan, X. Liao, F. Maréchal, J. Van herle, Y. Yang, C. Dong, L. Wang, Fuel cell-battery hybrid systems for mobility and off-grid applications: A review, Renewable and Sustainable Energy Reviews, 135 (2021) 110119.

[182] H. Chehrmonavari, A. Kakaee, S.E. Hosseini, U. Desideri, G. Tsatsaronis, G. Floerchinger, R. Braun, A. Paykani, Hybridizing solid oxide fuel cells with internal combustion engines for power and propulsion systems: A review, Renewable and Sustainable Energy Reviews, 171 (2023) 112982.

[183] S. Ma, X. Hu, Y. Zhao, X. Wang, C. Dong, Design and Evaluation of a Metal-Supported Solid Oxide Fuel Cell Vehicle Power System with Bioethanol Onboard Reforming, ACS Omega, 6 (2021) 29201-29214.

[184] W. Cai, F. Wang, E. Zhan, A.C. Van Veen, C. Mirodatos, W. Shen, Hydrogen production from ethanol over Ir/CeO2 catalysts: A comparative study of steam reforming, partial oxidation and oxidative steam reforming, Journal of Catalysis, 257 (2008) 96-107.

[185] E.I. Ortiz-Rivera, A.L. Reyes-Hernandez, R.A. Febo, Understanding the history of fuel cells, 2007 IEEE Conference on the History of Electric Power, 2007, pp. 117-122.

[186] J.M. Andújar, F. Segura, Fuel cells: History and updating. A walk along two centuries, Renewable and Sustainable Energy Reviews, 13 (2009) 2309-2322.

[187] S. Song, P. Tsiakaras, Recent progress in direct ethanol proton exchange membrane fuel cells (DE-PEMFCs), Applied Catalysis B: Environmental, 63 (2006) 187-193.

[188] J. Zhang, PEM Fuel Cell Electrocatalysts and Catalyst Layers: Fundamentals and Applications, Springer London2008.

[189] J. Durst, C. Simon, F. Hasché, H.A. Gasteiger, Hydrogen Oxidation and Evolution Reaction Kinetics on Carbon Supported Pt, Ir, Rh, and Pd Electrocatalysts in Acidic Media, Journal of The Electrochemical Society, 162 (2015) F190.

[190] F. Tzorbatzoglou, A. Brouzgou, P. Tsiakaras, Electrocatalytic activity of Vulcan-XC-72 supported Pd, Rh and PdxRhy toward HOR and ORR, Applied Catalysis B: Environmental, 174-175 (2015) 203-211.

[191] S.M.M. Ehteshami, Q. Jia, A. Halder, S.H. Chan, S. Mukerjee, The role of electronic properties of Pt and Pt alloys for enhanced reformate electro-oxidation in polymer electrolyte membrane fuel cells, Electrochimica Acta, 107 (2013) 155-163.

[192] Z.X. Liang, T.S. Zhao, Catalysts for Alcohol-Fuelled Direct Oxidation Fuel Cells, Royal Society of Chemistry2012.

[193] S.P.S. Badwal, S. Giddey, A. Kulkarni, J. Goel, S. Basu, Direct ethanol fuel cells for transport and stationary applications – A comprehensive review, Applied Energy, 145 (2015) 80-103.

[194] A. Brouzgou, A. Podias, P. Tsiakaras, PEMFCs and AEMFCs directly fed with ethanol: a current status comparative review, Journal of Applied Electrochemistry, 43 (2013) 119-136.

[195] Y. Chen, Fundamental Studies of Ethanol Oxidation Reaction in Direct Ethanol Fuel Cells Using Density Functional Theory (DFT) Calculations, Loughborough University2020.

[196] L. An, T.S. Zhao, Y.S. Li, Carbon-neutral sustainable energy technology: Direct ethanol fuel cells, Renewable and Sustainable Energy Reviews, 50 (2015) 1462-1468.

[197] H.R. Corti, E.R. Gonzalez, Direct alcohol fuel cells, Materials, Performance, Durability and Applications, Springer, Amsterdam, (2014).

[198] S. Song, W. Zhou, Z. Liang, R. Cai, G. Sun, Q. Xin, V. Stergiopoulos, P. Tsiakaras, The effect of methanol and ethanol cross-over on the performance of PtRu/C-based anode DAFCs, Applied Catalysis B: Environmental, 55 (2005) 65-72.

[199] J. Ling, G. Longtin, O. Savadogo, Comparison of ethanol and methanol crossover through different MEA components and structures by cyclic voltammetry, Asia-Pacific Journal of Chemical Engineering, 4 (2009) 25-32.

[200] S. Song, G. Wang, W. Zhou, X. Zhao, G. Sun, Q. Xin, S. Kontou, P. Tsiakaras, The effect of the MEA preparation procedure on both ethanol crossover and DEFC performance, Journal of Power Sources, 140 (2005) 103-110.

[201] T. Lopes, E. Antolini, E.R. Gonzalez, Carbon supported Pt–Pd alloy as an ethanol tolerant oxygen reduction electrocatalyst for direct ethanol fuel cells, International Journal of Hydrogen Energy, 33 (2008) 5563-5570.

[202] F. Colmati, E. Antolini, E.R. Gonzalez, Effect of temperature on the mechanism of ethanol oxidation on carbon supported Pt, PtRu and Pt3Sn electrocatalysts, Journal of Power Sources, 157 (2006) 98-103.

[203] H. Pramanik, S. Basu, A Study on Process Parameters of Direct Ethanol Fuel Cell, The Canadian Journal of Chemical Engineering, 85 (2007) 781-785.

[204] H. Pramanik, A.A. Wragg, S. Basu, Studies of some operating parameters and cyclic voltammetry for a direct ethanol fuel cell, Journal of Applied Electrochemistry, 38 (2008) 1321-1328.

[205] H. Pramanik, S. Basu, Modeling and experimental validation of overpotentials of a direct ethanol fuel cell, Chemical Engineering and Processing: Process Intensification, 49 (2010) 635-642.

[206] J. Tayal, B. Rawat, S. Basu, Bi-metallic and tri-metallic Pt–Sn/C, Pt–Ir/C, Pt–Ir–Sn/C catalysts for electro-oxidation of ethanol in direct ethanol fuel cell, International Journal of Hydrogen Energy, 36 (2011) 14884-14897.

[207] J. Tayal, B. Rawat, S. Basu, Effect of addition of rhenium to Pt-based anode catalysts in electro-oxidation of ethanol in direct ethanol PEM fuel cell, International Journal of Hydrogen Energy, 37 (2012) 4597-4605.

[208] J. Goel, S. Basu, Pt-Re-Sn as Metal Catalysts for Electro-Oxidation of Ethanol in Direct Ethanol Fuel Cell, Energy Procedia, 28 (2012) 66-77.

[209] Y. Wang, Nanomaterials for Direct Alcohol Fuel Cell, Jenny Stanford Publishing2016.

[210] H. Li, G. Sun, L. Cao, L. Jiang, Q. Xin, Comparison of different promotion effect of PtRu/C and PtSn/C electrocatalysts for ethanol electro-oxidation, Electrochimica Acta, 52 (2007) 6622-6629.

[211] Z.F. Pan, R. Chen, L. An, Y.S. Li, Alkaline anion exchange membrane fuel cells for cogeneration of electricity and valuable chemicals, Journal of Power Sources, 365 (2017) 430-445.

[212] F.J. Rodríguez-Varela, T.W. Napporn, Advanced Electrocatalysts for Low-Temperature Fuel Cells, Springer International Publishing2018.

[213] E.A. Monyoncho, T.K. Woo, E.A. Baranova, Ethanol electrooxidation reaction in alkaline media for direct ethanol fuel cells, in: C. Banks, S. McIntosh (Eds.) Electrochemistry: Volume 15, The Royal Society of Chemistry2018, pp. 0.

[214] M. Roschger, S. Wolf, K. Mayer, M. Singer, V. Hacker, Alkaline Direct Ethanol Fuel Cell: Effect of the Anode Flow Field Design and the Setup Parameters on Performance, Energies, 2022.

[215] Y. Li, Challenges and Perspectives in Alkaline Direct Ethanol Fuel Cells, in: L. An, T.S. Zhao (Eds.) Anion Exchange Membrane Fuel Cells: Principles, Materials and Systems, Springer International Publishing, Cham, 2018, pp. 325-346.

[216] D.M. Fadzillah, S.K. Kamarudin, M.A. Zainoodin, M.S. Masdar, Critical challenges in the system development of direct alcohol fuel cells as portable power supplies: An overview, International Journal of Hydrogen Energy, 44 (2019) 3031-3054.

[217] E.H. Yu, U. Krewer, K. Scott, Principles and Materials Aspects of Direct Alkaline Alcohol Fuel Cells, Energies, 2010, pp. 1499-1528.

[218] K.I. Ozoemena, Nanostructured platinum-free electrocatalysts in alkaline direct alcohol fuel cells: catalyst design, principles and applications, RSC Advances, 6 (2016) 89523-89550.

[219] C.-C. Yang, S.-J. Chiu, W.-C. Chien, Development of alkaline direct methanol fuel cells based on crosslinked PVA polymer membranes, Journal of Power Sources, 162 (2006) 21-29.

[220] C.-C. Yang, Y.-J. Lee, S.-J. Chiu, K.-T. Lee, W.-C. Chien, C.-T. Lin, C.-A. Huang, Preparation of a PVA/HAP composite polymer membrane for a direct ethanol fuel cell (DEFC), Journal of Applied Electrochemistry, 38 (2008) 1329-1337.

[221] H. Hou, G. Sun, R. He, Z. Wu, B. Sun, Alkali doped polybenzimidazole membrane for high performance alkaline direct ethanol fuel cell, Journal of Power Sources, 182 (2008) 95-99.

[222] H. Hou, S. Wang, W. Jin, Q. Jiang, L. Sun, L. Jiang, G. Sun, KOH modified Nafion112 membrane for high performance alkaline direct ethanol fuel cell, International Journal of Hydrogen Energy, 36 (2011) 5104-5109.

[223] F. Inambao, Bioethanol Technologies, IntechOpen2021.

[224] C. Wyman, Handbook on Bioethanol: Production and Utilization, Taylor & Francis1996.

[225] B. Gabrielle, N. Gagnaire, Life-cycle assessment of straw use in bio-ethanol production: A case study based on biophysical modelling, Biomass and Bioenergy, 32 (2008) 431-441.

[226] J.Y. Zhu, X.J. Pan, Woody biomass pretreatment for cellulosic ethanol production: Technology and energy consumption evaluation, Bioresource Technology, 101 (2010) 4992-5002.

[227] P. Rosha, F.M. Ali, H. Ibrahim, Recent advances in hydrogen production through catalytic steam reforming of ethanol: Advances in catalytic design, The Canadian Journal of Chemical Engineering, 101 (2023) 5498-5518.

[228] Ó.J. Sánchez, C.A. Cardona, Trends in biotechnological production of fuel ethanol from different feedstocks, Bioresource Technology, 99 (2008) 5270-5295.

[229] A. Demirbas, Biofuels securing the planet's future energy needs, Energy Conversion and Management, 50 (2009) 2239-2249.

[230] C. Xu, L. Cheng, P. Shen, Y. Liu, Methanol and ethanol electrooxidation on Pt and Pd supported on carbon microspheres in alkaline media, Electrochemistry Communications, 9 (2007) 997-1001.

[231] E.H. Yu, X. Wang, U. Krewer, L. Li, K. Scott, Direct oxidation alkaline fuel cells: from materials to systems, Energy & Environmental Science, 5 (2012) 5668-5680.

[232] B. Lan, Q.-L. Wang, Z.-X. Ma, Y.-J. Wu, X.-L. Jiang, W.-S. Jia, C.-X. Zhou, Y.-Y. Yang, Efficient electrochemical ethanol-to-CO2 conversion at rhodium and bismuth hydroxide interfaces, Applied Catalysis B: Environmental, 300 (2022) 120728.

[233] M.A.F. Akhairi, S.K. Kamarudin, Catalysts in direct ethanol fuel cell (DEFC): An overview, International Journal of Hydrogen Energy, 41 (2016) 4214-4228.

[234] Y. Chen, L. Zhuang, J. Lu, Non-Pt Anode Catalysts for Alkaline Direct Alcohol Fuel Cells, Chinese Journal of Catalysis, 28 (2007) 870-874.

[235] Y.-Y. Feng, Z.-H. Liu, W.-Q. Kong, Q.-Y. Yin, L.-X. Du, Promotion of palladium catalysis by silver for ethanol electro-oxidation in alkaline electrolyte, International Journal of Hydrogen Energy, 39 (2014) 2497-2504.

[236] J.B. Xu, T.S. Zhao, Y.S. Li, W.W. Yang, Synthesis and characterization of the Au-modified Pd cathode catalyst for alkaline direct ethanol fuel cells, International Journal of Hydrogen Energy, 35 (2010) 9693-9700.

[237] C.-C. Yang, S.-J. Chiu, K.-T. Lee, W.-C. Chien, C.-T. Lin, C.-A. Huang, Study of poly(vinyl alcohol)/titanium oxide composite polymer membranes and their application on alkaline direct alcohol fuel cell, Journal of Power Sources, 184 (2008) 44-51.

[238] S. Jadali, M.A. Kamyabi, J. Solla-Gullón, E. Herrero, Effect of Pd on the Electrocatalytic Activity of Pt towards Oxidation of Ethanol in Alkaline Solutions, Applied Sciences, 2021.

[239] Z. Zhang, L. Xin, K. Sun, W. Li, Pd–Ni electrocatalysts for efficient ethanol oxidation reaction in alkaline electrolyte, International Journal of Hydrogen Energy, 36 (2011) 12686-12697.

[240] R. Carrera-Cerritos, R. Fuentes-Ramírez, F.M. Cuevas-Muñiz, J. Ledesma-García, L.G. Arriaga, Performance and stability of Pd nanostructures in an alkaline direct ethanol fuel cell, Journal of Power Sources, 269 (2014) 370-378.

[241] L. Ma, D. Chu, R. Chen, Comparison of ethanol electro-oxidation on Pt/C and Pd/C catalysts in alkaline media, International Journal of Hydrogen Energy, 37 (2012) 11185-11194.

[242] S.Y. Shen, T.S. Zhao, J.B. Xu, Y.S. Li, Synthesis of PdNi catalysts for the oxidation of ethanol in alkaline direct ethanol fuel cells, Journal of Power Sources, 195 (2010) 1001-1006.

[243] Y.S. Li, T.S. Zhao, A high-performance integrated electrode for anion-exchange membrane direct ethanol fuel cells, International Journal of Hydrogen Energy, 36 (2011) 7707-7713.

[244] L. Ma, H. He, A. Hsu, R. Chen, PdRu/C catalysts for ethanol oxidation in anion-exchange membrane direct ethanol fuel cells, Journal of Power Sources, 241 (2013) 696-702.

[245] H. Mao, L. Wang, P. Zhu, Q. Xu, Q. Li, Carbon-supported PdSn–SnO2 catalyst for ethanol electro-oxidation in alkaline media, International Journal of Hydrogen Energy, 39 (2014) 17583-17588.

[246] J. Cai, Y. Huang, Y. Guo, Bi-modified Pd/C catalyst via irreversible adsorption and its catalytic activity for ethanol oxidation in alkaline medium, Electrochimica Acta, 99 (2013) 22-29.

[247] P.-C. Su, H.-S. Chen, T.-Y. Chen, C.-W. Liu, C.-H. Lee, J.-F. Lee, T.-S. Chan, K.-W. Wang, Enhancement of electrochemical properties of Pd/C catalysts toward ethanol oxidation reaction in alkaline solution through Ni and Au alloying, International Journal of Hydrogen Energy, 38 (2013) 4474-4482.

[248] C. Busó-Rogero, J. Solla-Gullón, F.J. Vidal-Iglesias, E. Herrero, J.M. Feliu, Oxidation of ethanol on platinum nanoparticles: surface structure and aggregation effects in alkaline medium, Journal of Solid State Electrochemistry, 20 (2016) 1095-1106.

[249] J. Fan, K. Qi, L. Zhang, H. Zhang, S. Yu, X. Cui, Engineering Pt/Pd Interfacial Electronic Structures for Highly Efficient Hydrogen Evolution and Alcohol Oxidation, ACS Applied Materials & Interfaces, 9 (2017) 18008-18014.

[250] F.J. Vidal-Iglesias, R.M. Arán-Ais, J. Solla-Gullón, E. Herrero, J.M. Feliu, Electrochemical Characterization of Shape-Controlled Pt Nanoparticles in Different Supporting Electrolytes, ACS Catalysis, 2 (2012) 901-910.

[251] S. Guerin, G.S. Attard, Electrochemical behaviour of electrodeposited nanostructured palladium+platinum films in 2 M H2SO4, Electrochemistry Communications, 3 (2001) 544-548.

[252] N. Alexeyeva, A. Sarapuu, K. Tammeveski, F.J. Vidal-Iglesias, J. Solla-Gullón, J.M. Feliu, Electroreduction of oxygen on Vulcan carbon supported Pd nanoparticles and Pd–M nanoalloys in acid and alkaline solutions, Electrochimica Acta, 56 (2011) 6702-6708.

[253] H. Erikson, A. Sarapuu, N. Alexeyeva, K. Tammeveski, J. Solla-Gullón, J.M. Feliu, Electrochemical reduction of oxygen on palladium nanocubes in acid and alkaline solutions, Electrochimica Acta, 59 (2012) 329-335.

[254] R.K. Pandey, V. Lakshminarayanan, Electro-Oxidation of Formic Acid, Methanol, and Ethanol on Electrodeposited Pd-Polyaniline Nanofiber Films in Acidic and Alkaline Medium, The Journal of Physical Chemistry C, 113 (2009) 21596-21603.

[255] R. Jiang, D.T. Tran, J.P. McClure, D. Chu, A Class of (Pd–Ni–P) Electrocatalysts for the Ethanol Oxidation Reaction in Alkaline Media, ACS Catalysis, 4 (2014) 2577-2586.

[256] Q. He, W. Chen, S. Mukerjee, S. Chen, F. Laufek, Carbon-supported PdM (M=Au and Sn) nanocatalysts for the electrooxidation of ethanol in high pH media, Journal of Power Sources, 187 (2009) 298-304.

[257] L.D. Zhu, T.S. Zhao, J.B. Xu, Z.X. Liang, Preparation and characterization of carbon-supported sub-monolayer palladium decorated gold nanoparticles for the electro-oxidation of ethanol in alkaline media, Journal of Power Sources, 187 (2009) 80-84.

[258] S. Shen, Y. Guo, L. Luo, F. Li, L. Li, G. Wei, J. Yin, C. Ke, J. Zhang, Comprehensive Analysis on the Highly Active and Stable PdAu/C Electrocatalyst for Ethanol Oxidation Reaction in Alkaline Media, The Journal of Physical Chemistry C, 122 (2018) 1604-1611.

[259] A.M. Makin Adam, A. Zhu, L. Ning, M. Deng, Q. Zhang, Q. Liu, Carbon supported PdSn nanocatalysts with enhanced performance for ethanol electrooxidation in alkaline medium, International Journal of Hydrogen Energy, 44 (2019) 20368-20378.

[260] L.M. Palma, T.S. Almeida, A.R. de Andrade, Comparative study of catalyst effect on ethanol electrooxidation in alkaline medium: Pt- and Pd-based catalysts containing Sn and Ru, Journal of Electroanalytical Chemistry, 878 (2020) 114592.

[261] A.N. Geraldes, D. Furtunato da Silva, J.C. Martins da Silva, O. Antonio de Sá, E.V. Spinacé, A.O. Neto, M. Coelho dos Santos, Palladium and palladium–tin supported on multi wall carbon nanotubes or carbon for alkaline direct ethanol fuel cell, Journal of Power Sources, 275 (2015) 189-199.

[262] W. Du, K.E. Mackenzie, D.F. Milano, N.A. Deskins, D. Su, X. Teng, Palladium–Tin Alloyed Catalysts for the Ethanol Oxidation Reaction in an Alkaline Medium, ACS Catalysis, 2 (2012) 287-297.

[263] R. Chen, J. Qi, J. Guo, P. Schubert, J. Hyden, E.J. Taylor, Tolerance of Impurities in Bioethanol on Pd/C and Pdru/C Catalysts Toward the Ethanol Oxidation Reaction in Alkaline Media, ECS Meeting Abstracts, MA2016-01 (2016) 1769.

[264] J. Torrero, M. Montiel, M.A. Peña, P. Ocón, S. Rojas, Insights on the electrooxidation of ethanol with Pd-based catalysts in alkaline electrolyte, International Journal of Hydrogen Energy, 44 (2019) 31995-32002.

[265] J. Guo, R. Chen, F.-C. Zhu, S.-G. Sun, H.M. Villullas, New understandings of ethanol oxidation reaction mechanism on Pd/C and Pd2Ru/C catalysts in alkaline direct ethanol fuel cells, Applied Catalysis B: Environmental, 224 (2018) 602-611.

[266] P. Kurzweil, Precious metal oxides for electrochemical energy converters: Pseudocapacitance and pH dependence of redox processes, Journal of Power Sources, 190 (2009) 189-200.

[267] H.A. Gasteiger, N. Markovic, P.N. Ross, Jr., E.J. Cairns, Methanol electrooxidation on well-characterized platinum-ruthenium bulk alloys, The Journal of Physical Chemistry, 97 (1993) 12020-12029.

[268] Z.-Y. Zhou, Q. Wang, J.-L. Lin, N. Tian, S.-G. Sun, In situ FTIR spectroscopic studies of electrooxidation of ethanol on Pd electrode in alkaline media, Electrochimica Acta, 55 (2010) 7995-7999.

[269] L. Jiang, A. Hsu, D. Chu, R. Chen, Ethanol electro-oxidation on Pt/C and PtSn/C catalysts in alkaline and acid solutions, International Journal of Hydrogen Energy, 35 (2010) 365-372.

[270] A. Elsheikh, J. McGregor, Synthesis and Characterization of PdAgNi/C Trimetallic Nanoparticles for Ethanol Electrooxidation, Nanomaterials, 2021.

[271] R.S. Amin, R.M. Abdel Hameed, K.M. El-Khatib, M. Elsayed Youssef, Electrocatalytic activity of nanostructured Ni and Pd–Ni on Vulcan XC-72R carbon black for methanol oxidation in alkaline medium, International Journal of Hydrogen Energy, 39 (2014) 2026-2041.

[272] M.D. Obradović, Z.M. Stančić, U.Č. Lačnjevac, V.V. Radmilović, A. Gavrilović-Wohlmuther, V.R. Radmilović, S.L. Gojković, Electrochemical oxidation of ethanol on palladium-nickel nanocatalyst in alkaline media, Applied Catalysis B: Environmental, 189 (2016) 110-118.

[273] C. Zhu, D. Wen, M. Oschatz, M. Holzschuh, W. Liu, A.-K. Herrmann, F. Simon, S. Kaskel, A. Eychmüller, Kinetically Controlled Synthesis of PdNi Bimetallic Porous Nanostructures with Enhanced Electrocatalytic Activity, Small, 11 (2015) 1430-1434.

[274] A. Dutta, J. Datta, Outstanding Catalyst Performance of PdAuNi Nanoparticles for the Anodic Reaction in an Alkaline Direct Ethanol (with Anion-Exchange Membrane) Fuel Cell, The Journal of Physical Chemistry C, 116 (2012) 25677-25688.

[275] S. Zhou, R. Yan, W. Zhou, C. Wu, W. Cheng, Highly efficient electrooxidation of ethanol on CuPtPd trimetallic catalyst, Journal of Electroanalytical Chemistry, 929 (2023) 117118.

[276] E. Leal da Silva, A. Cuña, M. Cadorin, J.S. Marcuzzo, C. Radtke, M.R. Baldan, A.C. Rodrigues-Siqueli, C. de Fraga Malfatti, Influence of the Support and SnO2 Content on the Electrocatalytic Properties of PdSn/C Electrocatalysts for EOR in Alkaline Medium, Waste and Biomass Valorization, 13 (2022) 1705-1716.

[277] J. Zhong, D. Bin, B. Yan, Y. Feng, K. Zhang, J. Wang, C. Wang, Y. Shiraishi, P. Yang, Y. Du, Highly active and durable flowerlike Pd/Ni(OH)2 catalyst for the electrooxidation of ethanol in alkaline medium, RSC Advances, 6 (2016) 72722-72727.